Design of Parameter Independent, High Performance Sensorless Controllers for Permanent Magnet Synchronous Machines

Xie, Ge

Publication date:
2015

Document Version
Publisher's PDF, also known as Version of record

Design of Parameter Independent, High Performance Sensorless Controllers for Permanent Magnet Synchronous Machines

by

Ge Xie

Dissertation submitted to the Faculty of Engineering and Science at Aalborg University
in partial fulfillment for the degree of
Doctor of Philosophy in Electrical Engineering

DEPARTMENT of ENERGY TECHNOLOGY
AALBORG UNIVERSITY
AALBORG, DENMARK
JULY 2015

Aalborg University
Department of Energy Technology
Pontopidanstræde 101
Aalborg East, DK-9220
Denmark
http://www.et.aau.dk

ISBN: 978-87-92846-74-7

To my parents and my girlfriend Ke Yu for their support

Preface

This thesis is submitted to Faculty of Engineering and Science at Aalborg University in partial fulfillment for the Ph.D. degree in Electrical Engineering.

This project is supported by Danfoss Power Electronics A/S, Denmark. Acknowledgements are given to Danfoss Power Electronics A/S and Department of Energy Technology, Aalborg University. I greatly appreciate the financial and technical support from Danfoss Power Electronics A/S to carry out this research project.

The project has been completed under the supervision of Associate Professor Kaiyuan Lu from the Department of Energy Technology, Aalborg University, Dr. Sanjeet Kumar Dwivedi and Mr. Jesper Riber Rosholm both from Danfoss Power Electronics A/S. First and foremost, I would like to express my sincere gratitude to my supervisor Associate Professor Kaiyuan Lu, for his professional and patient guidance during my Ph.D. period. Also, I would like to thank Dr. Sanjeet Kumar Dwivedi and Mr. Jesper Riber Rosholm, for their kindly support and discussions to my work.

I am grateful for the fruitful discussions and knowledge exchange I have had with my colleagues from the Department of Energy Technology, Aalborg University. Especially, I would like to thank my friends Dr. Dao Zhou, Dr. Yongheng Yang, Dr. Xiao Liu, Dr. Mingzhe Liu, Dr. Ke Ma, Dr. Xiongfei Wang, Dr. Chi Su, Dr. Jiakun Fang, Dr. Weihao Hu, Mr. Wenli Yao, Mr. Jie Tian, Mr. Dong Wang, Mrs. Qian Wu, Mr. Yang Feng, for their help and kindness. Much special appreciations are extended to Professor Frede Blaabjerg, Mads Lund, Walter Neumayr and Corina Busk Gregersen for their assistance in many ways.

Finally, I would like to express my deepest gratitude to my parents and my girlfriend Ke Yu for their constant support and encouragement.

Ge Xie
Aalborg, July 2015

Copyright Statement

Thesis title: Design of Parameter Independent, High Performance Sensorless Controllers for Permanent Magnet Synchronous Machines

Name of PhD student: Ge Xie

Name of supervisors: Dr. Kaiyuan Lu, Dr. Sanjeet Kumar Dwivedi

List of publication:

- Paper 1:

  Authors: Ge Xie, Kaiyuan Lu, Sanjeet Kumar Dwivedi, Jesper Riber Rosholm and Frede Blaabjerg

  Title: Minimum Voltage Vector Injection Method for Sensorless Control of PMSM for Low-Speed Operations

  The paper has been accepted in the IEEE Transaction on Power Electronics.

- Paper 2:

  Authors: Ge Xie, Kaiyuan Lu, Sanjeet Kumar Dwivedi, Jesper Riber Rosholm and Weiming Wu

  Title: Permanent Magnet Flux Online Estimation Based on Zero Voltage Vector Injection

  The paper has been accepted in the IEEE Transaction on Power Electronics Letters.

- Paper 3:

  Authors: Ge Xie, Kaiyuan Lu, Sanjeet Kumar Dwivedi and Jesper Riber Rosholm

  Title: High bandwidth zero voltage injection method for sensorless control of PMSM

The paper has been published in the 2014 17th International Conference on Electrical Machines and Systems (ICEMS), pp.3546-3552, Oct 2014.

- Paper 4:

  Authors: Ge Xie, Kaiyuan Lu, Sanjeet Kumar Dwivedi and Jesper Riber Rosholm

  Title: Improved INFORM Method by Minimizing the Inverter Nonlinear Voltage Error Effects

  The paper has been accepted in the 2015 2nd Workshop on Electrical Machines Design Control and Diagnosis (WEMDCD).

This present report combined with the above listed scientific papers has been submitted for assessment in partial fulfilment of the PhD degree. The scientific papers are not included in this version due to copyright issues. Detailed publication information is provided above and the interested reader is referred to the original published papers. As part of the assessment, co-author statements have been made available to the assessment committee and are also available at the Faculty of Engineering and Science, Aalborg University.

Abstract

The Permanent Magnet Synchronous Machine (PMSM) has become an attractive candidate for various industrial applications due to its high efficiency and torque density. In the PMSM drive system, simple and robust control methods play an important role in achieving satisfactory drive performances. For reducing the cost and increasing the reliability of the drive system, eliminating the mechanical sensor brings a lot of advantages to the PMSM drive system. Therefore, sensorless control was developed and has been increasingly used in different PMSM drive systems in the last 20 years. However, machine parameters such as resistance and inductance are involved in many existing sensorless control algorithms. Therefore, varying machine parameters due to different operation conditions may affect the accuracy of the position estimation and the drive performance consequently. For power converter manufactures, a generalized, universal sensorless controller that can be used for different types of PMSMs is desired. It is highly preferred that there should be no machine parameters involved in the sensorless controller.

The understanding of the PM machine model is a foremost requirement for the machine control. In this thesis, the mathematical models of the Permanent Magnet (PM) machine are first introduced. The control fundamentals including Field Oriented Control (FOC) strategy and two basic sensorless control methods are presented as well.

The experiment platform setup used to validate the proposed sensorless control algorithms is described next. Since the inverter voltage error may affect the performance of the sensorless control system, the nonlinear inverter voltage error is analyzed and discussed in detail. Two compensation methods are implemented and the results are given.

As a comparison example, one of the typical sensorless algorithm – the INFORM (Indirect flux detection by online reactance measurement) method is implemented and tested. It is demonstrated that the inverter voltage error may seriously affect the performance of the position estimator. To overcome this difficulty, a new implementation scheme of the INFORM method with easy inverter voltage error compensation strategy is therefore proposed.

In this thesis, two new machine parameter independent sensorless control methods are proposed. The zero voltage injection method is first introduced for e.g. medium speed operation. In this method, the zero voltage vector is injected between two FOC

PWM (Pulse-Width Modulation) periods. In the injection period, the voltage output from the inverter is forced to be zero. The rotor position and the speed are then estimated simply from the current changes during this zero voltage injection period. This method provides a good performance for the rotor position estimation. The transient fluctuation of the estimated rotor position error is around 20 degrees with a step load torque change from 0% to 100% of the rated torque. The position error in steady state is within ±2 electrical degrees for the best case. The proposed method may also be used for e.g. online machine parameter identification and an application example is given. For low speed operation, a new estimated d- or q-axis voltage injection sensorless algorithm is introduced. A voltage vector with constant magnitude is applied on the estimated d- or q-axis and inserted between two FOC PWM periods. The currents sampled before and after the injection period are then used for estimating the rotor position and speed. This method is further developed to suppress the inverter voltage error effects on the position estimation accuracy. Experimental results have shown that the transient position error during a step load change from no-load to full-load is around 20 degrees. The ripple in the rotor position error in steady state is around ±3 degrees with the real rotor speed as the feedback and ±6 degrees with the estimated rotor speed as the feedback. These two proposed methods ideally need one injection voltage vector only for the rotor position estimation. This will benefit increasing the control bandwidth and minimizing the current distortion. The implementations and extensive experimental results of these two methods are presented in detail in the thesis.

Abstrakt

Permanent Magnet synkron maskine (PMSM) er blevet en attraktiv kandidat til forskellige industrielle applikationer på grund af dens høje effektivitet og moment tæthed. I PMSM drivesystem, spiller enkle og robuste metoder en vigtig rolle i at opnå tilfredsstillende drev forestillinger. For at reducere omkostningerne og øge pålideligheden af drivesystemet, bringer eliminere den mekanisk sensor en masse fordele til PMSM drevsystem. Derfor, sensorless kontrol blev udviklet og er blevet i stigende grad brugt i forskellige PMSM drivsystemer i de sidste 20 år. Dog er maskine parametre som modstand og induktans involveret i mange eksisterende sensorless kontrol algoritmer. Derfor kan varierende maskine parametre på grund af forskellige driftsvilkår påvirke nøjagtigheden af position estimering og drive arbejdsindsats derfor. For magt converter fremstiller ønskes en generaliseret, universal sensorless controller, der kan bruges til forskellige typer af PMSMs. Det er meget foretrukket at der bør være nogen maskine parametre involveret i sensorless-controller.

Forståelsen af PM maskine modellen er først og fremmest krav til maskine kontrol. I denne afhandling, er de matematiske modeller af Permanent Magnet (PM) maskinen introduceret. Kontrol fundamentals felt orienteret kontrol (FOC) strategi og to grundlæggende sensorless kontrolmetoder præsenteres samt.

Opsætningen af eksperimentet platform bruges til at validere de foreslåede sensorless kontrol algoritmer er beskrevet næste. Da inverter spænding fejl kan påvirke effektiviteten af sensorless drevsystemet , er ikke-lineære inverter spænding fejl analyseret og drøftet i detaljer. To kompensation metoder er gennemført og resultaterne er givet.

Som et eksempel på sammenligning, en af de typiske sensorless algoritme INFORM (indirekte flux påvisning af online reaktans måling) bliver implementeret og testet. Det er påvist, at inverter spænding fejl alvorligt kan påvirke ydeevnen af position estimator. For at overvinde denne vanskelighed, foreslås derfor en ny implementering ordning af metoden INFORM med let inverter spænding fejl kompensation strategi.

I denne afhandling, er to nye maskine parameter uafhængige sensorless kontrolmetoder foreslået. Nul spænding injektion metoden er først indført for f.eks. medium hastighed operation. I denne metode sprøjtes den nul spænding vektor i mellem to FOC PWM (Pulse bredde Modulation) perioder. I perioden injektion er spænding output fra inverteren tvunget til at være nul. Rotoren position og hastighed

skønnes så blot fra de aktuelle ændringer i denne nul spænding injektion periode. Denne metode giver en god ydelse til rotorposition estimering. Forbigående udsving i den anslåede rotorposition fejl er omkring 20 grader med en trinvis belastning drejningsmoment ændring fra 0% til 100% af den nominelle moment. Position fejlen i steady state er inden for ±2 elektriske grader i bedste fald. Den foreslåede metode kan også bruges til f.eks. online maskine parameter identifikation og gives et ansøgning eksempel. For lav hastighed operation indføres en ny anslåede d - eller q-akse spænding injektion sensorless algoritme. En spænding vektor med konstant størrelsesorden er anvendt på den anslåede d - eller q-akse og indsættes mellem to FOC PWM perioder. Strømninger udtaget før og efter indsprøjtning bruges derefter til estimering af rotorposition og hastighed. Denne metode er videreudviklet til at undertrykke inverter spænding fejl effekter på position estimering nøjagtighed. Eksperimentelle resultater har vist, at den transiente position fejl under en trin belastning ændring fra ubelastet til fuld belastning er omkring 20 grader. Ripple i rotorposition fejl i steady state er omkring ±3 grader med virkelige rotor hastighed som feedback og ±6 grader med den anslåede rotor hastighed som feedback. Disse to foreslåede metoder skal ideelt set kun én injektion spænding vektor til rotorposition estimering. Det vil gavne stigende kontrol båndbredde og minimere den nuværende forvrængning. Implementeringer og omfattende eksperimentelle resultater af disse to metoder præsenteres i detaljer i afhandlingen.

Contents

Chapter 1
Introduction

This chapter presents the background of the project. The objectives of the research are introduced followed. The problem statement is formulated subsequently. Finally the outline of the dissertation is given.

1.1 Project background

Permanent Magnet Synchronous Machine (PMSM) has become the most promising drive motor candidate for many industrial applications, due to its high efficiency and high torque density [1]. Compared with the induction machine, PMSM does not need magnetizing component of stator current, since the excitation is provided by permanent magnets inside the machine. This reduces the current cost of the power supply and increases the efficiency. Besides, PM machines can be designed with less weight and volume over the induction machines. They also have higher torque to the inertia ratio which is very important for the fast electrical and mechanical dynamic responses.

In order to drive the PM machine with high efficiency and stability, different control methods for PMSMs have been developed in the last decades [2]. In general, there are two basic control strategies for PM machines: open-loop control and closed-loop control. In the open-loop control (e.g. V/f control) methods [3], the machine variables (such as the stator voltage and current, the rotor position and speed) need not to be known as the feedback. The voltage and frequency commands will be given by the controller without the comparison with the actual values. This will make the control system simpler. However, open-loop control system is unstable and responds slowly. In

the high performance drive systems, good stability and robustness can be achieved by closed-loop control method (such as vector control and direct torque control). For controlling the machine speed and torque accurately, the current of the machine, the rotor position and speed need to be known in the vector control or direct torque control methods. Field Oriented Control (FOC) is a classical closed-loop control method for PMSM [4], which uses the rotor speed as feedback for generating the reference torque and uses the rotor position for decoupling the stator currents, and then the torque component of the current can be controlled precisely.

In the normal closed-loop control systems, the sensors for obtaining the rotor position and speed information are needed. These additional sensors are expensive. The mechanical arrangement for the sensors will also considerably increase the cost of the entire drive system. When the machines are applied in some extreme industrial conditions, the rotor position sensors may become unreliable and their accuracy may probably be degraded. Due to these reasons, elimination of the mechanical sensor becomes necessary and is highly appreciated for many industrial applications. Therefore, many researches in developing the motor drive system without a position sensor have been carried out, which is known as the so-called "Sensorless control" [5]-[7]. In the sensorless control system, the rotor position sensor is eliminated. Instead, the rotor position is calculated by an estimator. The rotor position and speed can be estimated by sampling the real-time variables of the machine, such as voltages and currents. In principal, there are two kinds of methods for the position estimation: methods based on the voltage mode of the machine and methods based on the current mode of the machine. In the voltage mode based method, the rotor position information can be derived from a flux observer related to the voltage of the machine back-electromagnetic force (EMF) (known as the back-EMF voltage). In the current mode based method, the rotor position information is extracted from current signals which involve rotor saliency information. A typical example is to use a high frequency carrier signal that is injected into the machine and the signal processing technique is then used to obtain the rotor position information [8].

In many of sensorless control algorithms, the machine parameters such as resistance and inductance have to be involved [9], [10]. These parameters are always considered as constants. However, the temperature and saturation effects may change these parameters, and then affect the accuracy of the position estimation. Moreover, the machine parameters are often measured offline by using additional instrumentations. Therefore, a machine parameter independent sensorless controller is desired. This requires that there should be no machine parameter involved in the sensorless control algorithm, which is so-called "parameter independent sensorless control".

1.2 Research objectives

The machine parameters are important in many sensorless control systems. However, the parameters may also bring problems into the drive systems, if the sensorless control algorithms are sensitive to the machine parameter change. Therefore, elimination of the machine parameters can make the estimation more accurate and reliable for different industrial environments. For finding a high performance, parameter independent sensorless control method for PMSM, the objectives of this project are as follows.

- To design a parameter independent sensorless control algorithm, the modelling of PMSM and its control system should be illustrated in detail. The sensorless algorithm may then be implemented in the experimental test system.

- The inverter nonlinear voltage error and other limitations which may affect the accuracy of the rotor position estimation should be investigated and well compensated.

- The existing voltage pulses injection sensorless control method (e.g. the classical INFORM method) should be studied and implemented in the experimental system. The performance of the drive system based on the INFORM method should be carefully analyzed.

- Novel algorithms which can estimate the rotor position without using any machine parameters should be proposed. The stability and effectiveness of

these parameter independent sensorless algorithms should be compared with e.g. the classical INFORM method. The comparisons between the simulation and experimental results for the proposed methods also need to be illustrated.

1.3 Problem statement and Limitations

The challenges and limitations of the project are summarized as follows.

- In the parameter independent sensorless control algorithm, the current samples are the only variables used for the estimation. Therefore, the accuracy of the measurement will directly affect the performance of the estimator. How to obtain a clear and accurate current signal is the first important issue to be considered.

- In the Voltage Source Inverter (VSI), the nonlinear voltage error will affect the voltage output. The difference between the voltage command and the voltage output will bring an error into the current variations. Since the inverter voltage error distorts the output voltage, the injection voltage applied on the machine may be located with a wrong angle or a smaller magnitude. Thus the current change during the injection period may be incorrect. Therefore, this nonlinear voltage error in the inverter needs to be determined and compensated.

1.4 Outline of the Dissertation

The dissertation is organized in 8 chapters:

Chapter 1 Introduction

In this chapter, the project background and the objectives of the research are introduced. The problems and the limitations are presented followed. The outline of the dissertation is listed at the end.

Chapter 2 PM Machine and Control Fundamentals

The mathematical models of PM machine are derived in this chapter. The main control strategy used in the drive system is presented. Two main sensorless algorithms and parameter independent sensorless algorithm are also discussed and compared in this chapter.

Chapter 3 Experiment Platform Setup

The experiment platform setup is described in this chapter. The parameters of the test PMSM and load machine are listed. The inverter, DSP based controller and measurement equipment are also explained in detail.

Chapter 4 Inverter Voltage Error Analysis and Compensation

In this chapter, the inverter nonlinear voltage error is analyzed. The voltage error on the single phase and three-phase are determined and compared. Finally, the implementation of two compensation methods are discussed, the experimental results are also given and explained.

Chapter 5 INFORM Method and Improvements

This chapter introduces the standard INFORM method and an improved method. The theory of the INFORM method is illustrated. The simulation and experimental results of this method are given and compared. The implementation and the theoretical analysis of the improved method are presented, and the experimental results are given and compared with the standard method. A sector estimation method based on the INFORM voltage injection scheme is also introduced in this chapter.

Chapter 6 Zero voltage injection method

This chapter introduces the proposed zero voltage injection sensorless control method. In this method, the zero voltage vector is injected between two FOC PWM switching periods. In the injection period, the voltage output from the inverter is zero. However, the back-EMF will cause the current variation. The rotor position and the speed are then calculated by the measured current changes. The implementation and the mathematical analysis are presented. The simulation and experimental results are also

given and compared. A permanent magnet flux linkage online estimation method based on the zero voltage injection scheme is introduced at the end of this chapter.

Chapter 7 Estimated d-/q-axis Voltage Vector Injection Method

This chapter introduces the new estimated d-/q-axis voltage vector injection sensorless control method. In this method, the voltage vector with constant magnitude is inserted between two FOC PWM periods. The injected voltage vector can be on the estimated d- or q-axis. The currents sampled before and after the injection period are used for estimating the rotor position and speed. The implementation and analysis of this method are explained in detail. The simulation and experimental results are given and compared. The voltage error from the inverter may affect the algorithm. Therefore, a compensation method for minimizing the inverter voltage error is discussed and implemented. The experimental results with the voltage error compensation at different working conditions are also given.

Chapter 8 Conclusion

The main conclusions of the dissertation and recommendations for future work are highlighted in this chapter.

Bibliography

[1] K. J. Overshott, "Magnetism: it is permanent," *IEE Proceedings A Science, Measurement and Technology*, vol. 138, no. 1, pp. 22-30, Jan 1991.

[2] P. Vas, "Vector and Direct Torque Control of Synchronous Machines," *Oxford University Press*, 1998.

[3] G. D. Andreescu, C. E. Coman, A. Moldovan, I. Boldea, "Stable V/f Control System with Unity Power Factor for PMSM Drives," *International Conference on Optimization of Electrical and Electronic Equipment (OPTIM)*, pp. 432-438, May 2012.

[4] T. Rekioua, F. Meibody Tabar, R. Le Doeuff, "A new approach for the field-oriented control of brushless, synchronous, permanent magnet machines,"

Fourth International Conference on Power Electronics and Variable-Speed Drives, pp. 46-50, Jul 1990.

[5] K. Rajashekara, A. Kawamura, and K. Matsuse, "Sensorless Control of AC Motors," *New York: IEEE Press*, 1996.

[6] M. W. Degner, "Flux, Position, and Velocity Estimation in AC Machines Using Carrier Signal Injection," *University of Wisconsin-Madison*, 1998.

[7] J. M. Kim, S. J. Kang, and S. K. Sul, "Vector control of interior permanent magnet synchronous motor without a shaft sensor," *Twelfth Annual Conference on Applied Power Electronics Conference and Exposition*, vol. 2, pp. 743-748, Feb 1997.

[8] A. Piippo, M. Hinkkanen, and J. Luomi, "Sensorless control of PMSM drives using a combination of voltage model and HF signal injection," *IEEE 39th IAS Annual Meeting Conference on Industry Applications*, vol. 2, pp. 964-970, Oct 2004.

[9] M. J. Corley and R. D. Lorenz, "Rotor position and velocity estimation for a salient-pole permanent magnet synchronous machine at standstill and high speeds," *IEEE Transactions on Industry Applications*, vol. 34, no. 4, pp. 784-789, July/Aug 1998.

[10] R. Filka, P. Balazovic, and B. Dobrucky, "A seamless whole speed range control of interior PM synchronous machine without position transducer," *12th International Power Electronics and Motion Control Conference*, pp. 1008-1014, Aug 2006.

Chapter 2
PM Machine and Control Fundamentals

2.1 Introduction

This chapter introduces the mathematical model of PMSM. The purpose of modeling the PM machine is to provide a sufficient mathematical description for the physical machine behavior. The control strategies and the different sensorless algorithms may then be designed and evaluated. The three-phase PM machine model consists of electrical, magnetic and mechanical components. The results of the modeling work could be a dynamic or steady state mathematical model. The control strategy used in the project is Field Oriented Control, which is presented in the following sections. Two main typical sensorless algorithms: back-EMF based method and voltage carrier injection method are discussed and compared.

2.2 Modelling of PMSM

There are mainly two types of rotor configurations for PMSMs. They are surface mounted permanent magnet type and interior permanent magnet type. As shown in Figure 2.1, in the surface mounted permanent magnet type PMSMs, the magnets are mounted on the surface of the rotor, whereas in the interior permanent magnet type, the magnets are placed inside the rotor iron core. Two different rotor configurations bring different saliency characteristics to the machine. The inductances on the d- and q-axes are ideally equal to each other for the surface mounted version, whereas for the interior PMSM as shown in Figure 2.1(b), its q-axis inductance is higher than the d-axis inductance.

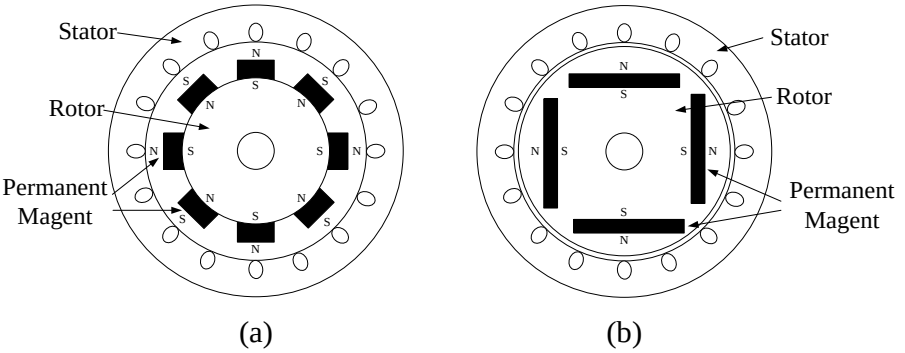

Figure 2.1: Different rotor configurations for PMSMs. (a) Surface magnets type. (b) Interior magnets type.

Figure 2.2 shows a conceptual diagram of a three-phase surface mounted PMSM with one pole pair. The stator windings of the machine are symbolized by one turn, and are shown as AA-, BB- and CC- with their current directions indicated. These three-phase stator coils are placed 120 electrical degrees apart from each other and the magnetic axes of three-phase stator are shown as a-, b- and c-axes. θ_r is the angle between the north pole of the rotor and the stator a-axis, which is denoted as the rotor position.

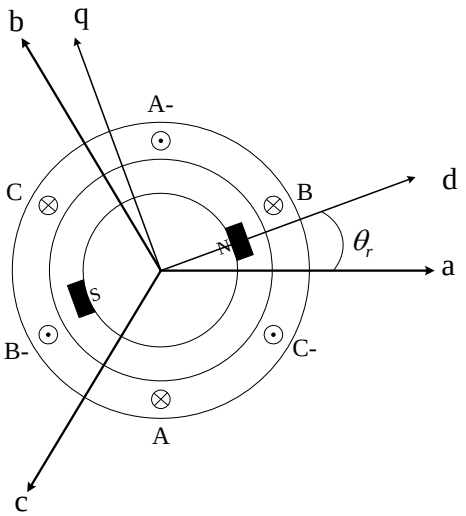

Figure 2.2: Conceptual diagram of a three-phase surface mounted PMSM.

2.2.1 Voltage equations in the stationary abc-reference frame

The voltage equations of the three-phase PM machine in the stationary abc-reference frame can be written as [1]:

$$\begin{bmatrix} v_a \\ v_b \\ v_c \end{bmatrix} = \begin{bmatrix} R & 0 & 0 \\ 0 & R & 0 \\ 0 & 0 & R \end{bmatrix} \begin{bmatrix} i_a \\ i_b \\ i_c \end{bmatrix} + \frac{d}{dt} \begin{bmatrix} \lambda_a \\ \lambda_b \\ \lambda_c \end{bmatrix} \tag{2.1}$$

where R is the stator winding resistance; v_a, v_b, v_c are the phase voltages on the stator; i_a, i_b, i_c are the phase currents on the stator; λ_a, λ_b, λ_c are the stator phase flux linkages.

In the PM machine model, the stator phase flux linkages are related to the phase currents and the PM flux linkage. For instance, the flux linkage on phase A can be described as:

$$\lambda_a = L_{aa} i_a + M_{ab} i_b + M_{ac} i_c + \lambda_{pm,a} \tag{2.2}$$

where L_{aa} is the self-inductance on phase A; M_{ab}, M_{ac} are the mutual inductances between phase A and B, phase A and C respectively. $\lambda_{pm,a}$ is the PM flux linkage on phase A. According to Figure 2.2, the PM flux on the a-axis can be derived as:

$$\lambda_{pm,a} = \lambda_{mpm} \cos(\theta_r) \tag{2.3}$$

λ_{mpm} is the magnitude of the permanent magnet flux linkage. Then the three-phase stator flux linkages can be written as:

$$\begin{bmatrix} \lambda_a \\ \lambda_b \\ \lambda_c \end{bmatrix} = \begin{bmatrix} L_{aa} & M_{ab} & M_{ac} \\ M_{ba} & L_{bb} & M_{bc} \\ M_{ca} & M_{cb} & L_{cc} \end{bmatrix} \begin{bmatrix} i_a \\ i_b \\ i_c \end{bmatrix} + \lambda_{mpm} \begin{bmatrix} \cos(\theta_r) \\ \cos(\theta_r - 120°) \\ \cos(\theta_r + 120°) \end{bmatrix} \tag{2.4}$$

In (2.4), the self-inductances on the three-phase stator windings can be defined as:

$$L_{aa} = L_\sigma + L_A - L_B \cos 2\theta_r \tag{2.5}$$

$$L_{bb} = L_\sigma + L_A - L_B \cos 2(\theta_r - 120°) \tag{2.6}$$

$$L_{cc} = L_\sigma + L_A - L_B \cos 2(\theta_r + 120°) \tag{2.7}$$

where L_σ is the leakage inductance, L_A and L_B are defined as:

$$L_A = \frac{L_{aad} + L_{aaq}}{2} \tag{2.8}$$

$$L_B = \frac{L_{aad} - L_{aaq}}{2} \tag{2.9}$$

where L_{aad} is the self-inductance on the a-axis when $\theta_r = 0$, L_{aaq} is the value when $\theta_r = 90°$.

Then the mutual inductances between stator phases can be defined as:

$$M_{ab} = M_{ba} = -\frac{1}{2} L_A - L_B \cos 2(\theta_r - 60°) \tag{2.10}$$

$$M_{ac} = M_{ca} = -\frac{1}{2} L_A - L_B \cos 2(\theta_r + 60°) \tag{2.11}$$

$$M_{bc} = M_{cb} = -\frac{1}{2} L_A - L_B \cos 2\theta_r \tag{2.12}$$

2.2.2 Voltage equations in the stationary αβ-reference frame

The voltage equations of PM machine can be also represented in a space vector form, which is very helpful when the machine is controlled by the vector control based algorithm. A rectangular two dimensional coordinates system with mutually perpendicular stationary α- and β- axes is used for locating the space vector. The α-axis is aligned to the magnetic axis of the stator phase A, as shown in Figure 2.3.

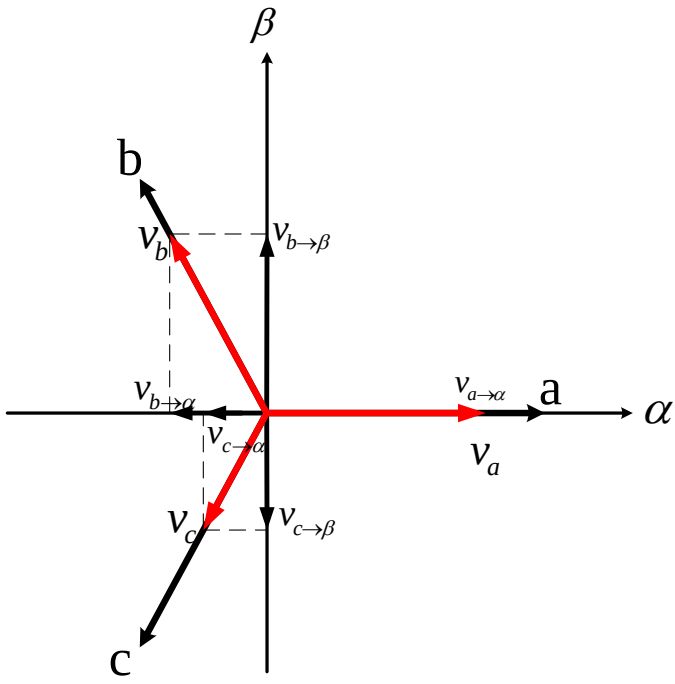

Figure 2.3: Transformation between abc- and αβ-reference frame.

According to Clarke transformation, the variables can be transferred from the abc-reference frame to the αβ-reference frame by:

$$C = \frac{2}{3}\begin{bmatrix} 1 & -\frac{1}{2} & -\frac{1}{2} \\ 0 & \frac{\sqrt{3}}{2} & -\frac{\sqrt{3}}{2} \end{bmatrix} \tag{2.13}$$

Therefore, the machine voltage equations can be represented as:

$$\begin{bmatrix} v_\alpha \\ v_\beta \end{bmatrix} = C\begin{bmatrix} v_a \\ v_b \\ v_c \end{bmatrix} = \begin{bmatrix} R & 0 \\ 0 & R \end{bmatrix}\begin{bmatrix} i_\alpha \\ i_\beta \end{bmatrix} + \frac{d}{dt}\begin{bmatrix} \lambda_\alpha \\ \lambda_\beta \end{bmatrix} \tag{2.14}$$

where:

$$\begin{bmatrix} \lambda_\alpha \\ \lambda_\beta \end{bmatrix} = C\begin{bmatrix} L_{aa} & M_{ab} & M_{ac} \\ M_{ba} & L_{bb} & M_{bc} \\ M_{ca} & M_{cb} & L_{cc} \end{bmatrix} C^{-1}\begin{bmatrix} i_\alpha \\ i_\beta \end{bmatrix} + \lambda_{mpm} C\begin{bmatrix} \cos(\theta_r) \\ \cos(\theta_r - 120°) \\ \cos(\theta_r + 120°) \end{bmatrix} \tag{2.15}$$

By substituting (2.5)~(2.12), expression (2.15) can be derived as:

$$\begin{bmatrix}\lambda_\alpha\\ \lambda_\beta\end{bmatrix}=\begin{bmatrix}L_\sigma+\frac{3}{2}L_A-\frac{3}{2}L_B\cos(2\theta_r) & -\frac{3}{2}L_B\sin(2\theta_r)\\ -\frac{3}{2}L_B\sin(2\theta_r) & L_\sigma+\frac{3}{2}L_A+\frac{3}{2}L_B\cos(2\theta_r)\end{bmatrix}\begin{bmatrix}i_\alpha\\ i_\beta\end{bmatrix}+\lambda_{mpm}\begin{bmatrix}\cos\theta_r\\ \sin\theta_r\end{bmatrix} \quad (2.16)$$

Equation (2.14) and (2.16) are normally expressed in the vector form as:

$$\bar{v}_{\alpha\beta}=R\bar{i}_{\alpha\beta}+\frac{d}{dt}\bar{\lambda}_{\alpha\beta} \quad (2.17)$$

$$\bar{\lambda}_{\alpha\beta}=(L_d i_d+\lambda_{mpm}+jL_q i_q)e^{j\theta_r} \quad (2.18)$$

2.2.3 Voltage equations in the rotating dq-reference frame

Equation (2.17) and (2.18) describes the voltage equation in the stationary αβ-reference frame, the rotor position dependent variables are still involved in the expressions. Therefore, a suitable rotating dq-reference frame depending on the rotor position is introduced to simplify the voltage equation. In the dq-reference frame, the inductances and the PM flux linkage can be seen as constants and are independent from each other. As shown in Figure 2.4, the transformation matrix between the αβ-reference frame and the dq-reference frame can be written as:

$$P=\begin{bmatrix}\cos\theta_r & \sin\theta_r\\ -\sin\theta_r & \cos\theta_r\end{bmatrix} \quad (2.19)$$

Then (2.14) can be written as:

$$\begin{bmatrix}v_d\\ v_q\end{bmatrix}=P\begin{bmatrix}v_\alpha\\ v_\beta\end{bmatrix}=R\begin{bmatrix}i_d\\ i_q\end{bmatrix}+\frac{d}{dt}\begin{bmatrix}\lambda_d\\ \lambda_q\end{bmatrix}+\omega_r\begin{bmatrix}0 & -1\\ 1 & 0\end{bmatrix}\begin{bmatrix}\lambda_d\\ \lambda_q\end{bmatrix} \quad (2.20)$$

Where v_d , v_q , i_d , i_q , λ_d , λ_q are the stator voltages, currents and flux linkages in the dq-reference frame respectively; ω_r is the rotor speed.

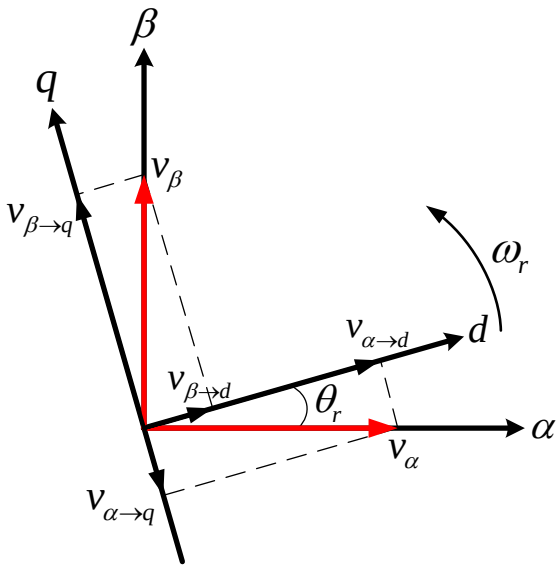

Figure 2.4: Transformation between αβ - and dq-reference frame.

Since the rotor N pole is aligned with the d-axis, the inductances on the d-, q-axes are equivalent to:

$$L_d = L_\sigma + \frac{3}{2} L_{aad} \tag{2.21}$$

$$L_q = L_\sigma + \frac{3}{2} L_{aaq} \tag{2.22}$$

The flux linkages on the d- and q-axes can then be simplified as:

$$\begin{bmatrix} \lambda_d \\ \lambda_q \end{bmatrix} = \begin{bmatrix} L_d & 0 \\ 0 & L_q \end{bmatrix} \begin{bmatrix} i_d \\ i_q \end{bmatrix} + \lambda_{mpm} \begin{bmatrix} 1 \\ 0 \end{bmatrix} \tag{2.23}$$

2.2.4 The electromagnetic torque equation

The expression for the electromagnetic torque generated by the PM machine can be derived from the power equation of the machine. The instantaneous power of the machine can be described in dq-reference frame as:

$$P = \frac{3}{2} \left(v_d i_d + v_q i_q \right) \tag{2.24}$$

By substituting v_d and v_q from (2.20), equation (2.24) can be rewritten as:

$$P = \frac{3}{2}\left(Ri_d^2 + Ri_q^2\right) + \frac{3}{2}\left(L_d i_d \frac{d}{dt} i_d + L_q i_q \frac{d}{dt} i_q\right) + \frac{3}{2}\left[\omega_r \left(L_d i_d i_q + \lambda_{mpm} i_q - L_q i_d i_q\right)\right] \tag{2.25}$$

In (2.25), the third term is used for energy conversion. Therefore, the power transformation from electrical energy to mechanical energy should be expressed as:

$$P_e = \frac{3}{2}\left[\omega_r \left(L_d i_d i_q + \lambda_{mpm} i_q - L_q i_d i_q\right)\right] \tag{2.26}$$

Considering that the electromechanical power should be equal to the multiplication of the rotor mechanical speed and the electromechanical torque:

$$P_e = \frac{\omega_r}{p} T_e \tag{2.27}$$

where p is the number of the machine pole pairs. Thus, the electromechanical torque of the machine can be written as:

$$T_e = \frac{3}{2} p\left[\lambda_{mpm} i_q + \left(L_d - L_q\right) i_d i_q\right] \tag{2.28}$$

2.3 Field oriented control of PMSM

Since the PM machine model can be described in dq-reference frame, the inductance and the flux linkage are independent with the rotor position. According to the electromechanical torque equation (2.28), the torque of the machine can be controlled by the current on the d-axis and q-axis. This can be referred to the rotor permanent magnet flux oriented control.

As a high efficient control strategy, Field Oriented Control (FOC) becomes a successful control strategy for PMSMs [2], [3]. As shown in Figure 2.5, in the classical FOC system, the abc-reference frame voltage and current of the electrical machine will be transformed to the rotating dq-reference frame. Therefore, the rotor position is needed for the reference frame transformation. The rotor position angle can be obtained

from e.g. an encoder or an estimator. In the FOC system, the rotor speed is used as the feedback which compares with the reference speed and uses a PI controller for obtaining the q-axis current command. The reference current on the d-axis is usually set to be zero for e.g. surface mounted PMSM drive system. The voltage commands in the dq-reference frame are both given by the PI controllers which use the reference and actual currents as inputs. These two voltage commands are then transformed to the abc-reference frame by using the rotor position information. The inverter gating signals are finally determined by inverter pulse width modulation techniques (like the well-known Space Vector Pulse-Width Modulation technique) [4].

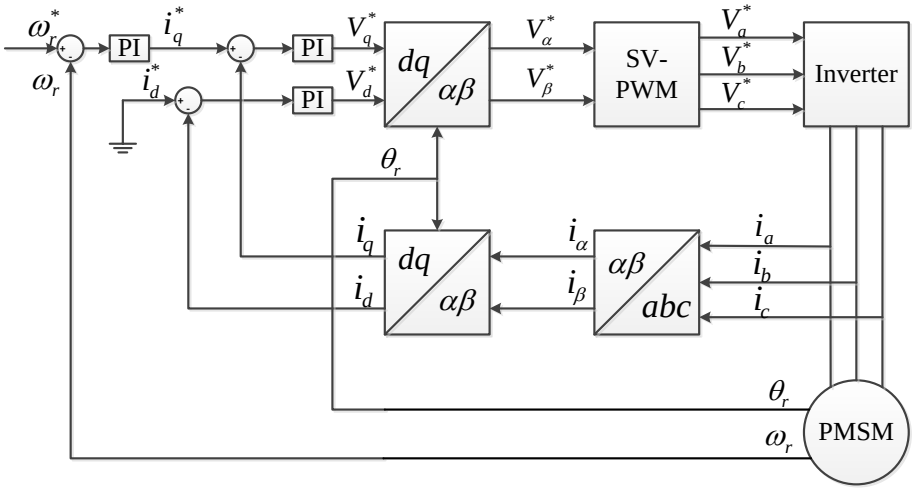

Figure 2.5: Diagram of FOC system.

2.4 Sensorless control of PMSM

As mentioned in section 2.3, in the Field Oriented Control system, knowing about the rotor position and speed information is necessary. For obtaining the rotor position without the mechanical position sensor, sensorless control method is investigated and developed in last 20 years. The following subsections are a state-of-the-art review of the existing sensorless control methods for PMSM.

2.4.1 Back-EMF based methods

The main idea of the Back-EMF method is using the fundamental voltage and current components of the machine to estimate the rotor PM flux linkage vector [5]. This method has a good performance when the machine works in the medium to high speed range, because the back-EMF voltage is proportional to the speed and has a good signal-to-noise ratio in this working range. A classical rotor position estimation derivation is given as follows.

For deriving the back-EMF voltage, the machine voltage equations (2.20) can be represented in a vector form:

$$\bar{v}_{dq} = R\bar{i}_{dq} + \frac{d}{dt}\bar{\lambda}_{dq} + j\omega_r\bar{\lambda}_{dq} \tag{2.29}$$

where:

$$\bar{\lambda}_{dq} = L_d i_d + \lambda_{mpm} + jL_q i_q \tag{2.30}$$

The machine model may then be transferred to the αβ-reference frame by introducing the rotor position information in the voltage equation. In the αβ-reference frame, the machine model becomes [6]:

$$\bar{v}_{\alpha\beta} = R\bar{i}_{\alpha\beta} + L_q\frac{d}{dt}\bar{i}_{\alpha\beta} + j\omega_r\lambda_{eq}e^{j\theta_r} \tag{2.31}$$

where:

$$\lambda_{eq} = \lambda_{mpm} + (L_d - L_q)i_d \tag{2.32}$$

The back-EMF voltage may then be derived as:

$$\bar{E}_{\alpha\beta} = \bar{v}_{\alpha\beta} - R\bar{i}_{\alpha\beta} - L_q\frac{d}{dt}\bar{i}_{\alpha\beta} = j\omega_r\lambda_{eq}e^{j\theta_r} \tag{2.33}$$

Under steady state operation condition, the back-EMF voltage can be considered to be 90 degrees in advance of the rotor flux vector, which is aligned with the rotor d-axis:

$$\angle\bar{E}_{\alpha\beta} = \angle j\omega_r\lambda_{eq}e^{j\theta_r} = \angle\omega_r\lambda_{eq}e^{j(\theta_r+90°)} = \theta_r + 90° \tag{2.34}$$

The rotor position may then be found from (2.34).

There are many sensorless algorithms based on the back-EMF method are studied and developed in recent years.

- **Model Reference Adaptive System (MRAS)**

  The Model Reference Adaptive System (MRAS) based methods are often applied in the sensorless drive of induction machines [7]-[9]. In the classical MRAS method, the rotor flux in the adaptive model is used to compare with the one in the reference model. The rotor speed is then estimated by the fluxes difference between the two models using adequate adaptive mechanism. The estimated rotor position is determined by integrating the estimated speed. The similar idea has also been applied for the PMSMs recently [10]-[12]. In [10] and [12], the MRAS algorithm provided an estimated rotor position with -30 degree and -20 degree error during the acceleration, respectively.

- **Extended Kalman Filter (EKF)**

  The Kalman filter dynamics results from the consecutive cycle of prediction and filtering [13]. The dynamics of these cycles is derived and interpreted in the frame work of Gaussian probability density functions. It is shown that the Kalman filter is a linear, discrete time system that evaluates the state estimation. The Extended Kalman Filter (EKF) implements the Kalman filter for a system dynamics results from the linearization of the original nonlinear filter dynamics around the previous state estimation [14]. The EKF can be used for both induction machines [15] and PMSMs [16]-[18]. In [14], the estimated rotor position has a 5.4 degrees DC bias and ±10 degrees ripple when the machine operates at steady state.

- **Observer based estimator**

  The redundant observer uses the voltage equations of the PM machine in the dq-reference frame for the estimation [19]. In this reference frame, the Park transform uses the estimated position information instead of the position given by a sensor. This can introduce errors into the d-axis and q-axis voltage. Then

a PI controller is used to drive the errors to zero by estimating the rotor position. Parameter errors may lead to estimation errors. Therefore, the parameter estimation may also be added to the redundant observer [20]. In [20], the redundant observer provides an estimated rotor position with a 0.035 rad ripple at steady state.

The Luenberger observer uses the principle with a model of the system and an observer compensator [21]. The observer compensator changes the input to the system model to minimise the observed error. From the observer, internal states that are not possible to measure directly may be extracted from the system model [22].

- **Neural network**

  As an intelligent control algorithm, the neural network is widely known for its strong capacities of self-learning, self-adapting and self-organization [23]. It is now used to combine with other control method e.g. PID control for the PMSM drive. A structured neural networks method for sensorless control of AC machines using the zero sequence carrier signal voltage is introduced in [24]. This method allows effective compensation of saturation-induced saliencies as well as other secondary saliencies. Experimental results show an error between -5 and -8 degrees in the estimated position in [25].

Back-EMF based methods use an internal model of the machine for the rotor position estimation. Different mathematical methods can be applied to minimize the error between the model and the practical system. However, at zero speed and low speed, since the back-EMF is small, the noise in estimated back-EMF signals becomes a greater portion leading to a large error in the estimated rotor position. The error can also be affected by the variation of the resistance and the inductances.

2.4.2 Voltage carrier injection based method

Since the back-EMF is hard to be detected at low speed and standstill, voltage carrier injection based sensorless control methods are proposed for the low speed range operation [26]. In the voltage carrier injection methods, an additional carrier signal is

added to the fundamental machine voltage. The carrier signal frequency is usually much higher than the fundamental frequency (500 Hz to 2.5 kHz, with a switching frequency of 5 kHz). The current response which contains the rotor saliency information is used for calculating the rotor position. A common rotor position estimation derivation based on the high frequency voltage signal injection method is described as follows.

Since the high frequency voltage signal injection method is used in low speed range, in the PM machine voltage equations, the rotor speed can be approximated to be zero. Equation (2.31) may be represented as:

$$\bar{v}_{\alpha\beta} = R\bar{i}_{\alpha\beta} + L_1 \frac{d}{dt}\bar{i}_{\alpha\beta} + L_2 \frac{d}{dt}\bar{i}^*_{\alpha\beta} e^{j2\theta_r} \tag{2.35}$$

where $L_1 = \dfrac{L_d + L_q}{2}$, $L_2 = \dfrac{L_d - L_q}{2}$, $\bar{i}^*_{\alpha\beta}$ is the conjugate vector of $\bar{i}_{\alpha\beta}$.

When the injection voltage is described as:

$$\bar{v}_{c\alpha\beta} = V_c e^{j\omega_c t} \tag{2.36}$$

The subscript c refers to "carrier". Considering the frequency of the injection voltage is very high, the voltage drop on the stator resistance may be seen as to be much smaller than the voltage drop on the inductance. Thus term $R\bar{i}_{\alpha\beta}$ can be neglected in the high frequency model, then (2.35) may be simplified for the injection voltage as:

$$\bar{v}_{c\alpha\beta} = L_1 \frac{d}{dt}\bar{i}_{c\alpha\beta} + L_2 \frac{d}{dt}\bar{i}^*_{c\alpha\beta} e^{j2\theta_r} \tag{2.37}$$

By resolving (2.37) for the current term $\bar{i}_{c\alpha\beta}$,

$$\bar{i}_{c\alpha\beta} = \frac{V_c}{j\omega_c} \frac{1}{L_1^2 - L_2^2} \left(L_1 e^{j\omega_c t} - L_2 e^{j(-\omega_c t + 2\theta_r)} \right) \tag{2.38}$$

Then,

$$\bar{i}_{c\alpha\beta} e^{j\omega_c t} = \frac{V_c}{j\omega_c} \frac{1}{L_1^2 - L_2^2} \left(L_1 e^{j2\omega_c t} - L_2 e^{j2\theta_r} \right) \tag{2.39}$$

The fundamental component of (2.39) can be abstracted by a linear low pass filter:

$$LPF\left(\bar{i}_{c\alpha\beta}e^{j\omega_c t}\right)= j\frac{V_c L_2}{\omega_c\left(L_1^2-L_2^2\right)}e^{j2\theta_r} \tag{2.40}$$

The rotor position may then be obtained as:

$$\theta_r = \frac{1}{2}\left[\arg\left(LPF\left(\bar{i}_{c\alpha\beta}e^{j\omega_c t}\right)\right)-90°\right] \tag{2.41}$$

The following overview of the injection methods are separated based on the type of injected signal.

- **Rotating αβ-reference frame voltage injection**

  The technique of injecting a rotating high frequency voltage in the αβ-reference frame to estimate the rotor position is well researched in [27]-[29]. In this kind of injection method, a constant amplitude voltage vector rotating with a high frequency is added into the fundamental voltage vector. The high frequency current response is filtered out by a band pass filter and then used for estimating the rotor position. The measured current filtered by the low pass filter is used as the feedback for the current controller. Figure 2.6 shows the diagram for the rotating αβ-reference frame voltage injection scheme.

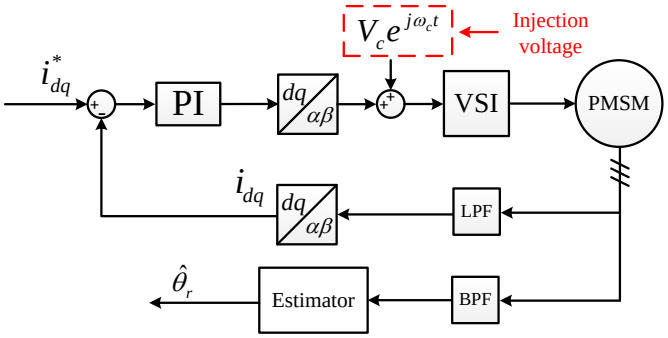

Figure 2.6: Diagram of rotating αβ-reference frame voltage injection.

- **Synchronous dq-reference frame voltage injection**

  The synchronous frame voltage injection methods have been introduced in many publications e.g. [30]-[33]. In this injection scheme, the voltage vector

can be applied on either estimated d- or q-axis. The estimated rotor position $\hat{\theta}_r$ is defined in the estimated dq-reference frame. The difference between the estimated frame and the actual frame is defined as $\tilde{\theta}_r$. A PLL tracking algorithm is used for adjusting the rotor position error $\tilde{\theta}_r$ to be zero. Therefore, the estimated rotor position may then be obtained from the PLL controller. Figure 2.7 shows the diagram for the synchronous frame voltage injection scheme.

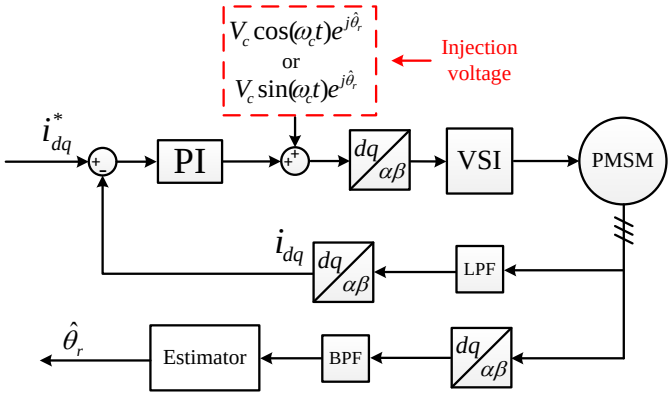

Figure 2.7: Diagram of synchronous frame voltage injection.

- **Voltage pulses injection**

  The voltage pulses injection methods are also studied and developed in recent years [34], [35]. This kind of approaches is to detect the rotor saliency by injecting the voltage pulses in transient conditions. The current response during the voltage excitation period gives the information about the rotor position. The INFORM method which proposed by Schroedl is a classical voltage pulses injection method [36]. The magnetic saliency is detected by measuring the change of the complex stator current vector during the test voltage pulses injection periods. The estimated rotor position error in the standard INFORM method is around 6 degrees [37]. In the further work by Schroedl, it is also shown that the applied test vector sequence can be

enhanced to achieve better performance with normal fundamental machine current control [37].

The common idea of the voltage carrier injection based methods is to apply the additional voltage excitation on the machine stator. The current response is then used to obtain the rotor saliency information. These voltage injection based methods are parameter insensitive and easy to implement. The main disadvantage of this kind of methods is the significant current distortion. With the additional injection voltage, the stator current may have a significant high frequency harmonics. These high frequency component need to be filtered by the low pass filter. Therefore, the performance of the control system may then be affected.

2.4.3 Parameters independent sensorless control

In many sensorless control algorithms discussed above, the machine parameters such as resistance [20], [21], [26] and inductance [20], [27], [30], [31] need to be known. However, the machine parameters may not be constant in different operating conditions. For eliminating the influence from the machine parameter variations and improving the control system reliability, a machine parameters independent sensorless control method is desired.

There already exist several machine parameter independent sensorless algorithms e.g. the INFORM method [36]. These methods use the current response caused by the injection voltage as the only variable to estimate the rotor position. However, these existing parameter independent sensorless control methods still can be improved and with respect to implementation simplicity and robustness against inverter voltage error. Therefore, some new approaches for parameter independent sensorless control system are also proposed and evaluated in this dissertation.

2.5 Summary

The mathematical model of PMSM has been given in this chapter. The voltage equations of the machine were represented in different coordinate systems. When the voltage equations were transformed to the dq-reference frame, the currents were

decoupled to two independent components. This makes the vector control based method becomes much easier to be used in the drive system.

The Field Oriented Control method and two main sensorless control methods have also been described in this chapter. The comparison of two main sensorless control methods reveals that, the parameter independent sensorless control algorithm becomes a promising and valuable research.

Bibliography

[1] D. O'Kelly, S. Simmons, "Introduction to Generalized Electrical Machine Theory," *Maidenhead: McGraw- Hill,* 1968.

[2] W. Leonhard, "Control of Electrical Drives," *Secaucus, NJ, USA: Springer-Verlag New York, Inc.,* 1991.

[3] D. W. Novotny, T. A. Lipo, "Vector Control and Dynamics of AC Drives," *Oxford: Oxford University Press,* 1996.

[4] G. Xie, K. Y. Lu, D. S. Kumar, R. J. Riber, "High bandwidth zero voltage injection method for sensorless control of PMSM," *17th International Conference on Electrical Machines and Systems (ICEMS),* pp. 3546-3552, Oct 2014.

[5] J. S. Kim, S. L. Sul, "High Performance PMSM Drives without Rotational Position Sensors Using Reduced Order Observer," *IEEE Thirtieth IAS Annual Meeting Conference on Industry Applications,* vol. 1, pp. 75-82, Oct 1995.

[6] I. Boldea, M. C. Paicu, G. D. Andreescu, "Active Flux Concept for Motion-Sensorless Unified AC Drives," *IEEE Transactions on Power Electronics,* vol. 23, no. 5, pp. 2612-2618, Sep 2008.

[7] G. Yang, T. H. Chin, "Adaptive-speed identification scheme for a vector-controlled speed sensorless inverter-induction motor drive," *IEEE Transactions On Industry Applications,* vol. 29, no. 4, pp. 820–825, Jul/Aug 1993.

[8] R. Blasco-Gimenez, G. M. Asher, M. Sumner, K. J. Bradley, "Dynamic performance limitations for MRAS based sensorless induction motor drives. I. Stability analysis for the closed loop drive," *IEE Proceedings-electric Power Applications*, vol. 143, no. 2, pp. 113-122, Mar 1996.

[9] L. Zhen, L. Y. Xu, "Sensorless field orientation control of induction machines based on a mutual MRAS scheme," *IEEE Transactions on Industrial Electronics*, vol. 45, no. 5, pp. 824-831, Oct 1998.

[10] H. Nian, Y. K. He, L. Huang, H. Ying, "Sensorless operation of an inset PM bearingless motor implemented by the combination approach of MRAS and HF signal injection," *The Sixth World Congress on Intelligent Control and Automation, WCICA*, vol. 2, pp. 8163-8167, June 2006.

[11] J. Zhang, Q. Jiang, "Sensorless commutation of micro PMSMs for high-performance high-speed applications," *Eighth International Conference on Electrical Machines and Systems (ICEMS)*, vol. 3, pp. 1795–1800, Sept. 2005.

[12] H. M. Kojabadi, M. Ghribi, "MRAS-based adaptive speed estimator in PMSM drives," *International Workshop on Advanced Motion Control (AMC)*, pp. 569–572, Mar 2006.

[13] R. E. Kalman, "A new approach to linear filtering and prediction problems," *Transactions of the ASME–Journal of Basic Engineering*, vol. 82, no. Series D, pp. 35-45, 1960.

[14] M. Boussak, "Implementation and experimental investigation of sensorless speed control with initial rotor position estimation for interior permanent magnet synchronous motor drive," *IEEE Transactions on Power Electronics*, vol. 20, no. 6, pp. 1413-1422, Nov 2005.

[15] M. Khafallah, A. El Afia, A. Cheriti, F. El Mariami, A. Saad, B. El Moussaoui, "EKF based speed sensorless vector control of an induction machine," *IEEE International Conference on Industrial Technology*, vol. 3, pp. 1338 – 1344, Dec 2004.

[16] S. Bolognani, L. Tubiana, and M. Zigliotto, "Extended kalman filter tuning in sensorless PMSM drives," *IEEE Transactions on Industry Applications*, vol. 39, no. 6, pp. 1741-1747, Nov/Dec 2003.

[17] S. Stasi, L. Salvatore, and F. Cupertino, "Sensorless control of PM synchronous motors based on LKF estimation of rotor position," *IEEE 28th Annual Conference* on *Industrial Electronics Society (IECON),* vol. 1, pp. 686-691, Nov 2002.

[18] Y. H. Kim, Y. S. Kook, "High performance IPMSM drives without rotational position sensors using reduced-order EKF," *IEEE Transactions on Energy Conversion,* vol. 14, no. 4, pp. 868-873, Dec 1999.

[19] S. Caux and M. Fadel, "Kalman filter and redundant observer comparison for sensorless PMSM velocity control," *IEEE International Symposium on Industrial Electronics (ISIE),* vol. 3, pp. 887-892, Jun 2005.

[20] B. Gerard, S. Caux, P. Maussion, "Redundant Position Observer Improvement for Sensorless PMSM at Low Speed," *IEEE International Symposium on Industrial Electronics,* vol. 3, pp. 2083-2088, Jul 2006.

[21] R. Filka, P. Balazovic, B. Dobrucky, "A seamless whole speed range control of interior PM synchronous machine without position transducer," *12th International Power Electronics and Motion Control Conference*, pp. 1008-1014, Aug 2006.

[22] M. Trabelsi, M. Jouili, M. Boussak, Y. Koubaa, M. Gossa, "Robustness and Limitations of Sensorless Technique Based on Luenberger State-Observer for Induction Motor Drives Under Inverter Faults," *IEEE International Symposium on Industrial Electronics (ISIE),* pp. 716-721, Jun 2011.

[23] Q. D. Guo, R. F. Luo, L. M. Wang, "Neural Network Adaptive Observer Based Position and Velocity Sensorless Control of PMSM," *4th International Workshop on Advanced Motion Control,* vol.1, pp. 41-46, Mar 1996.

[24] P, Garcia, F. Briz, D. Raca, R. D. Lorenz, "Saliency Tracking-Based, Sensorless Control of AC Machines Using Structured Neural Networks," *Fourtieth IAS Annual Meeting on Industry Applications,* vol. 1, pp. 319-326, Oct 2005.

[25] T. D. Batzel, K. Y. Lee, "An approach to sensorless operation of the permanent magnet synchronous motor using diagonally recurrent neural networks," *IEEE Transactions on Energy Conversion*, vol. 18, no. 1, pp. 100-106, Mar 2003.

[26] J. M. Kim, S.J. Kang, S.K. Sul, "Vector control of interior permanent magnet synchronous motor without a shaft sensor," *Twelfth Annual Conference on Applied Power Electronics Conference and Exposition (APEC)*, vol. 2, pp. 743-748, Feb 1997.

[27] M. W. Degner, R. D. Lorenz, "Using Multiple Saliencies for the Estimation of Flux, Position, and Velocity in AC Machines," *IEEE Transaction on Industry Applications*, vol. 34, no. 5, pp. 1097-1104, Sep/Oct 1998.

[28] N. Teske, G. M. Asher, M. Sumner, K. J. Bradley, "Suppression of Saturation Saliency Effects for the Sensorless Position Control of Induction Motor Drives Under Loaded Conditions," *IEEE Transactions on Industrial Electronics*, vol. 47, no. 5, pp. 1142-1150, Oct 2000.

[29] N. Teske, G. M. Asher, M. Sumner, K. J. Bradley, "Analysis and Suppression of High-Frequency Inverter Modulation in Sensorless Position-Controlled Induction Machine Drives," *IEEE Transaction on Industry Applications*, vol. 39, no. 1, pp. 10-18, Jan/Feb 2003.

[30] M. J. Corley, R. D. Lorenz, "Rotor Position and Velocity Estimation for a Salient-Pole Permanent Magnet Synchronous Machine at Standstill and High Speeds," *IEEE Transaction on Industry Applications*, vol. 34, no. 4, pp. 784-789, July/Aug. 1998.

[31] J. H. Jang, S. K. Sul, J. I. Ha, K. Ide, M. Sawamura, "Sensorless Drive of Surface-Mounted Permanent-Magnet Motor by High-Frequency Signal Injection Based on Magnetic Saliency," *IEEE Transaction on Industry Applications*, vol. 39, no. 4, pp. 1031-1038, Jul/Aug 2003.

[32] M. Linke, R. Kennel, J. Holtz, "Sensorless position control of permanent magnet synchronous machines without limitation at zero speed," *IEEE 28th Annual Conference on Industrial Electronics Society (IECON)*, pp. 674-679, 2002.

[33] J. Holtz, "Acquisition of Position Error and Magnet Polarity for Sensorless Control of PM Synchronous Machines," *IEEE Transaction on Industry Applications,* vol. 44, no. 4, pp. 11721180, Jul/Aug 2008.

[34] P. Vadstrup, R. D. Lorenz, "Robust estimator design for signal injection-based IPM synchronous machine drives," *IEEE Industry Applications Society (IAS) Annual Meeting,* vol. 2, pp. 957-963, Oct 2004.

[35] R. Filka, P. Balazovic, B. Dobrucky, "A seamless whole speed range control of interior PM synchronous machine without position transducer," *12th International Power Electronics and Motion Control Conference*, pp. 1008-1014, Aug 2006.

[36] M. Schroedl, "Sensorless Control of AC Machines at Low Speed and Standstill Based on the "INFORM" Method," *IEEE IAS Annual Meeting,* pp. 270-277, Oct 1996.

[37] E. Robeischl, M. Schroedl, "Optimized INFORM Measurement Sequence for Sensorless PM Synchronous Motor Drives With Respect to Minimum Current Distortion," *IEEE Transaction on Industry Applications,* vol. 40, no. 2, pp. 591-598, Mar/Apr 2004.

Chapter 3
Experimental Platform Setup

3.1 Introduction

For validating the different sensorless control algorithms, an experimental platform is setup in the department of energy technology at Aalborg University. Figure 3.1 shows the block diagram of the platform. A Surface-Mounted Permanent Magnet Synchronous Machine is used as the test machine. The SMPMSM is connected to a DC machine which is used as the load motor. The load machine is connected to a DC power supply with a manual control switch. The test machine is supplied by a Voltage Source Inverter. The rotor position and speed of the test machine are obtained from an encoder, and the currents on the test machine stator are sampled by three Hall transducers. The rotor position information and the measured currents will then be sent into the DSP controller, and then the three-phase PWM switching signals are calculated by the real-time control algorithm inside the DSP. For real-time monitoring the variables inside the DSP, a D/A module is used to export the data to the oscilloscope. The phase currents of the test machine are also shown in the scope. An USB/JTAG cable is applied for the communication between the computer and the DSP controller.

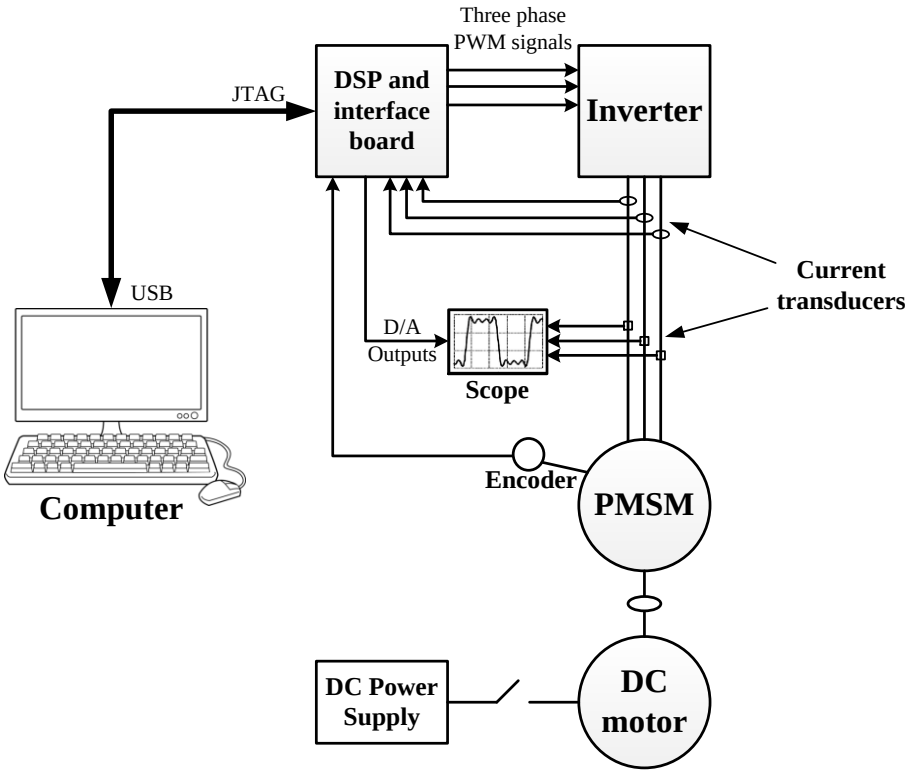

Figure 3.1: Diagram of the experimental platform setup.

3.2 Permanent magnet synchronous machine

Figure 3.2 and Figure 3.3 show the picture of the permanent magnet synchronous machine used as the test motor and the nameplate of the machine. This SEM company made machine has two pole pairs, the maximum voltage and current are 260 V and 16 A respectively, other machine parameters are listed in Table 3.1.

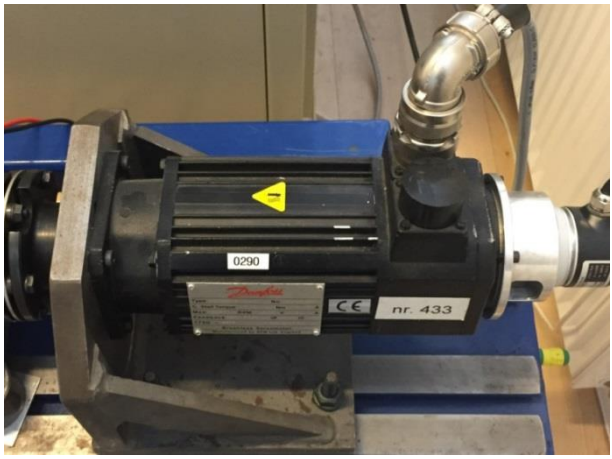

Figure 3.2: Picture of PMSM.

Figure 3.3: Nameplate of PMSM.

Table 3.1

Parameters of SMPMSM	
Rated power [W]	470
Max. phase voltage [V]	380
Rated current [A]	2.9
Rated speed [rpm]	2850
Rated frequency [Hz]	95

Rated torque [Nm]	1.58
Stator resistance [Ω]	2.35
d-axis inductance [mH]	10
q-axis inductance [mH]	15.4
PM flux linkage [Wb.turns]	0.132
Pole pairs	2

3.3 Load machine

As shown in Figure 3.4, a single phase DC shunt machine is used as the load machine. A DC power supply and a manual control switch are connected to the DC machine as the load system. The load drive system can provide both continue and step load. The nameplate of the DC machine is shown in Figure 3.5. The machine parameters are listed in Table 3.2.

Figure 3.4: Picture of DC load machine.

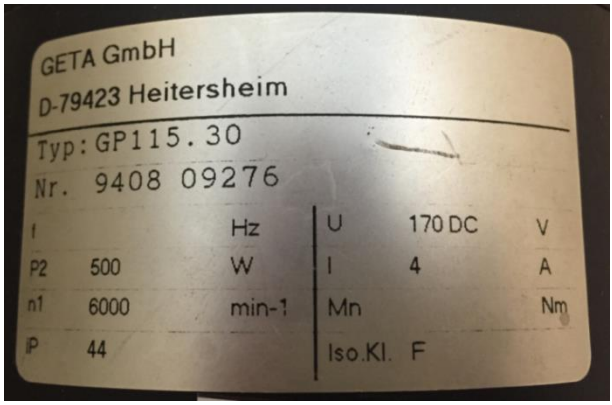

Figure 3.5: Nameplate of DC load machine.

Table 3.2

Parameters of Load DC machine	
Rated power [W]	500
Rated DC voltage [V]	170
Rated current [A]	4
Rated speed [rpm]	6000

3.4 Drive system

3.4.1 Inverter

Figure 3.6 shows the inverter made by Danfoss Power Electronics A/S, the model is FC302 series automation drive. Figure 3.7 shows the nameplate of the inverter. The inverter is controlled by an interface board which uses optical fibers for the three-phase gate signal inputs. The interface board can also provide different choices for the dead-time setup, from 2μs to 4 μs, as shown in Figure 3.8.

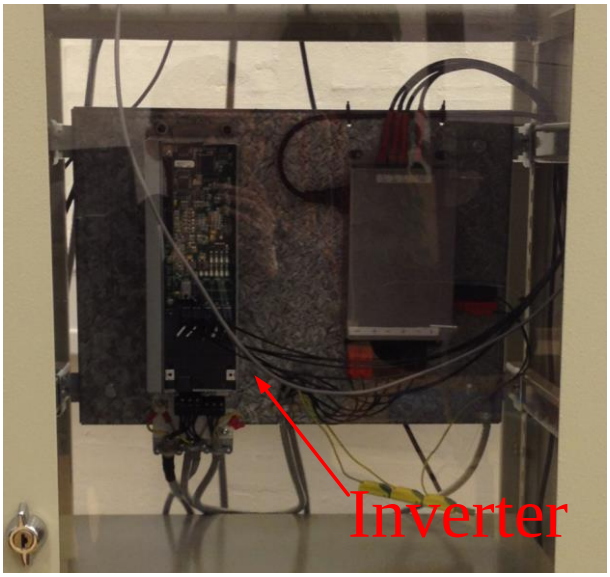

Figure 3.6: Picture of inverter.

Figure 3.7: Nameplate of inverter.

Figure 3.8: Picture of inverter interface board.

3.4.2 DSP controller

As shown in Figure 3.9, a TMS320F28335 DSP control board is used for implementing the control methods and providing the PWM signals for the inverter. The interface board is designed for receiving the electric signal inputs and sending the optical signal outputs.

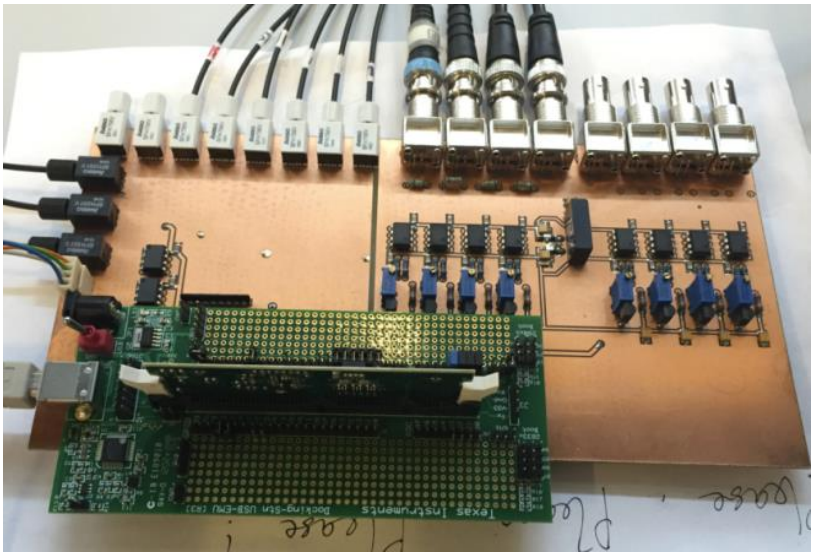

Figure 3.9: Picture of DSP controller and interface board.

3.4.3 Measurement equipment

Figure 3.10 and Figure 3.11 show the current transducers used for the current measurement and the encoder used for obtaining the real rotor position and speed. The current transducers use LA 55-P LEM made as the model. The encoder model is 2R2048-D-2M-S, which has 2048 pulses.

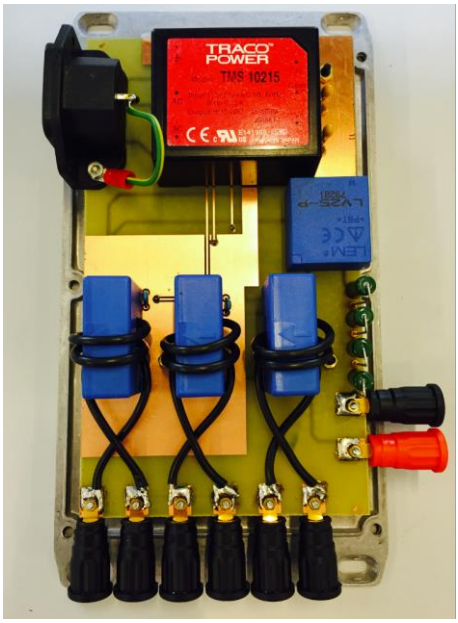

Figure 3.10: Picture of current transducers.

Figure 3.11: Picture of encoder.

Due to the current transducer introduces a background noise into the sample, a hardware filter for obtaining a clear and accurate current signal is needed. As shown in Figure 3.12, a RC filter is connected between DSP pin and the LEM module output. Then the background noise will be significantly reduced. The cutoff frequency of the

filter is set around 200 kHz, the resistance is chosen as 683 Ω, the capacitance is 1 nF. Figure 3.13 shows the performance of the hardware RC filter. With the filter, the sampled current ripple decreases from ±0.02 A to ±0.005 A.

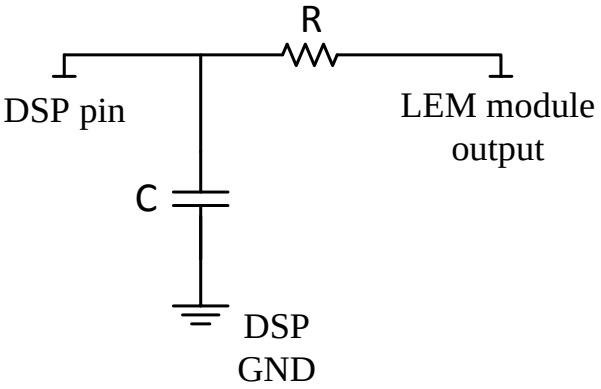

Figure 3.12: Topology of RC filter.

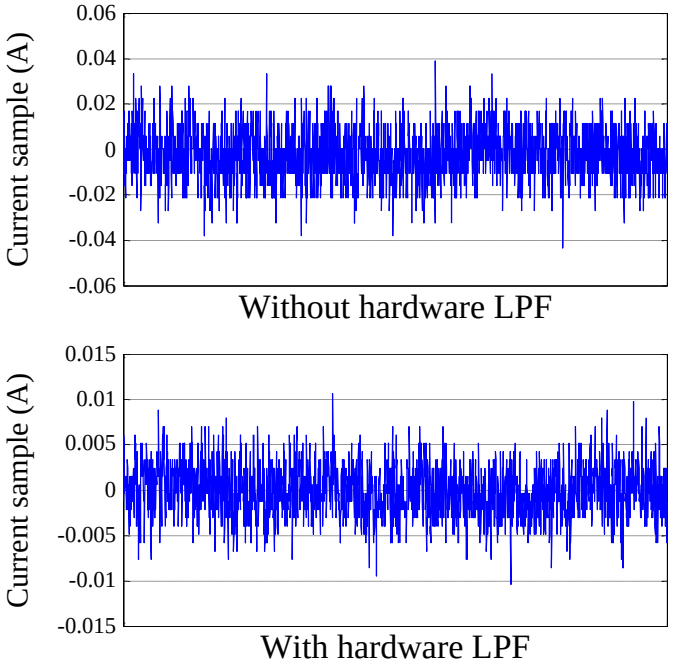

Figure 3.13: Performance of RC filter.

3.5 Summary

This chapter has introduced the hardware platform for the experiment. The inverter and the test machine are setup well, and a hardware filter is designed for obtaining the better current sample signal.

Chapter 4

Inverter Voltage Error Analysis and Compensation

4.1 Introduction

In the Pulse Width Modulation (PWM) controlled Voltage Source Inverter (VSI), the dead-time, the switching time delay and other nonlinear switch characteristics may distort the output voltage. In most of the sensorless drive systems, there is no voltage sensors used for measuring the terminal voltage on the machine. When the sensorless control algorithm is based on the voltage injection scheme, the inverter voltage error may affect the rotor position estimation especially in the low speed operation range for sensorless controlled motor drives. Therefore, various effective inverter nonlinear voltage error compensation methods have been studied and proposed to improve the performance of sensorless drives [1], [2]. This chapter analyzes the nonlinear inverter voltage error and indicates the complicated nature of accurate inverter voltage error compensation.

4.2 Principle of inverter voltage error generation

4.2.1 Dead-time voltage error

To avoid the shoot through fault of IGBT on the same leg of inverter, the gate signal for driving the IGBT has to set up a dead-time [3]. In this way, one of the IGBTs on the same leg can be safely turned off before turning on the other IGBT. This brings the main component of the inverter voltage error.

Figure 4.1 shows the dead-time effect on the single phase. As shown in Figure 4.1(b), compared with the voltage command, the gate signal has a delay when the switch turns on, which is called dead-time. It has different consequences on the output inverter voltage depending on the current direction. When the current on the single phase is positive, the voltage error ΔV is deducted from the output voltage V_{AN}; when the current becomes negative, the voltage error ΔV is added to the output voltage.

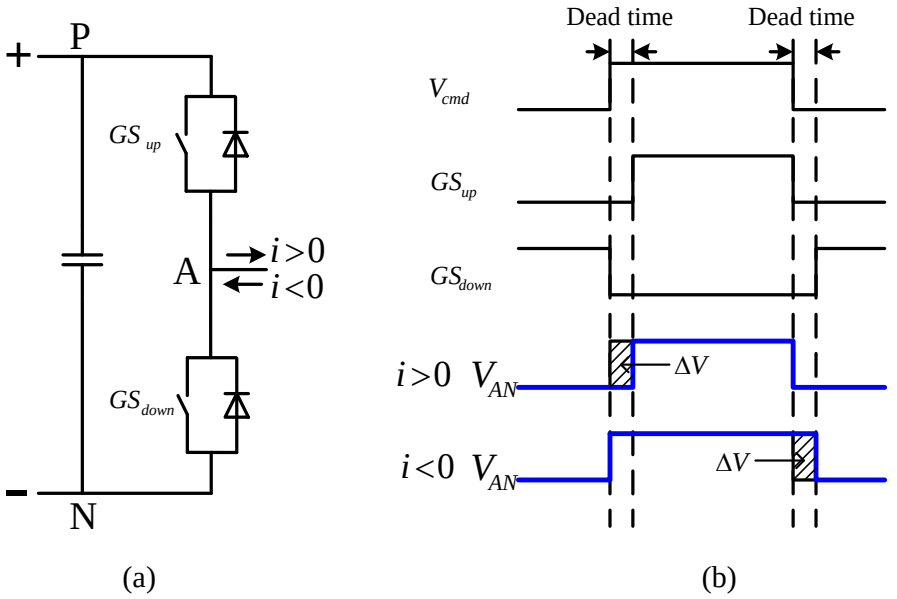

Figure 4.1: Dead-time voltage error on the single phase.

4.2.2 Nonlinear voltage error

Theoretically, the phase voltage switching edge should be ideally sharp before and after the dead-time, as shown in Figure 4.1(b). However, the fact is that the turn on and turn off of power switch cannot be infinitely fast and the phase voltage cannot change instantly either. Because of the characteristic of the IGBT, the real output voltage in each PWM cycle changes with a slope, especially when additional snubber capacitor is added [4]. When trying to turn off a switch that is with the IGBT conducting, the switching off action ideally will immediately change the conducting status of that leg causing the output voltage to change. But due to the snubber capacitor, even though the

IGBT is off, the current will charge the parallel capacitor. The voltage cannot step down immediately, but instead, will change slowly [4].

Figure 4.2 shows the nonlinear voltage error considering the parasitic and snubber capacitance. Compared to Figure 4.1(b), when the current is positive, the output voltage cannot step down from the DC link voltage to zero, but with a slope. The gray area is nonlinear voltage error caused by the parasitic capacitance. When the phase current is negative, the output voltage cannot increase step from zero to V_{DC}, the output voltage will increase gradually with a slope. The gray area in Figure 4.2 for e.g. $i > 0$ will actually compensate the voltage loss caused by the dead-time, as shown in the red dotted box. As a consequence, the total voltage error over one switching period is reduced compared to Figure 4.1(b). When the phase current becomes smaller, during the same time interval, the snubber capacitor voltage variation due to this small charging current will become smaller and the voltage error due to dead-time can be largely compensated, as shown in Figure 4.3. As expected, when the current approaches zero, the inverter voltage error will also approach zero even the constant dead-time is always present [5], [6].

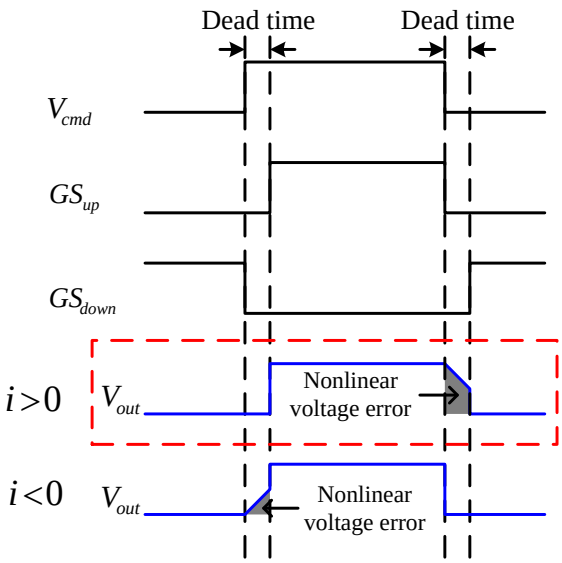

Figure 4.2: Nonlinear voltage error with the parasitic and snubber capacitance.

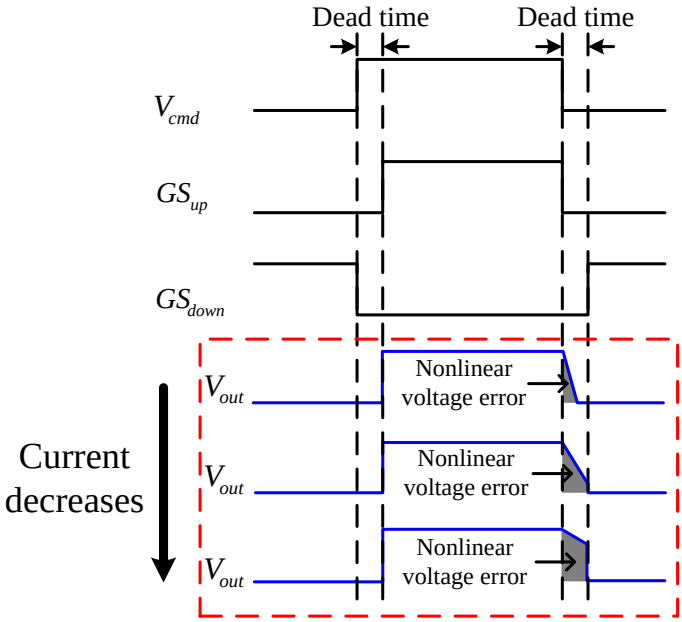

Figure 4.3: Nonlinear voltage error under different currents.

In different inverters, the switch characteristics may be different from each other, and the dead-time may also be set to be different values [6], [7]. Therefore, the inverter voltage error needs to be measured practically and then be well compensated. Many compensation algorithms for the inverter nonlinear voltage error have been studied in [8]-[10].

4.3 Inverter voltage error experimental determination

4.3.1 Single phase voltage error measurement

Assuming that the voltage errors on the three-phase bridges of the inverter are the same, it may be easy to obtain the inverter voltage error on a single phase. For measuring the nonlinear inverter voltage error on a single phase, a RL load is connected between phase A output and the negative terminal of the DC-link capacitor, as shown in Figure 4.4. In this case, the currents of phase B and C are both 0. The output voltage is regulated by controlling the duty cycle of phase A. The DC-link voltage of the inverter is 550 V, the switching frequency is 10 kHz, and the dead-time is set to be 2 μs.

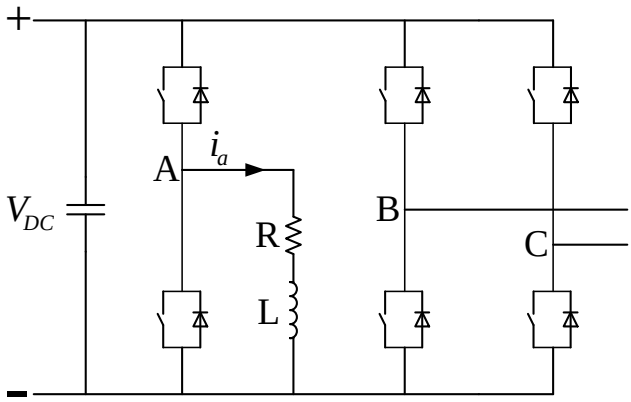

Figure 4.4: Topology for measuring the voltage error on the single phase of the inverter (without currents on the other two phases).

Figure 4.5 shows the measurement result of the inverter nonlinear voltage error on a single phase of the inverter. For this test inverter, when current on the single phase is smaller than 1.2 A, the voltage error is in the nonlinear zone. When the phase current is greater than 1.2 A, the voltage error becomes linear and proportional to the current. In this linear zone, the switch may be seen as a pure resistance representing switch internal resistive voltage drop, the similar result is given in [5], [7].

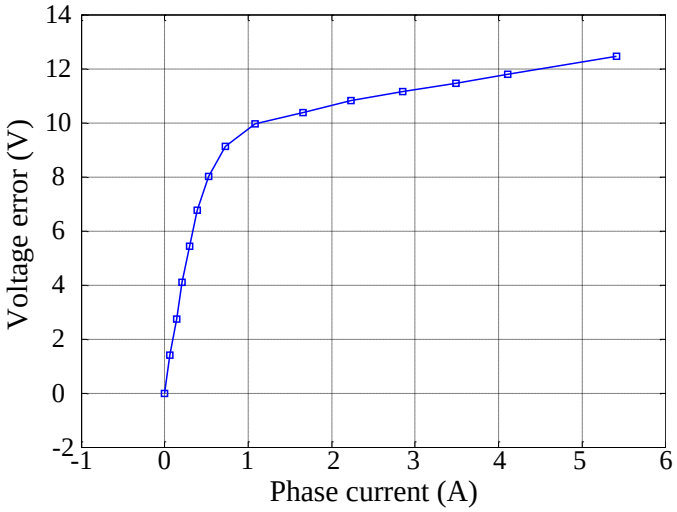

Figure 4.5: Measured voltage error on the single phase of the inverter.

4.3.2 Three-phase voltage error measurement

However, since the inverter controls a three-phase PMSM, currents will be presented in all the three phases. The voltage error on the particular one phase may be affected by the currents on the other two phases. To demonstrate this phenomenon, the test of Figure 4.5 is repeated with non-zero currents on phase B and phase C. To achieve this, the inverter is connected to a three-phase load as shown in Figure 4.6. The magnitude of the voltage vector and its orientation are changed and the currents on the three phases will change correspondingly. The inverter voltage error for phase A is then recorded.

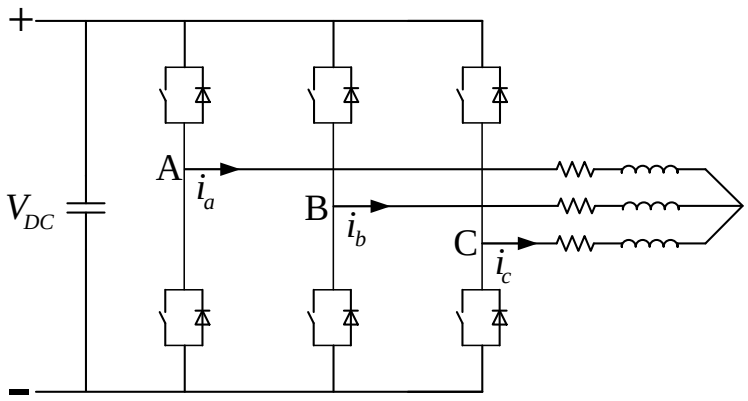

Figure 4.6: Topology for measuring the voltage error on the single phase of the inverter (with currents on the other two phases).

Figure 4.7 shows the measured single phase inverter voltage error for phase A. In Figure 4.7, when the phase angle of the voltage vector is changed from -20 to 20 degrees (0 degree is the phase a-axis), the inverter voltage error on phase A has different characteristics. Different phase B and C currents have a clear influence on the phase A inverter voltage error. Because of this influence, compensating three-phase inverter voltage errors at the same time will be much more complicated. This also indicates that many other inverter voltage error measurement methods (e.g. [6]) which measure only one single phase voltage error might not be accurate enough.

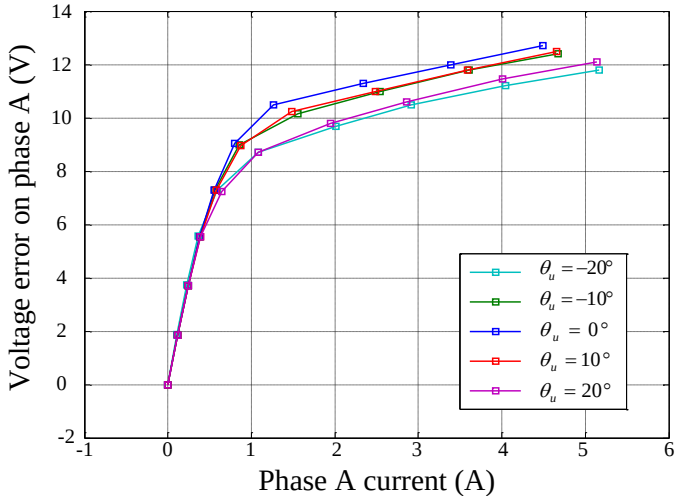

Figure 4.7: Measured voltage error on the phase A influenced by phase angle of voltage vector.

Figure 4.8 and Figure 4.9 show the three-phase currents when the machine is operating at no-load condition. The test machine is controlled by an open-loop rotating voltage vector command. The magnitude and the frequency of the voltage command are constant (V/f control), and then the PMSM works at the constant synchronous speed. As shown in Figure 4.8, the frequency of the voltage command is 0.5 Hz, and the magnitude of the voltage is set to be 4.7 V. At this low frequency, the machine phase resistance of 2.35 Ω will be predominant. Therefore, the amplitude of the current should be near 2 A. However, the amplitude of the measured current is around 0.3 A only, and there is an apparent distortion when the current is close to zero, as shown in Figure 4.8. Figure 4.9 shows the result of the same experiment, but the magnitude of the voltage command increases to 9.4 V. The ideal three-phase currents should be near to 4 A, but the actual amplitude of the currents is around 0.75 A only. The inverter voltage error will bring non-legible output voltage error at low voltage outputs and its effects should be compensated.

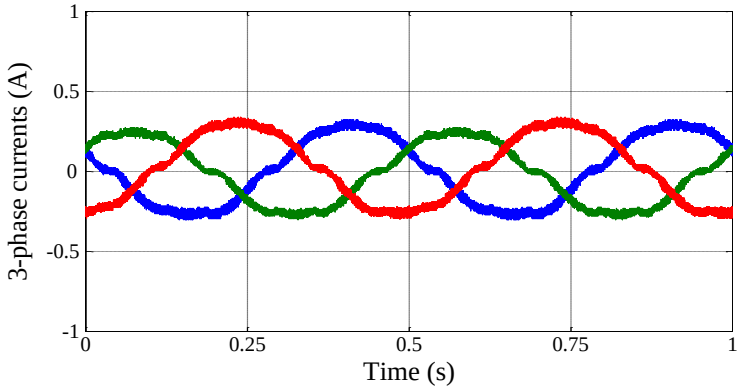

Figure 4.8: Three phase currents with the rotating voltage vector (the desired current magnitude is 2 A).

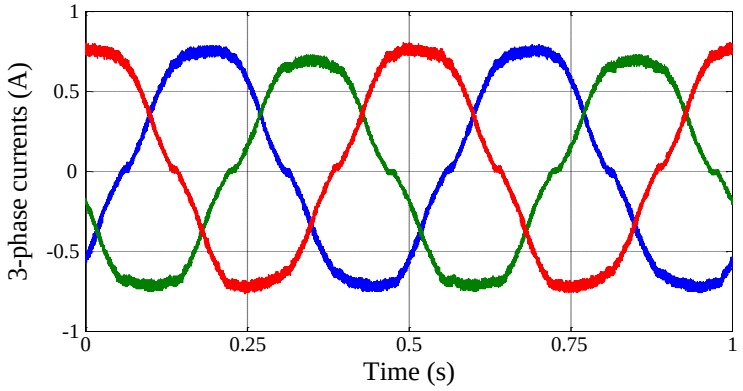

Figure 4.9: Three phase currents with the rotating voltage vector (the desired current magnitude is 4 A).

4.4 Compensation method implementation

4.4.1 Dead-time compensation

According to Figure 4.1, the voltage error caused by the dead-time is assumed to be constant. Therefore, a constant voltage component should be compensated on each single phase. The sign of the compensated voltage depends on the current polarity. The compensation strategy can be described as:

$$\begin{cases} V_{a\_com}^{*} = V_{a}^{*} + \Delta V & (i_a > 0) \\ V_{a\_com}^{*} = V_{a}^{*} - \Delta V & (i_a < 0) \\ V_{b\_com}^{*} = V_{b}^{*} + \Delta V & (i_b > 0) \\ V_{b\_com}^{*} = V_{b}^{*} - \Delta V & (i_b < 0) \\ V_{c\_com}^{*} = V_{c}^{*} + \Delta V & (i_c > 0) \\ V_{c\_com}^{*} = V_{c}^{*} - \Delta V & (i_c < 0) \end{cases} \tag{4.1}$$

where V_a^*, V_b^*, V_c^* are the voltage commands on the three phases; $V_{a\_com}^*$, $V_{b\_com}^*$, $V_{c\_com}^*$ are the voltage commands with the compensation; ΔV is the dead-time voltage error, which can be calculated by:

$$\Delta V = V_{DC} \frac{T_{dead-time}}{T_s} \tag{4.2}$$

Figure 4.10 and Figure 4.11 show the three-phase currents with constant dead-time voltage error compensation. The machine still operates with open-loop V/f control, but the voltage commands are adjusted according to equation (4.1). The machine operates at 0.5 Hz and the desired magnitudes of the voltage on the three phases are the same as before, i.e. 4.7 V and 9.4 V respectively. In this experiment, the switching period is set as 100 μs, and the dead-time is 2 μs. The voltage on the DC link is around 550 V, so the dead-time voltage error can be calculated by (4.2), which gives 11 V and is larger than the desired output magnitudes.

The maximum desired phase voltage command is 4.7 V, but the compensation voltage is 11 V. This may lead to the current on one single phase is always higher than zero, as the red line shown in Figure 4.10. This is because when the phase current is positive, the compensation voltage will be chosen as +11 V according to (4.1); and then this +11 V voltage clams the current to be always higher than zero. Three-phase currents have clear nonzero offsets and this is not a desired operation condition.

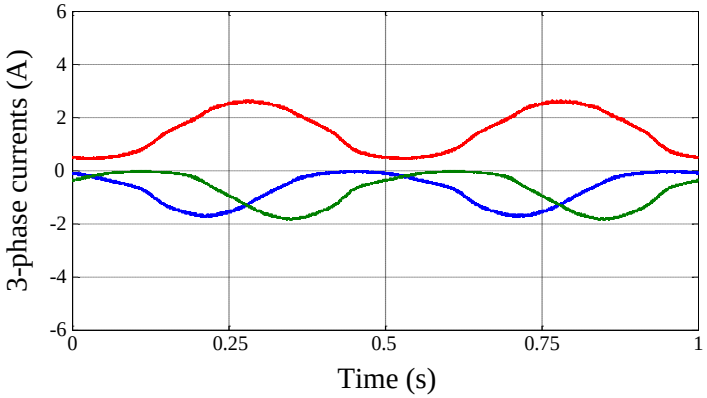

Figure 4.10: Three-phase currents with the dead-time voltage compensation (the desired current magnitude is 2 A).

However, when the magnitude of the voltage command increases to 9.4 V, the compensation voltage cannot keep the current always higher than zero. The three-phase currents become those as Figure 4.11. There is a step transition in the current in each 60 degrees electrical angle. This is because when the current experiences zero-crossing, the compensation voltage will introduce a step change from +11 V to -11 V (or from -11 V to 11 V). So the current has a nearly step change correspondingly. These results illustrate that constant dead-time voltage error compensation has bad performance at low output voltage commands.

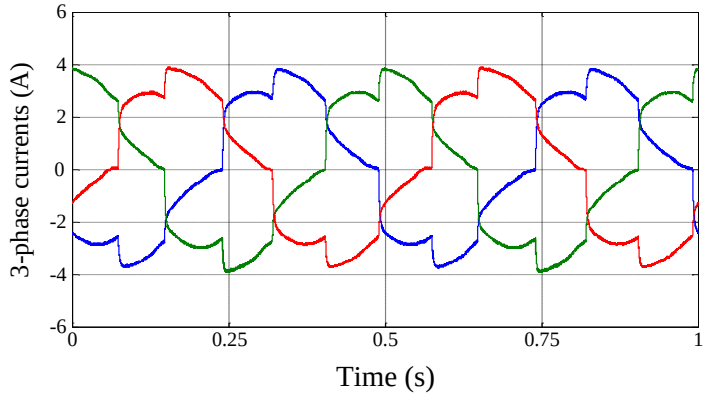

Figure 4.11: Three-phase currents with the dead-time voltage compensation (the desired current magnitude is 4 A).

4.4.2 Voltage error curve fitting based compensation

As discussed above, the constant dead-time voltage error compensation brings many problems such as highly distorted phase current waveforms. And in extreme cases, the current polarity cannot be controlled. Therefore, a compensation algorithm considering snubber capacitor effects which reduces the dead-time inverter voltage error when current reduces is necessary. Figure 4.5 shows the actual nonlinear voltage error profile of the test inverter. As a straight forward solution, this voltage error curve can be fitted as a look-up table. Once the phase current is measured, the compensation voltage may then be determined by using this off-line measured table.

Figure 4.12 shows the topology when the look-up table compensation method is used on the single phase of the inverter. In this experiment, the phase A and C of the machine are connected to the phase A output of the inverter and negative terminal of the DC-link capacitor as an RL load. A sinusoidal voltage command is given to phase A of the inverter.

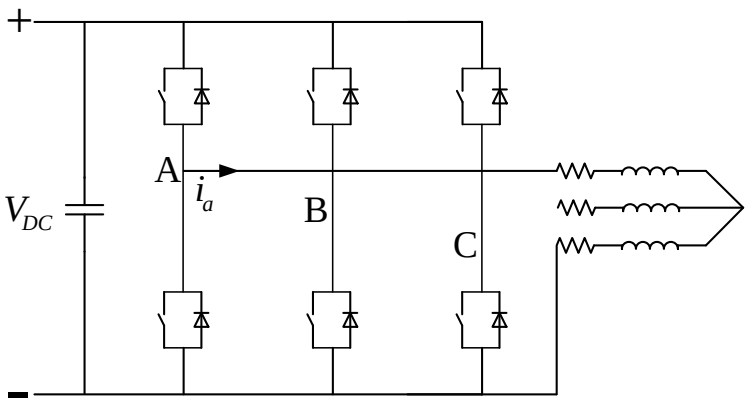

Figure 4.12: Topology for the single phase compensation.

Figure 4.13 and Figure 4.14 show the experimental results when the inverter voltage error is compensated using the measured nonlinear voltage error curve on a single phase. Figure 4.13 shows the result when the magnitude of the voltage command is 9.4 V (the resistance of the load becomes 4.7 Ω which is twice as the machine phase

resistance 2.35 Ω) and the frequency is 0.5 Hz. The current waveform is very close to a sinusoidal signal, and the amplitude of the current is also close to the ideal value of 2 A. When the magnitude of the reference voltage increases from 9.4 V to 18.8 V, the current amplitude also increases from 2 A to 4 A as well, as shown in Figure 4.14. The results shown in Figure 4.13 and 4.14 prove that by using a look-up table searching the measured nonlinear voltage error curve, the inverter voltage error can be accurately compensated on a single phase.

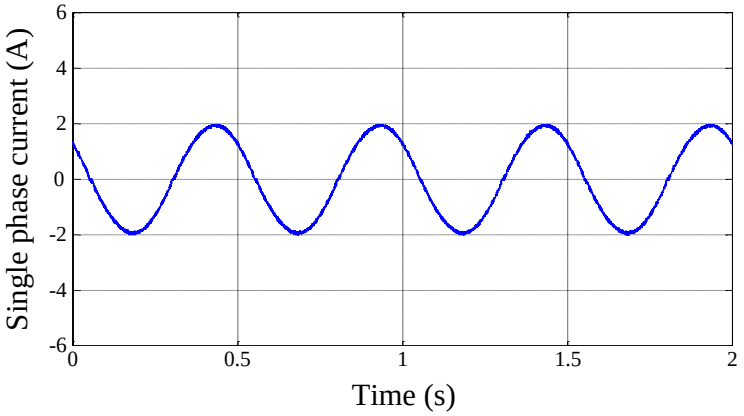

Figure 4.13: Single phase current with the look-up table compensation (the desired current magnitude is 2 A).

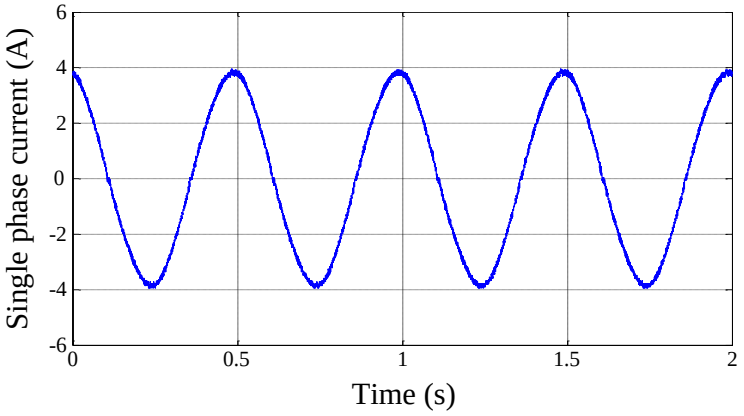

Figure 4.14: Single phase current with the look-up table compensation (the desired current magnitude is 4 A).

Ideally, when this look-up table method is used for all three phases, the rotating voltage vector command should also be able to provide a good sinusoidal three-phase currents waveform. However, Figure 4.15 and 4.16 show that the three-phase currents still have quite visible distortions when this method is applied for three-phase inverter legs. This distortion in the current may be caused by the voltage error which has been introduced in Figure 4.7.

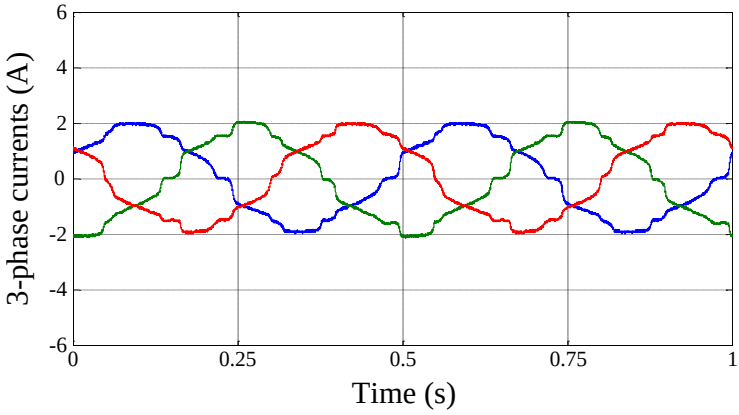

Figure 4.15: Three-phase currents with the look-up table compensation (the desired current magnitude is 2 A).

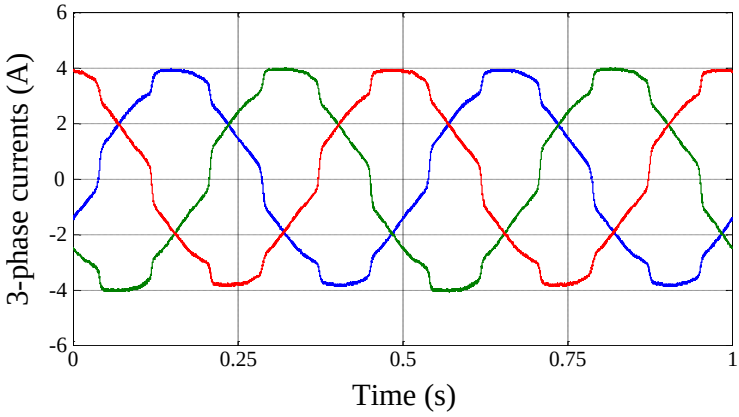

Figure 4.16: Three-phase currents with the look-up table compensation (the desired current magnitude is 2 A).

4.4.3 Limitations of the compensation

In most of the DSP or dSPACE based control systems, the gate signal outputs have a switching period delay for the execution. This is illustrated in Figure 4.17. When the value of the switching counter is equal to 0 (the beginning of period 1), an PWM interrupt will be triggered and the current will be sampled as i_0. Using this measured current, the FOC algorithm will be executed and a new the voltage command will be calculated during switching period 1. This voltage command V_1^* will be loaded to the DSP register at the time when the switching counter is equal to 1 (the beginning of period 2). This means the voltage command will be implemented in the next switching period 2. Similarly, the compensation value for the voltage error which depends on the current i_0 will be calculated in period 1, and used in period 2. However, at the beginning of period 2, the current may change to i_1. The compensation used in period 2 will then be incorrect since it is calculated based on i_0. This may bring an extra error for the previously discussed voltage error compensation method.

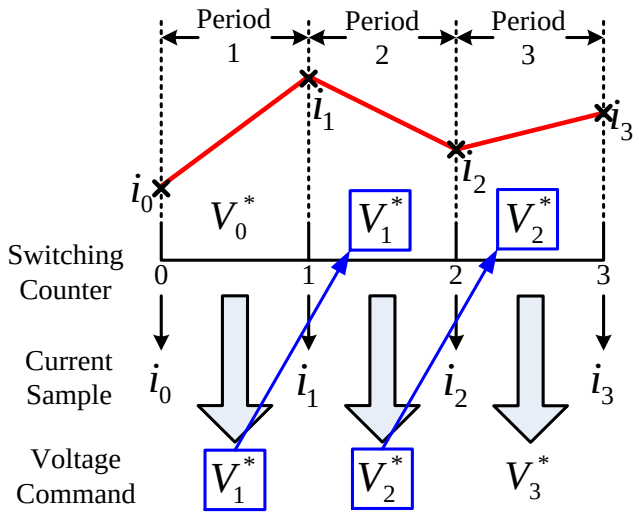

Figure 4.17: Diagram of the voltage command delay.

The nonlinear inverter voltage error is always related to the phase current. The measured current will bring a background noise into the control system. This will affect the accuracy of the compensation especially near zero-crossing. In the voltage injection based methods, the injected voltage may cause a big variation in the phase current within one switching period. Therefore, the compensation may have a big error due to the time delay in digital implementation as discussed above.

4.5 Summary

The inverter voltage error has been presented in this chapter. The dead-time effect causes the main error in the output voltage. The IGBT characteristic and the parasite capacitance also bring a distortion into the output voltage. These reasons cause the nonlinear voltage error in the inverter output voltage.

For determining the inverter voltage error, the experimental measurements have been done both on the single phase and three phases of the inverter. The experimental results illustrated that the current on one single phase would affect the voltage error on the other two phases. This makes the compensation for all the three phases becomes very complex.

This chapter has also compared two different nonlinear voltage error compensation strategies. When the constant dead-time voltage error was used as the compensation value, the output voltage may have an unexpected step change when the current is near zero. Therefore, the voltage error curve fitting based look-up table method was tested in the test platform. The test results shown that this look-up table method can greatly compensate the voltage error on the single phase. However, when the method was used for three phases of the inverter, the output voltage will have a small distortion because of the slight change on the voltage error curve which was affected by the currents on the other phases. Other limitations of the nonlinear voltage compensation have also been discussed at the end of the chapter. Due to the complexity of compensating the inverter nonlinear voltage error accurately, it is preferred to find an implementation method that can avoid generation large inverter voltage error (as will be presented in

chapter 6), or an algorithm that can minimize the voltage error effects in estimating the rotor position (as will be presented in chapter 7).

Bibliography

[1] Y. Inoue, K. Yamada, S. Morimoto, M. Sanada, "Effectiveness of Voltage Error Compensation and Parameter Identification for Model-Based Sensorless Control of IPMSM," *IEEE Transactions on Industry Applications*, vol. 45, no. 1, pp. 213-221, Jan/Feb 2009.

[2] W. Sun, Y. Yu, G. L. Wang, D. G. Xu, "Accurate Inverter Error Compensation Using Self-Tuning Stator Current Estimation Error in Sensorless Induction Motor Drives," *IEEE Industry Applications Society Annual Meeting*, pp. 1-6, Oct 2014.

[3] Y. Murai, A. Riyanto, H. Nakamura, K. Matsui, "PWM Strategy for High Frequency Carrier inverters Eliminating Current-Clamps during Switching Dead-Time," *IEEE Industry Applications Society Annual Meeting*, vol.1, pp. 317-322, Oct 1992.

[4] Z. D. Zhang, L. Y. Xu, "Dead-Time Compensation of Inverters Considering Snubber and Parasitic Capacitance," *IEEE Transaction on Power Electronics*, vol. 29, no. 6, pp. 3179-3187, Jun 2014.

[5] A. R. Weber, G. Steiner, "An Accurate Identification and Compensation Method for Nonlinear Inverter Characteristics for AC Motor Drives," *IEEE International Instrumentation and Measurement Technology Conference*, pp. 821-826, May 2012.

[6] I. R. Bojoi, E. Armando, G. Pellegrino, S. G. Rosu, "Self-commissioning of inverter nonlinear effects in AC drives," *2nd IEEE ENERGYCON Conference & Exhibition*, pp. 213-218, Sep 2012.

[7] G. Pellegrino, R. I. Bojoi, P. Guglielmi, F. Cupertino, "Accurate Inverter Error Compensation and Related Self-Commissioning Scheme in Sensorless Induction

Motor Drives," *IEEE Transaction on Industry Applications*, vol. 46, no. 5, pp. 1970-1978, Sep/Oct 2010.

[8] G. Pellegrino, P. Guglielmi, E. Armando, I. R. Bojoi, "Self-Commissioning Algorithm for Inverter Non-Linearity Compensation in Sensorless Induction Motor Drives," *Industry Applications Society Annual Meeting*, pp. 1-7, Oct 2008.

[9] J. Holtz, J. Quan, "Sensorless Vector Control of Induction Motors at Very Low Speed Using a Nonlinear Inverter Model and Parameter Identification," *IEEE Transactions on Industry Applications*, vol. 38, no. 4, pp. 1087-1095, Jul/Aug 2002.

[10] D.H. Lee, J. W. Ahn, "A Simple and Direct Dead-Time Effect Compensation Scheme in PWM-VSI," *IEEE Transactions on Industry Applications*, vol. 50, no. 5, pp. 3017-3025, Sep/Oct 2014.

Chapter 5
INFORM Method and Improvements

5.1 Introduction

In traditional sensorless control methods, back-EMF based methods cannot be used in very low speed range and standstill [1], and the machine parameters have to be involved in the estimation [2], [3]. High frequency sinusoidal signal injection based methods bring the Low-Pass-filters (LPFs) and Band-Pass-Filters (BPFs) into the drive system [4], [5], which may lower the performance of the control system. Therefore, different types of voltage pulse injection methods for obtaining the rotor position have been investigated and developed in the last decades [6], [7]. Being different from the traditional high frequency steady state voltage injection method, voltage pulse injection based methods have attracting advantages like the elimination of band-pass filter or low-pass filters in the control system. The INFORM (Indirect Flux detection by On-line Reactance Measurements) method is a classical voltage pulses injection based method which was introduced in 1992 [8]. In the INFORM method, the current variations caused by the injection voltages are directly used for estimating the rotor position. The machine parameters will not be involved in the calculation. Therefore, the INFORM method is one kind of parameter independent sensorless control method. However, since the current variations are the only variables used for the estimation, the accuracy of the injected voltage vectors on the machine terminals may dramatically affect the performance of the estimation. To illustrate these effects, the performance of the original INFORM method is first presented in this chapter, and an improved INFORM implementation is proposed next. A further application: sector control which based on the INFORM method is also introduced.

5.2 INFORM method

5.2.1 Implementation of the INFORM method

The INFORM method is a classical rotor position estimation method which utilizes the saliency of the rotor. The basic idea of the INFORM method is to create desired current responses by injecting three test voltage pulses, and the rotor position is determined from measured current responses [9]. As shown in Figure 5.1, the voltage vectors with the constant magnitudes are injected on the a-, b-, and c-axes sequentially after the normal PWM command reserved for the PI controllers used in FOC. The currents are sampled at the beginning of each switching period, and the current variations in the αβ-reference frame may then be determined by the currents sampled before and after the injection periods.

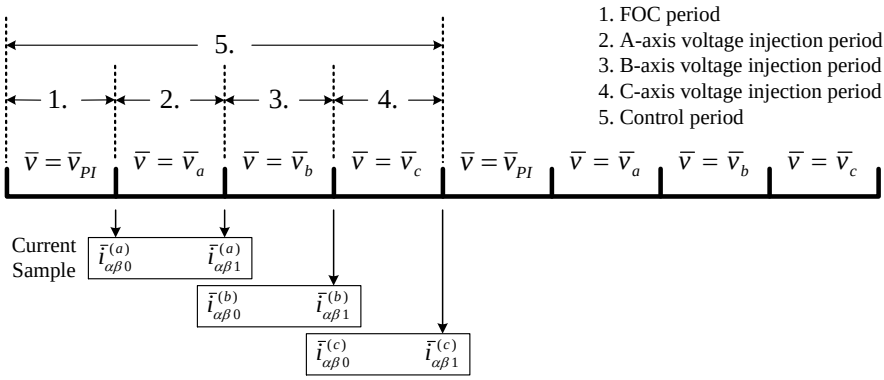

Figure 5.1: Voltage injection scheme of INFORM method in implementation.

5.2.2 Mathematical analysis of the INFORM method

As discussed in section 2.3.2, Since the INFORM method is usually used in the low speed range sensorless control for PMSM, the voltage equation in the αβ-reference frame may be represented as:

$$\bar{v}_{\alpha\beta} = R\bar{i}_{\alpha\beta} + L_1 \frac{d}{dt}\bar{i}_{\alpha\beta} + L_2 \frac{d}{dt}\bar{i}^{*}_{\alpha\beta} e^{j2\theta_r} \tag{5.1}$$

where $L_1 = \frac{L_d + L_q}{2}$, $L_2 = \frac{L_d - L_q}{2}$, $\bar{i}^*_{\alpha\beta}$ is the conjugate vector of $\bar{i}_{\alpha\beta}$. When the injection voltage $\bar{v}_{\alpha\beta} >> R\bar{i}_{\alpha\beta}$, (5.1) may be simplified to:

$$\bar{v}_{\alpha\beta} = L_1 \frac{d}{dt}\bar{i}_{\alpha\beta} + L_2 \frac{d}{dt}\bar{i}^*_{\alpha\beta} e^{j2\theta_r} \tag{5.2}$$

Solving (5.2) for $\frac{d}{dt}\bar{i}_{\alpha\beta}$, it may be obtained that:

$$\frac{d}{dt}\bar{i}_{\alpha\beta} = \frac{1}{L_1^2 - L_2^2}\left(L_1\bar{v}_{\alpha\beta} + L_2\bar{v}^*_{\alpha\beta} e^{j2\theta_r}\right) \tag{5.3}$$

where $\bar{v}^*_{\alpha\beta}$ is the conjugate vector of $\bar{v}_{\alpha\beta}$. In a short period (e.g. one switching period), $\frac{di}{dt}$ may be approximated by $\frac{\Delta i}{\Delta t}$. Therefore, (5.3) may then be written in the classical INFORM form as [9]:

$$\Delta\bar{i}_{\alpha\beta} = \left(c_1 + c_2 e^{j2(\theta_r - \theta_u)}\right)\Delta t\bar{v}_{\alpha\beta} \tag{5.4}$$

where, $c_1 = \frac{L_1}{L_1^2 - L_2^2}$, $c_2 = \frac{-L_2}{L_1^2 - L_2^2}$, θ_u is the voltage vector angle in the αβ-reference frame, and $\bar{v}_{\alpha\beta} = V_m e^{j\theta_u}$. As shown in Figure 5.1, $\Delta\bar{i}_{\alpha\beta}$ can be calculated by $\Delta\bar{i}_{\alpha\beta} = \bar{i}_{\alpha\beta 1} - \bar{i}_{\alpha\beta 0}$ for each injection period.

When the test voltage pulses are sequentially injected on the phase a-, b-, c-axes, the injection voltages may be represented as: $\bar{V}_{\alpha\beta 1} = V_m e^{j0}$, $\bar{V}_{\alpha\beta 2} = V_m e^{j\frac{2\pi}{3}}$, $\bar{V}_{\alpha\beta 3} = V_m e^{j\frac{4\pi}{3}}$ respectively. Then (5.4) gives:

$$\Delta\bar{i}^{(a)}_{\alpha\beta} = \bar{i}^{(a)}_{\alpha\beta 1} - \bar{i}^{(a)}_{\alpha\beta 0} = \left(c_1 + c_2 e^{j2\theta_r}\right)\Delta t V_m \tag{5.5}$$

$$\Delta\bar{i}^{(b)}_{\alpha\beta} = \bar{i}^{(b)}_{\alpha\beta 1} - \bar{i}^{(b)}_{\alpha\beta 0} = \left(c_1 + c_2 e^{j2\left(\theta_r - \frac{2\pi}{3}\right)}\right)\Delta t V_m e^{j\frac{2\pi}{3}} \tag{5.6}$$

$$\Delta\bar{i}_{\alpha\beta}^{(c)} = \bar{i}_{\alpha\beta 1}^{(c)} - \bar{i}_{\alpha\beta 0}^{(c)} = \left(c_1 + c_2 e^{j2\left(\theta_r - \frac{4\pi}{3}\right)} \right) \Delta t V_m e^{j\frac{4\pi}{3}} \tag{5.7}$$

Equations (5.5), (5.6), (5.7) may be combined in a vector form as:

$$\Gamma = \Delta\bar{i}_{\alpha\beta}^{(a)} + \Delta\bar{i}_{\alpha\beta}^{(b)} e^{j\frac{2\pi}{3}} + \Delta\bar{i}_{\alpha\beta}^{(c)} e^{j\frac{4\pi}{3}} = 3c_2 V_m e^{j2\theta_r} \Delta t \tag{5.8}$$

where the rotor position θ_r may then be estimated by:

$$\theta_r = \frac{1}{2} \arg \Gamma \tag{5.9}$$

5.3 Simulation and experimental analysis

5.3.1 Simulation results

The INFORM method is first implemented in a simulation model which is built in Matlab/Simulink. The machine parameters use the actual values of the test PM machine. The switching frequency is set as 10k Hz which is the same as the value used in the experiment.

Figure 5.2 shows the machine module in the simulation system, where the voltage equations of the stator in the dq-reference frame and the electromagnetic torque equation are used in the model.

Figure 5.3 shows the FOC module designed in the system, where the d-axis current reference is set to be 0. The PI controllers for i_d and i_q are designed for controlling the current loops; the PI controller for speed is used for controlling the speed loop.

Figure 5.4 shows the voltage selector module. In this voltage selector, a counter is set 1 to 4 sequentially as a cycle, and the magnitude of the injection voltage is set as 30 V. The voltage outputs and the counter value are shown in Figure 5.5. When counter value is equal to 1, the voltage output is chosen as the voltage command from the FOC module; when the counter counts from 2 to 4, the output voltages are aligned with phase a-, b-, and c- respectively. As shown in the bottom row in Figure 5.5, the blue

line shows the voltage command on the α-axis, and the red line shows the β-axis voltage command.

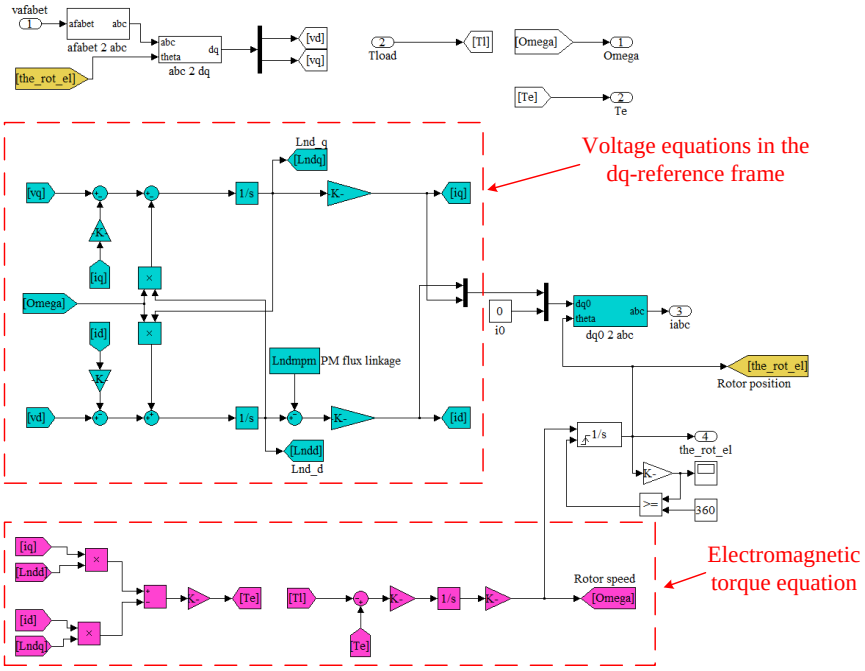

Figure 5.2: Diagram of PMSM simulation model.

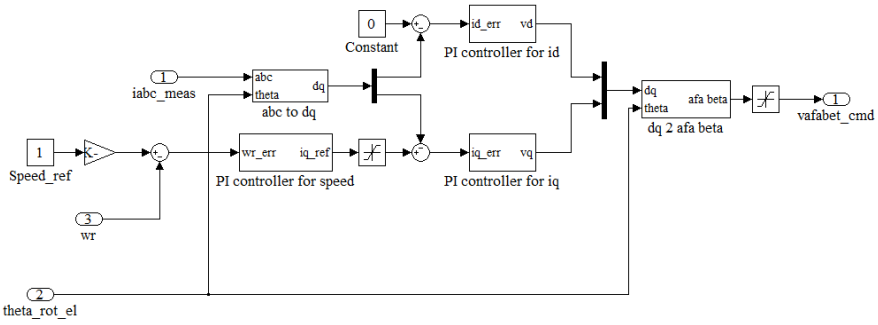

Figure 5.3: Diagram of FOC simulation module.

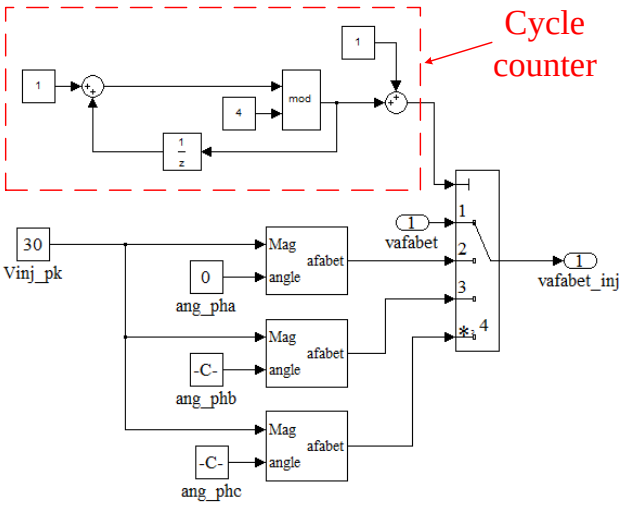

Figure 5.4: Diagram of output voltage selector.

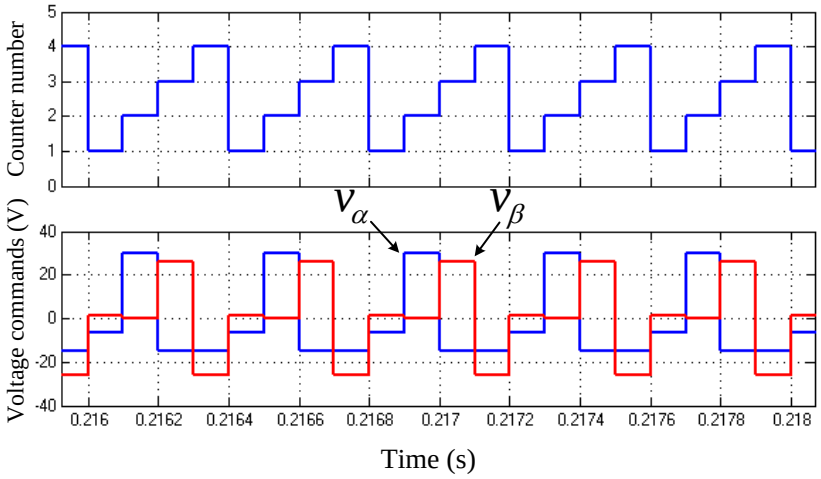

Figure 5.5: Counter signal and voltage commands outputs from the selector.

Figure 5.6 shows the simulation results when the INFORM method is implemented in the simulation FOC system. In this simulation, the PI parameters for the current controller are turned as: $K_p = 70$, $K_i = 20000$; the values for the speed controller are maintained as: $K_p = 2$, $K_i = 30$. The reference speed in the system is set to be 15 rpm. The estimated rotor position is used as the feedback for decoupling the stator currents. As shown in Figure 5.6, the injection voltage brings the ripple into the current, since the magnitude of the injection voltage vector is 30 V, the corresponding current ripple is around ±0.3 A in the d- and q-axes currents. A -0.3 degrees DC bias in the estimated rotor position is caused by the back-EMF which was also neglected in (6.1). This is evident from observed results that when the rotor speed decreases, this DC bias will reduce correspondingly. In the simulation, the estimated rotor position will not be affected by the step load. The INFORM algorithm provides a good performance both in transient and steady state.

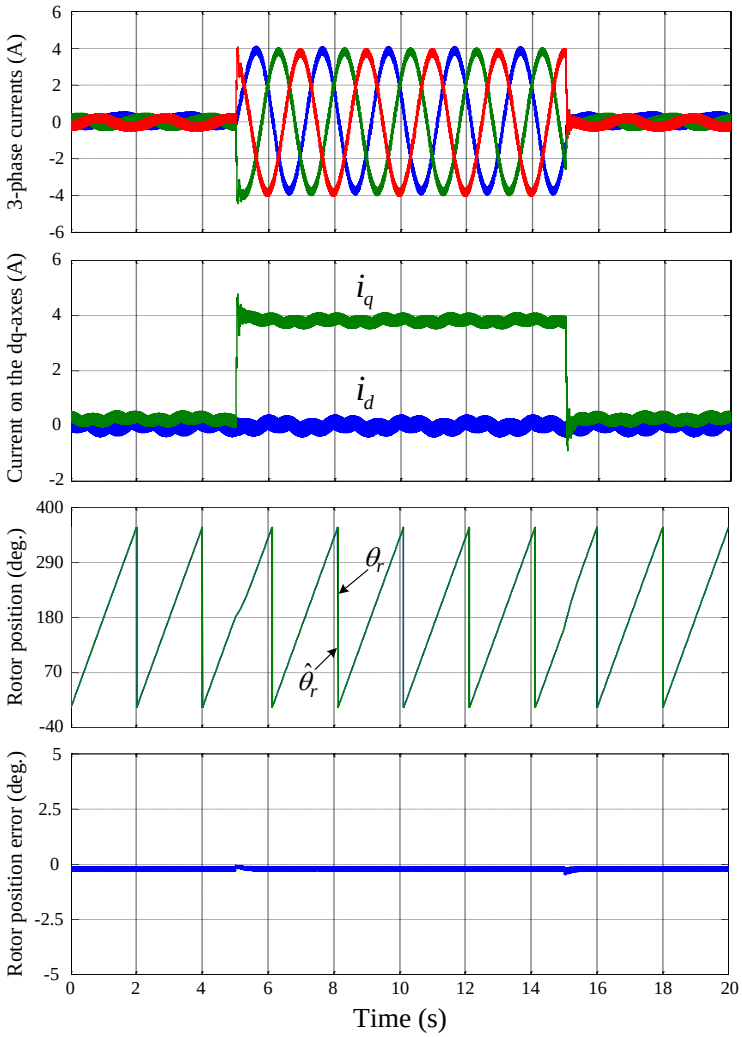

Figure 5.6: Simulation results of INFORM method with 90% rated torque step at 15 rpm.

5.3.2 Experimental results

When the INFORM method is implemented in the practical experimental drive system, the system performance and the estimated rotor position are shown in Figure 5.7. In the experiment, the PI parameters for the current loop and speed loop are set to be same as the value used in the simulation: $K_p = 70$, $K_i = 20000$ and $K_p = 2$, $K_i = 30$ respectively. The real rotor position and speed from the encoder are used as the feedbacks. Considering with the dead-time voltage error, the magnitude of injection voltage vector is set to be 50 V. The reference speed is set to be 15 rpm, which is the same as the value in the simulation.

Compared with the simulation results shown in Figure 5.6, Figure 5.7 shows the experimental results that the current ripple on the q-axis increases to ±0.5 A with load. The ripple in the estimated rotor position is ±10 degrees without the load and ±16 degrees with the 90% rated load. A -15 degrees DC bias appears when the load is applied on the machine, which means the real rotor position delays the estimated one by 15 degrees when the machine works with load. The enlarged fluctuation and DC bias in the estimated rotor position may be both caused by the inverter voltage error. The inverter voltage error may affect the magnitude and location of the injected voltage vector. For minimizing this extra disturbance by the inaccuracy of the injection voltage, the inverter voltage error needs to be well compensated.

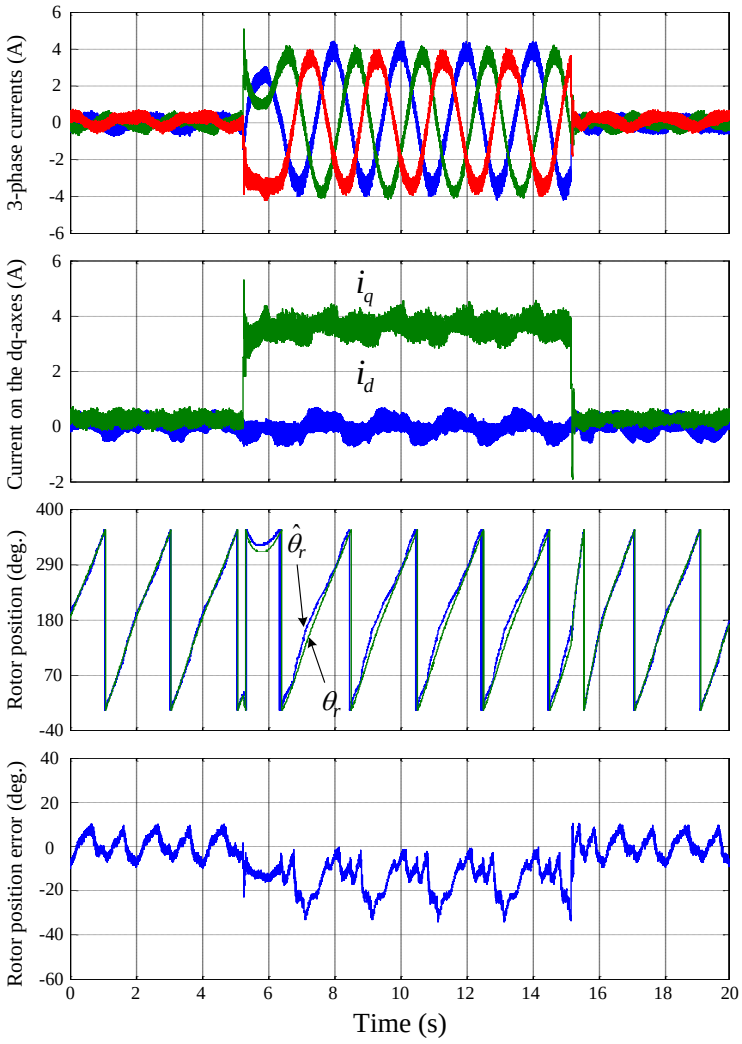

Figure 5.7: Experimental results of INFORM method with 90% rated torque step at 15 rpm.

5.4 Improved INFORM method

5.4.1 Implementation in drive system

In the INFORM method, the voltage pulses are injected sequentially on the stator three-phase axes. In the standard Space-Vector PWM modulation, the duty cycles for generating three test voltage pulses are illustrated as Figure 5.8. The ideal duty cycle is shown with the dotted lines. In the first voltage injection period, the voltage vector is applied on the a-axis. The duty cycles of the voltage commands are set to be larger than 50% for phase A, smaller than 50% and with the same duty ratio for both phase B and C. However, the phase currents may be different when the machine operates at different conditions. The resultant voltage error for each phase may be different, as indicated with the solid lines in Figure 5.8. As discussed in chapter 4, the nonlinear voltage error on the single phase may be also affected by the currents on the other two phases. Therefore, compensating the voltage error for all three phases at the same time is very difficult, especially when the currents may not be measured precisely.

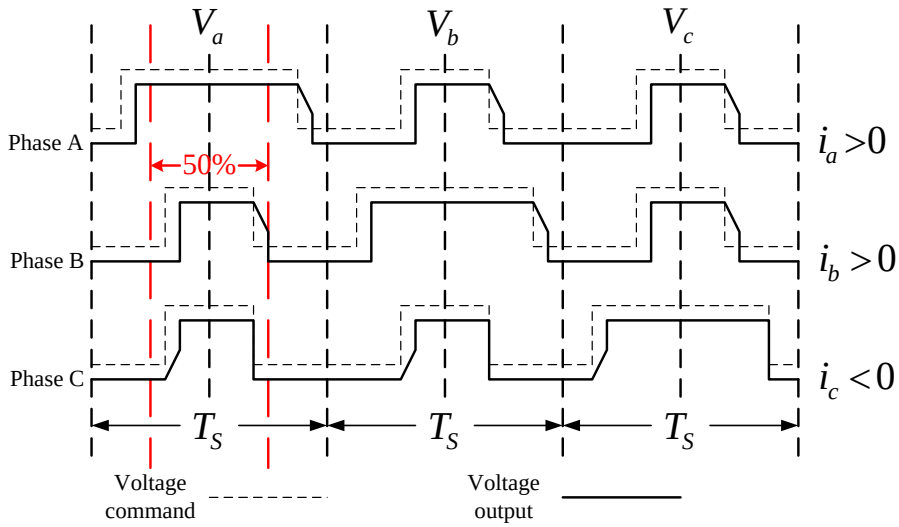

Figure 5.8: Traditional Space-Vector PWM outputs for injection voltage vectors.

As shown in Figure 5.9, For suppressing the nonlinear voltage error existing in different phases, the duty cycles of two phases may be forced to be 0, when these two phases are not aligned to the injection axis. When the voltage is injected on the a-axis,

the duty cycles on the phase B and C are both set to be 0, and the duty cycle on the phase A becomes $D_a^{(proposed)} = D_a^{(traditional)} - D_b^{(traditional)}$. Ideally, there will be no voltage outputs on phase B and C, and then the resultant voltage vector will be on the desired a-axis. Compared with Figure 5.8, in the first injection period, the voltage error on the phase B and C are eliminated. The voltage compensation may need to be implemented on the phase A only.

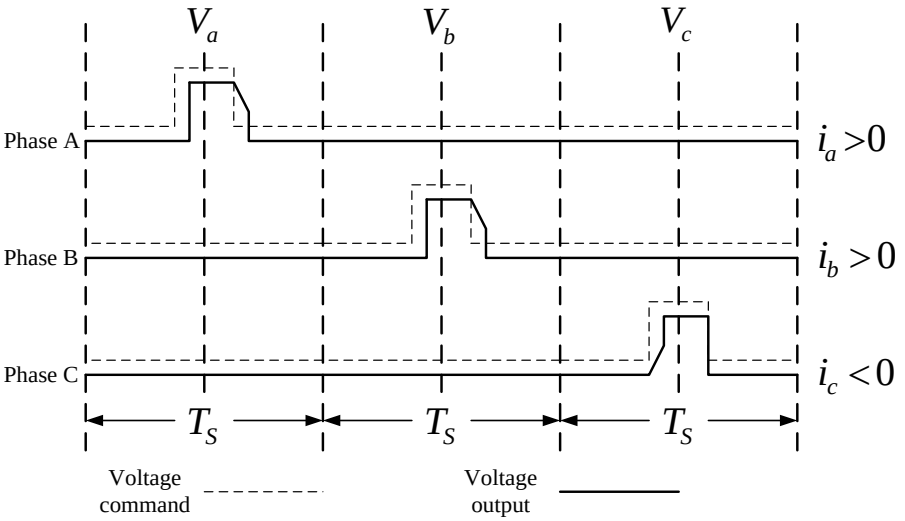

Figure 5.9: Optimized Space-Vector PWM outputs for injection voltage vectors.

As discussed in chapter 4.2, the nonlinear voltage error of the inverter used in the experimental platform has been determined as shown in Figure 4.4. Therefore, the voltage error needs to be compensated on one single phase with the curve shown in Figure 4.4 in each injection periods only. The limitation mentioned in chapter 4.3.3 can be also avoided by the 0% duty cycle. E.g. the compensation on the phase B, in Figure 5.9, the current sample at the beginning of first switching period (V_a period) will be used for calculating the compensation voltage for the second switching period (V_b period). The voltage output on the phase B in the first switching period is 0. Therefore, the current on the phase B will change slowly, and then the compensation voltage will

not significantly change during the first switching period. The compensation error caused by the DSP implementation delay may then be minimized.

5.4.2 Experimental results with improved SVPWM

Figure 5.10 shows the result when the improved SVPWM algorithm (shown as Figure 5.9) is applied in the system, but the inverter voltage error is not compensated. Compared with Figure 5.7, the currents with these two different SVPWM algorithms have similar profiles. The estimated position ripples is still large, which is ±10 degrees without the load and -15±17 degrees with the 90% rated load respectively. At no-load operation condition, the position error behaviors very similarly to Figure 5.7. This is because the small current causes the smaller voltage error, and the smaller voltage error brings less affect into the estimated rotor position. However, since the load is added on the machine, the inverter voltage error increases with the current. Different inverter voltage error associated to these two different SVPWM scheme results in different position error waveform for the same injection voltage vector. This comparison has clearly shown that the voltage vector injection based method is sensitive to the output voltage distortions.

It may be noticed that, the DC bias is still in the rotor position error when the load is applied on the machine, for both the standard and improved SVPWM algorithms. This DC bias is mainly due to that the inverter output voltage vector is not perfectly aligned with the desired axis during the injection periods, as illustrated in Figure 5.11. This may be validated by adjusting the original estimation algorithm (5.4) to:

$$\Delta\bar{i}_{\alpha\beta} = \left(c_1 + c_2 e^{j2(\theta_r - \theta_u - \Delta\theta)}\right)\Delta t\bar{V}_{\alpha\beta} \tag{5.10}$$

where a voltage vector drift angle $\Delta\theta$ (denoted in Figure 5.11) is used to indicate the right voltage vector location. The simulation model can easily confirm that the injection voltage drift angle causes the DC bias in the estimated rotor position. The voltage error angle may be compensated in the estimated rotor position. then equation (5.9) becomes:

$$\theta_r = \frac{1}{2}\arg\Gamma + \Delta\theta \tag{5.11}$$

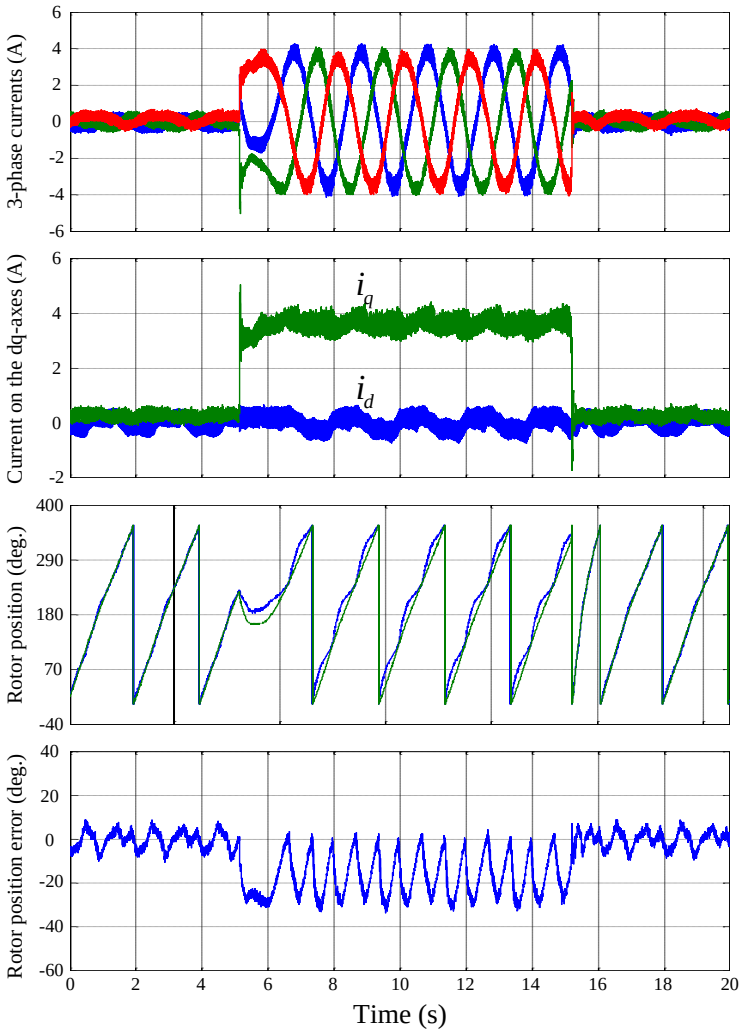

Figure 5.10: Experimental results of INFORM method with 90% rated torque step at 15 rpm (with optimized SVPWM algorithm).

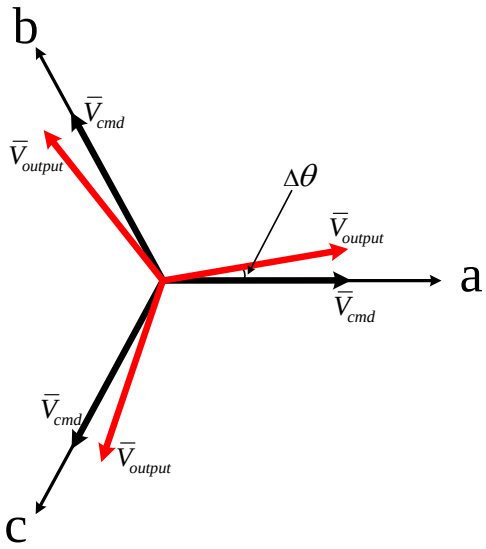

Figure 5.11: Diagram of command and actual output voltage vector.

Figure 5.12 shows the drive system performance when the voltage vector drift angle is compensated. This angle is found to be 6 degrees at the rated operation condition. The improved SVPWM is used for generating the injection voltage vectors. The machine operates at 15 rpm with the real rotor position and speed as the feedback. The ripple in the rotor position error is ±8 degrees without the load and ±18 degrees with the 90% rated load, which is close to the results shown in Figure 5.10. But the DC bias in the position error is now removed. The reason for the voltage vector drifting away from the desired axis might be due to extra voltage disturbances e.g. the conducting voltage drops of the IGBT and diode voltage losses contributed from phase B and C.

Figure 5.13 shows the experimental results of the INFORM method when the nonlinear inverter voltage error is compensated. In this experiment, the improved SVPWM implementation is applied. The single phase inverter voltage error is also compensated by the measured curve fitted look-up table during the injection periods. Compared with the results shown in Figure 5.12, the ripple in the estimated position is greatly reduced. The ripple in the estimated rotor position error maintains under ±10 degrees both with and without the load.

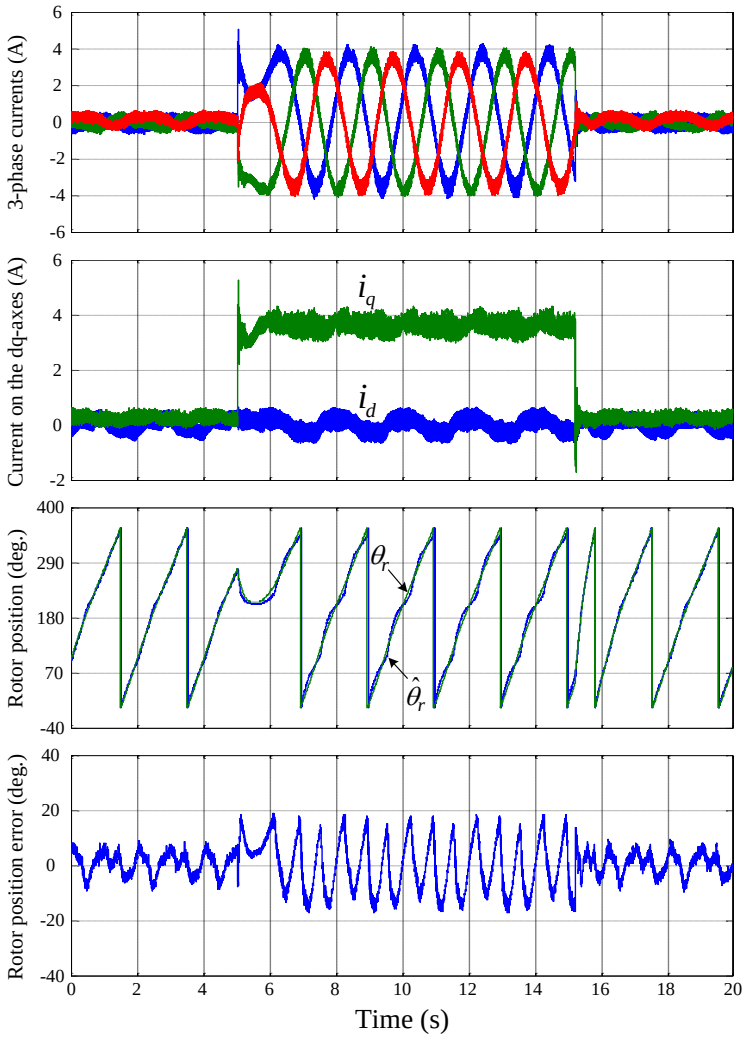

Figure 5.12: Experimental results of INFORM method with 90% rated torque step at 15 rpm (with voltage error angle compensation).

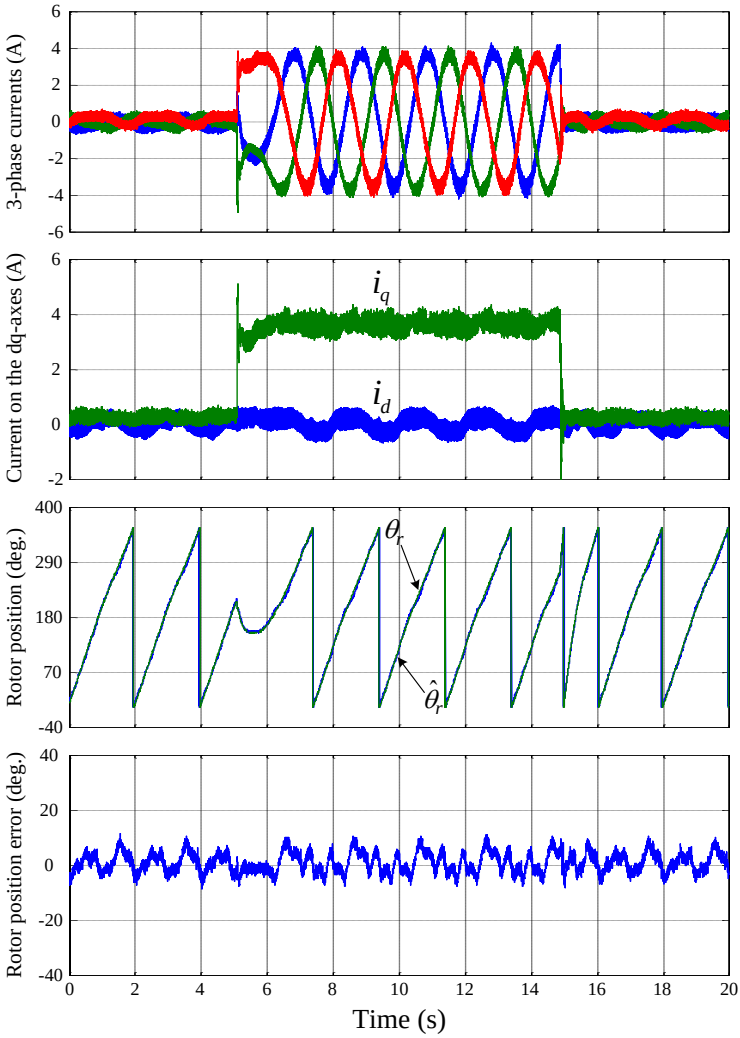

Figure 5.13: Experimental results of INFORM method with 90% rated torque step at 15 rpm (with voltage error angle and nonlinear voltage error compensation).

It can be demonstrated from the experimental results shown in Figure 5.13 that, the INFORM method may give satisfactory performances for the drive system. But it was also illustrated that this method is sensitive to different voltage errors which may cause the injection voltage vector drift away from the desired axes. This may result in DC bias in the estimated rotor position error. The inverter voltage error may bring a large ripple into the estimated rotor position and it must be compensated. The modified

SVPWM may require the inverter voltage error compensation to be implemented on one phase only in every injection period, this largely simplifies the compensation.

5.5 Sector estimation based on INFORM method

For obtaining a good system performance based on the INFORM method, the optimization and voltage compensation are very necessary and important. However, implementing the optimization and compensation is difficult and with limitations, e.g. the inverter voltage error cannot be measured precisely. Since the INFORM method highly depends on the current measurement accuracy, a sector estimation algorithm is proposed. The sector estimation method can be easily achieved by detecting the current polarity, and the value of the current becomes unnecessary. Thus, the problems caused by the current measurement can be simply avoided. In addition, this method may limit the maximum position error to ideally 15 degrees under any transient conditions. This could be useful to ensure a stable operation of the drive that is independent on load change conditions.

5.5.1 Mathematical analysis of the algorithm

The same as the INFORM method, the sector estimation method also uses the voltage injection scheme shown in Figure 5.1. Then equation (5.4) can be written as:

$$\Delta\bar{i}_{\alpha\beta} = \left(c_1 + c_2 e^{j2(\theta_r-\theta_u)}\right)\Delta t V_m e^{j\theta_u} \tag{5.12}$$

By multiplying $e^{-j\theta_u}$ on the both sides of (5.12), it may be derived that:

$$\Delta\bar{i}_{\alpha\beta} e^{-j\theta_u} = \left(c_1 + c_2 e^{j2(\theta_r-\theta_u)}\right)\Delta t V_m \tag{5.13}$$

$$\arg(\Delta\bar{i}_{\alpha\beta}) - \theta_u = \arg\left(c_1 + c_2 e^{j2(\theta_r-\theta_u)}\right) \tag{5.14}$$

The vector diagram for (5.14) is shown as Figure 5.14, it may be easy to notice that:

$$\arg(\Delta\bar{i}_{\alpha\beta}) - \theta_u > 0 \Rightarrow \theta_r - \theta_u \in \left(0, \frac{\pi}{2}\right) \cup \left(\pi, \frac{3\pi}{2}\right) \tag{5.15}$$

$$\arg(\Delta\bar{i}_{\alpha\beta}) - \theta_u < 0 \Rightarrow \theta_r - \theta_u \in \left(\frac{\pi}{2}, \pi\right) \cup \left(\frac{3\pi}{2}, 2\pi\right) \tag{5.16}$$

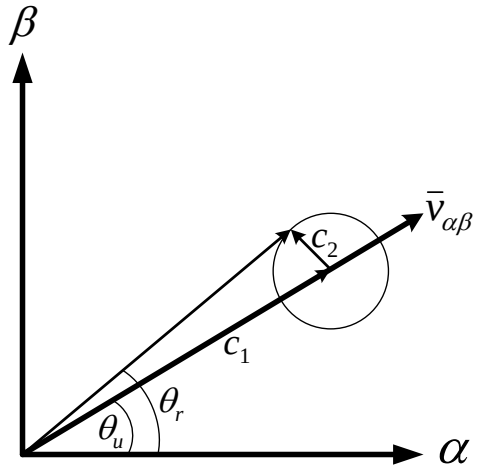

Figure 5.14: Diagram of injection voltage vector.

Since the three injection voltages are injected on the a-, b-, c-axes sequentially, the angle of the injection voltage θ_u will be 0, $\frac{2\pi}{3}$, $\frac{4\pi}{3}$ in these three injection periods. Then the left side of (5.14) can be defined as:

$$\arg(\Delta\bar{i}_{\alpha\beta1}^{(a)}) = \arg(\Delta\bar{i}_{\alpha\beta1}) - \theta_u = \arg(\Delta\bar{i}_{\alpha\beta1}) \tag{5.17}$$

$$\arg(\Delta\bar{i}_{\alpha\beta2}^{(b)}) = \arg(\Delta\bar{i}_{\alpha\beta2}) - \theta_u = \arg(\Delta\bar{i}_{\alpha\beta2}) - \frac{2\pi}{3} \tag{5.18}$$

$$\arg(\Delta\bar{i}_{\alpha\beta3}^{(c)}) = \arg(\Delta\bar{i}_{\alpha\beta3}) - \theta_u = \arg(\Delta\bar{i}_{\alpha\beta3}) - \frac{4\pi}{3} \tag{5.19}$$

By substituting (5.15) and (5.16), equation (5.17) gives:

$$\arg(\Delta\bar{i}_{\alpha\beta1}) > 0 \Rightarrow \theta_r \in \left(0, \frac{\pi}{2}\right) \cup \left(\pi, \frac{3\pi}{2}\right) \tag{5.20}$$

$$\arg(\Delta\bar{i}_{\alpha\beta1}) < 0 \Rightarrow \theta_r \in \left(\frac{\pi}{2}, \pi\right) \cup \left(\frac{3\pi}{2}, 2\pi\right) \tag{5.21}$$

Similarly, (5.18) and (5.19) give:

$$\arg(\Delta\bar{i}_{\alpha\beta2}^{(b)}) > 0 \Rightarrow \theta_r \in \left(0, \frac{\pi}{6}\right) \cup \left(\frac{2\pi}{3}, \frac{7\pi}{6}\right) \cup \left(\frac{5\pi}{3}, 2\pi\right) \tag{5.22}$$

$$\arg(\Delta\bar{i}_{\alpha\beta2}^{(b)}) < 0 \Rightarrow \theta_r \in \left(\frac{\pi}{6}, \frac{2\pi}{3}\right) \cup \left(\frac{7\pi}{6}, \frac{5\pi}{3}\right) \tag{5.23}$$

$$\arg(\Delta\bar{i}_{\alpha\beta3}^{(c)}) > 0 \Rightarrow \theta_r \in \left(\frac{\pi}{3}, \frac{5\pi}{6}\right) \cup \left(\frac{4\pi}{3}, \frac{11\pi}{6}\right) \tag{5.24}$$

$$\arg(\Delta\bar{i}_{\alpha\beta3}^{(c)}) < 0 \Rightarrow \theta_r \in \left(0, \frac{\pi}{3}\right) \cup \left(\frac{5\pi}{6}, \frac{4\pi}{3}\right) \cup \left(\frac{11\pi}{6}, 2\pi\right) \tag{5.25}$$

According to (5.20)~(5.25), the signs of $\arg(\Delta\bar{i}_{\alpha\beta1}^{(a)})$, $\arg(\Delta\bar{i}_{\alpha\beta2}^{(b)})$ and $\arg(\Delta\bar{i}_{\alpha\beta3}^{(c)})$ may confirm the rotor position in a 30 degrees sector, e.g. when $\arg(\Delta\bar{i}_{\alpha\beta1}) > 0$, $\arg(\Delta\bar{i}_{\alpha\beta2}^{(b)}) > 0$, and $\arg(\Delta\bar{i}_{\alpha\beta3}^{(c)}) < 0$, the rotor position will in $\left(0, \frac{\pi}{6}\right)$ or $\left(\pi, \frac{7\pi}{6}\right)$.

The vector plane can be divided into 12 average sectors, each sector is 30 degrees, as shown in Figure 5.15. In Figure 5.15, the rotor position may be located in 2 different sectors, and the angle between these 2 sectors is 180 degrees (e.g. $\left(0, \frac{\pi}{6}\right)$ or $\left(\pi, \frac{7\pi}{6}\right)$). Therefore, the polarity of the machine rotor needs to be determined, and then the rotor position may be located in the unique sector. The polarity detection is also necessary in the INFORM method.

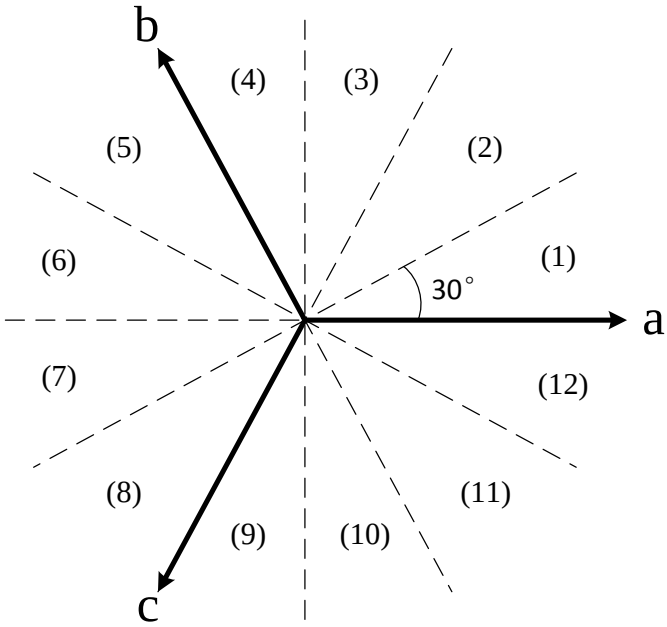

Figure 5.15: Sectors distribution in vector plane.

Table 5.1 shows the sectors corresponding to the signs of the current variation angles. Since the sector which the rotor position located in is known, the middle axis of each sector is used as the estimated rotor position. In this case, the rotor position error between the estimated rotor position and the real rotor position will be clamped under 15 degrees.

Table 5.1

Polarity	Sector	Rotor position angle (deg.)	Sign of $\arg(\Delta\bar{i}_{\alpha\beta1}^{(a)})$	Sign of $\arg(\Delta\bar{i}_{\alpha\beta2}^{(b)})$	Sign of $\arg(\Delta\bar{i}_{\alpha\beta3}^{(c)})$
Positive	1	(0, 30)	+	+	-
	2	(30, 60)	+	-	-
	3	(60, 90)	+	-	+
	4	(90, 120)	-	-	+
	5	(120, 150)	-	+	+
	6	(150, 180)	-	+	-

Negative	7	(180, 210)	+	+	-
	8	(210, 240)	+	-	-
	9	(240, 270)	+	-	+
	10	(270, 300)	-	-	+
	11	(300, 330)	-	+	+
	12	(330, 360)	-	+	-

5.5.2 Simulation results

The voltage injection scheme is implemented in the Matlab/Simulink model which is exactly the same as the one used in the INFORM method simulation. However, the rotor position estimation algorithm is changed to the sector estimation method. In this simulation, the machine reference speed is set to be 6 rpm. The magnitude of the injection voltage vector is 30 V. The real rotor position is used as the feedback for decoupling the stator currents. The PI parameters use the same values as in the INFORM method: $K_p = 70$, $K_i = 20000$ for the current controller; and $K_p = 2$, $K_i = 30$ for the speed controller. The simulation results are shown in Figure 5.16. Compared with the results shown in Figure 5.6, the currents of the machine stator have a similar profile. The estimated rotor position becomes constant while it is located in a single sector, and the estimated rotor position has a stair waveform with 12 steps when the rotor rotates for one cycle. The rotor position error is shown as a ±15 degrees saw-tooth waveform. The details of the rotor position are shown in Figure. 5.17.

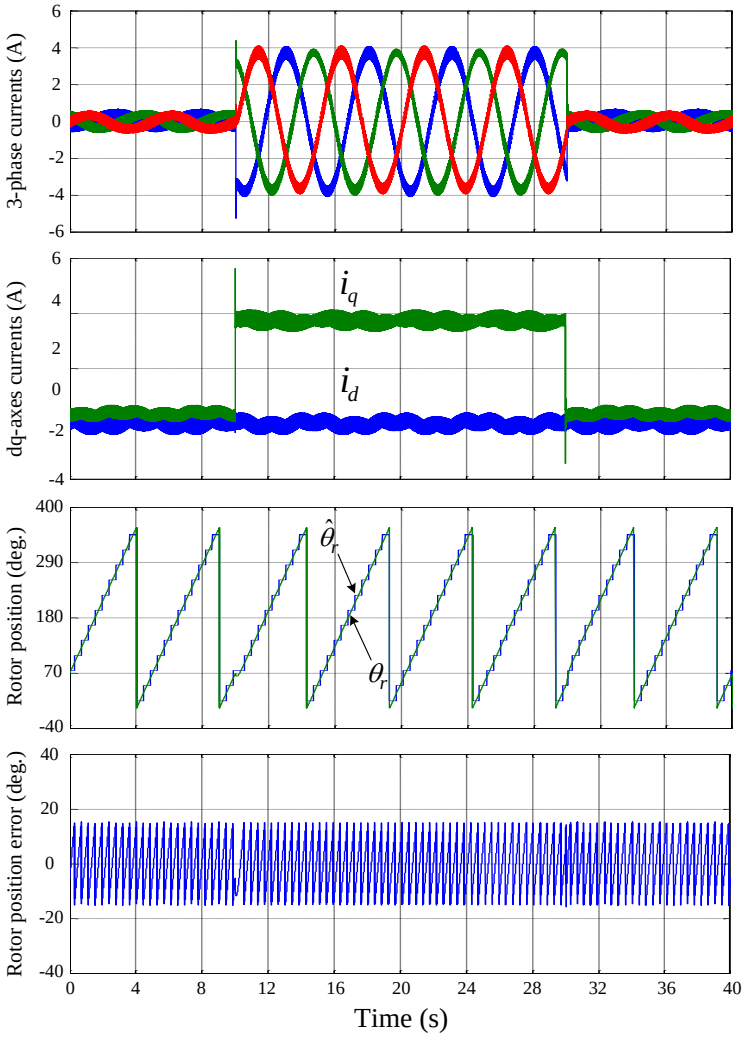

Figure 5.16: Simulation results of sector estimation method with 90% rated torque step at 6 rpm.

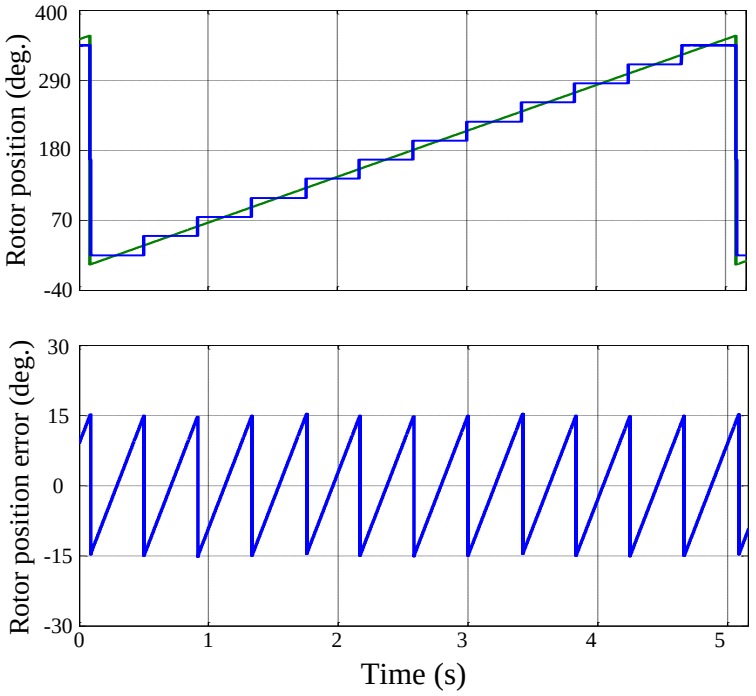

Figure 5.17: Simulation results of rotor position details.

5.5.3 Experimental results

The sector estimation algorithm is then tested in a FOC drive system with the real rotor position and speed as the feedback, and the machine operates at 6 rpm. There is no voltage error compensation to be applied in this experiment. Therefore, for reducing the effect of the dead-time voltage error, the magnitude of the injected voltage increases from 30 V to 50 V. Figure 5.18 shows the experimental results when the machine operates in the dynamic situation. Compared with the performance of the INFORM method shown in Figure 5.10, the ripple in the current increases with the injection voltage, the peak to peak values are 1 A in INFORM method with 30V injection voltage and 1.4 A in sector estimation method with 50V injection voltage respectively. When the 90% rated load is added on the machine, a -15 degrees DC bias appears in the position error, which is similar as the standard INFORM methods. The rotor position error increases from the theoretical ±15 degrees to around ±20 degrees when the load is applied on the machine.

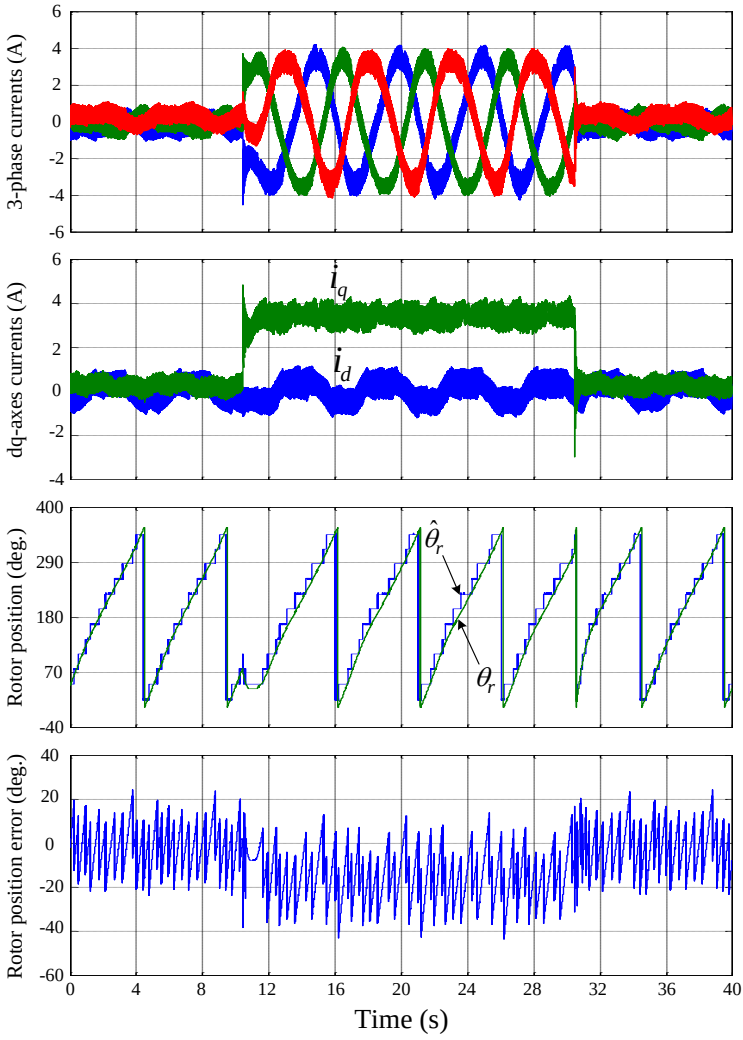

Figure 5.18: Experimental results of sector estimation method with 90% rated torque step at 6 rpm.

Figure 5.19 shows the details of the real and estimated rotor positions, and the position error between them when the machine operates at 6 rpm without the load. Consistent with the simulation, the estimated rotor position is a stair waveform. However, there is a fluctuation in the rotor position error, and this is caused by the inverter voltage error.

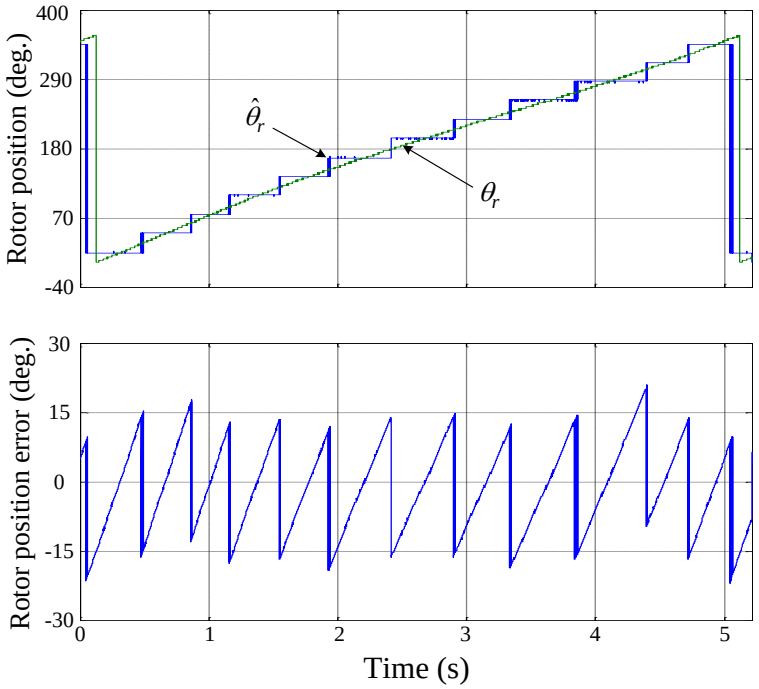

Figure 5.19: Experimental results of rotor position details.

Being different from the INFORM method, sector estimation method detects the sector where the rotor position located. However, middle axis of the sector is not the unique candidate for the estimated rotor position. The boundary of the sector may also be used as the estimated rotor position. When the machine is working with the rated load, the boundary where the sector begins may be chosen as the estimated rotor position (e.g. when the rotor position is detected in sector 1, the estimated rotor position is chose to be equal to 0 degree). Therefore, the DC bias in the rotor position error caused by the inverter voltage error may be compensated by the optimized selection of sector edge. Figure 5.20 shows the performance of the drive system with the axis selection optimization. The magnitude of the rotor position error is 30 degrees with no load and 40 degrees with 90% rated load respectively. The DC bias in the position error is mostly compensated. It may be observed from Figure 5.20 that the position error behaviors consistently during steady state or transient operation conditions.

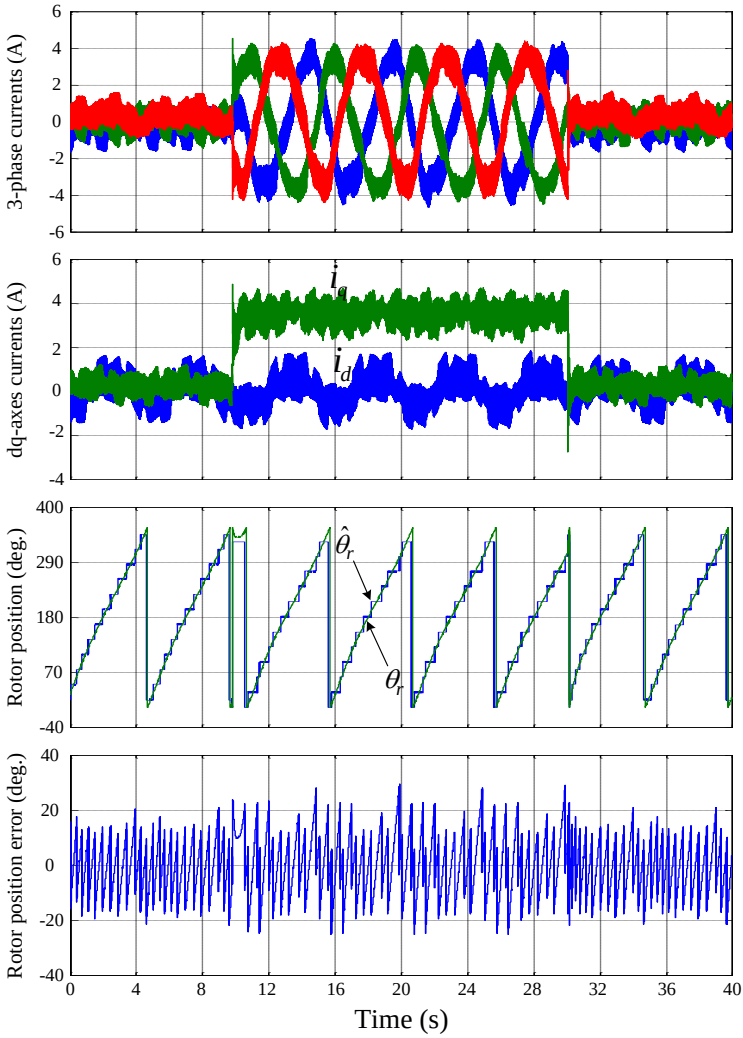

Figure 5.20: Experimental results of sector estimation method with 90% rated torque step at 6 rpm (with optimized selection of sector edge).

5.6 Summary

For obtaining the rotor position and speed information in high performance PMSM drive system at low speed range, different signal injection methods have been investigated and developed. As a voltage injection based method, the INFORM method is a classical and effective sensorless control method and has been widely used in different industrial drive systems. In this chapter, the INFORM method has been

studied in detail. In the INFORM method, the current variation during the injection period is the only variable used for estimating the rotor position. Therefore the accuracy of the injection voltage may affect the performance of the rotor position estimator. A new strategy was introduced for compensating the inverter nonlinear voltage error in the injection voltage.

The simulation and experimental results of the sensorless FOC system with the original INFORM method are given in this chapter. The experimental results show that the inverter voltage error causes a DC bias and a big fluctuation in the estimated rotor position when the machine operates with the load. Since the voltage error is largely compensated, the improved INFORM method shows a good performance for the drive system, the disturbance in the estimated rotor position is also minimized.

A new algorithm for the rotor position estimation based on the INFORM injection scheme has been presented in this chapter also. The sector estimation control method determines the sector where the rotor located by using the signs of the current variations. This algorithm can ideally keep the rotor position error smaller than 15 degrees even during rated step load transients. Therefore, this sector estimation algorithm can be used with other sensorless method (e.g. standard INFORM method) for guaranteeing that the rotor position error can be controlled at a relatively small value (e.g. 15 degrees) during transients, ensuring stable operation of the drive under different conditions

Bibliography

[1] D. Montesinos, S. Galceran, A. Sudria, O. Gomis, F. Blaabjerg, "Low cost sensorless control of permanent magnet motors - an overview and evaluation," *IEEE International Conference on Electric Machines and Drives*, pp. 1681-1688, May 2005.

[2] B. Gerard, S. Caux, P. Maussion, "Redundant Position Observer Improvement for Sensorless PMSM at Low Speed," *IEEE International Symposium on Industrial Electronics*, vol. 3, pp. 2083-2088, Jul 2006.

[3] R. Filka, P. Balazovic, B. Dobrucky, "A seamless whole speed range control of interior PM synchronous machine without position transducer," *12th International Power Electronics and Motion Control Conference*, pp. 1008-1014, Aug 2006.

[4] T. C. Lin, Z. Q. Zhu, "Sensorless operation capability of surface-mounted permanent magnet machine based on high-frequency signal injection methods," *Ninth International Conference on Ecological Vehicles and Renewable Energies (EVER)*, pp. 1-7, Mar 2014.

[5] J. H. Jang, S. K. Sul, J. I. Ha, K. Ide, M. Sawamura, "Sensorless Drive of Surface-Mounted Permanent-Magnet Motor by High-Frequency Signal Injection Based on Magnetic Saliency," *IEEE Transaction on Industry Applications*, vol. 39, no. 4, pp. 1031-1038, Jul/Aug 2003.

[6] J. M. Liu, Z. Q. Zhu, "Novel Sensorless Control Strategy With Injection of High-Frequency Pulsating Carrier Signal Into Stationary Reference Frame," *IEEE Transaction on Industry Applications*, vol. 50, no. 4, pp. 2574-2583, Jul/Aug 2014.

[7] Y. D. Yoon, S. K. Sul, K. Ide, "High-Bandwidth Sensorless Algorithm for AC Machine Based on Square-Wave-Type Voltage Injection," *IEEE Transaction on Industry Applications*, vol. 47, no.3, pp. 1361-1370, May/Jun 2011.

[8] M. Schroedl, "Sensorless control of A.C. machines," *VDI Fortschrittberichte 21*, no. 117, 1992.

[9] M. Schroedl, "Sensorless Control of AC Machines at Low Speed and Standstill Based on the "INFORM" Method," *IEEE IAS Annual Meeting*, pp. 270-277, Oct 1996.

Chapter 6
Zero Voltage Injection Method

6.1 Introduction

For obtaining the machine rotor position and speed information, many voltage pulses injection based methods such as the INFROM method [1] and the methods proposed in [2], [3] have been studied and developed. However, these sensorless control methods may need multiple voltage pulses for calculating the rotor position. This may greatly reduce the control frequency of the drive system and introduce a large distortion into the stator currents. In the INFORM method, three voltage pulses are needed on the phase a-, b-, and c- axes respectively, the control period becomes 4 times as the original FOC period [1]. For reducing the current ripple and increasing the system control frequency, a single zero voltage pulse injection method is proposed in this chapter. Since there is no effective voltage output from the inverter during the injection period, the zero voltage injection method utilizes the back-EMF effect as the injection voltage to generate the current ripple. In this method, the zero voltage vector is inserted between two neighboring FOC PWM periods. The rotor position and speed are directly estimated from the current ripple measured within the injection period. Based on the back-EMF voltage, this method is aimed at medium to high speed range (i.e. higher than 10% of the rated frequency). In general, the lowest frequency depends on the machine parameters such as PM flux linkage, back-EMF and stator time constant. In this chapter, the implementation and the mathematical analysis of this algorithm are described. The simulation and experimental results are given and compared. Finally, another application based on this method for online PM lux linkage estimation is discussed.

6.2 Zero voltage injection method

6.2.1 Implementation of the zero voltage injection method

In the zero voltage injection sensorless control algorithm, the zero voltage vector is inserted conveniently between the PWM periods commanded by the FOC PI controllers, as shown in Figure 6.1. The currents in the αβ-reference frame will be measured at the time instant before and after the injection period. The rotor position and speed may then be calculated by these current samples directly.

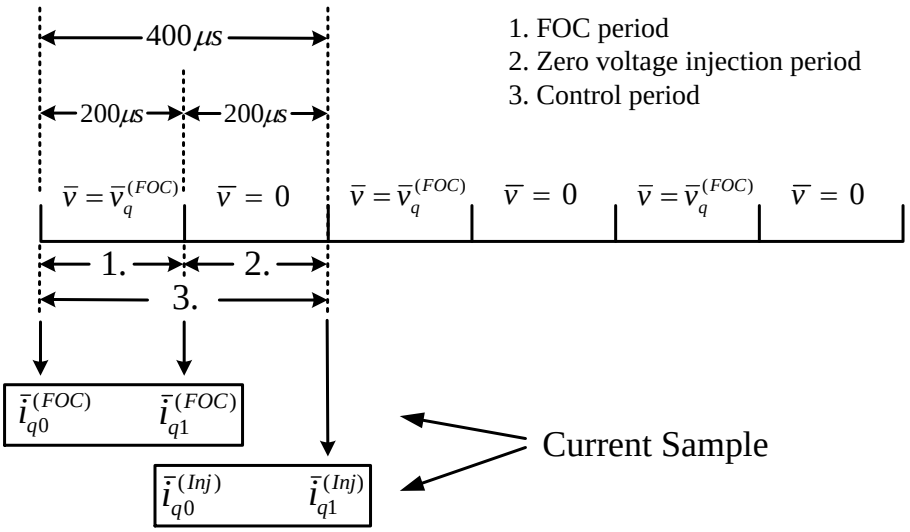

Figure 6.1: Zero voltage injection scheme in implementation.

For realizing zero output voltage in the traditional Space-Vector Modulation (SVM) technique, zero voltage command will generate 50% duty cycles for all the three-phase inverter legs. Therefore, the switches need to be turned on and off once during the zero voltage period. However, as discussed in section 4.2, when the phase current is not equal to zero, the nonlinear inverter voltage error may make the output phase voltage differ from zero, as the first switching period shown in Figure 6.1. To suppress this nonlinear voltage error in a simple way, the commanded duty cycles in this zero voltage injection PWM period may be set to be 0% or 100% for all three inverter legs, as the second and third switching periods in Figure 6.2. This will effectively remove

the voltage error caused by dead-time. The voltage error related to the dead-time is predominant in the inverter nonlinear voltage error. However, the switch forward resistive voltage drop and the voltage drop on the diode (shown as the difference between the dotted lines and solid lines in Figure 6.2) will still be present.

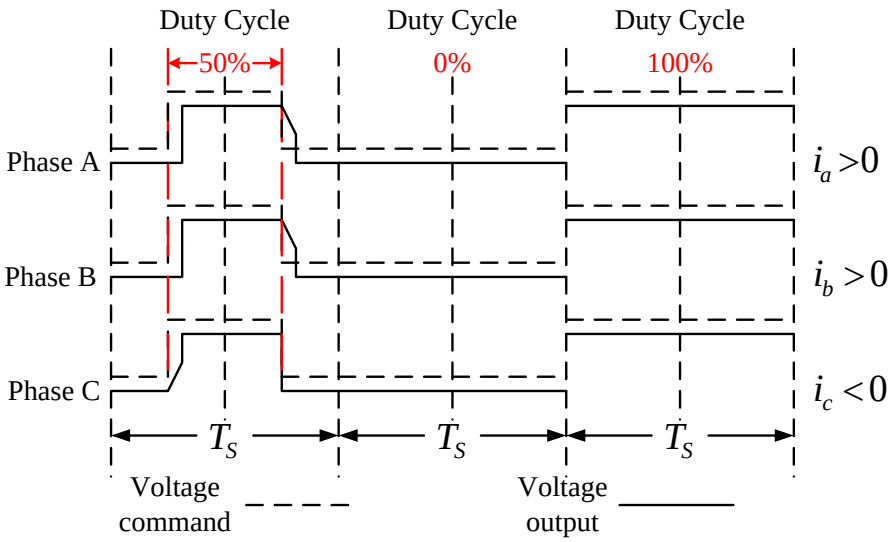

Figure 6.2: Different duty cycle strategies.

6.2.2 Mathematical analysis of the algorithm

As discussed in section 2.1.3, equation (2.18) and (2.20) can be combined as:

$$\begin{bmatrix} v_d \\ v_q \end{bmatrix} = R\begin{bmatrix} i_d \\ i_q \end{bmatrix} + \begin{bmatrix} L_d & 0 \\ 0 & L_q \end{bmatrix}\begin{bmatrix} \frac{d}{dt} i_d \\ \frac{d}{dt} i_q \end{bmatrix} + \omega_r \begin{bmatrix} 0 & -L_q \\ L_d & 0 \end{bmatrix}\begin{bmatrix} i_d \\ i_q \end{bmatrix} + \omega_r \lambda_{mpm}\begin{bmatrix} 0 \\ 1 \end{bmatrix} \tag{6.1}$$

For deriving the current variations on the d- and q-axes, (6.1) can be rewritten in a convenient matrix form as:

$$\begin{bmatrix} \frac{d}{dt} i_d \\ \frac{d}{dt} i_q \end{bmatrix} = \begin{bmatrix} -\frac{R}{L_d} & \frac{L_q}{L_d}\omega_r \\ -\frac{L_d}{L_q}\omega_r & -\frac{R}{L_q} \end{bmatrix}\begin{bmatrix} i_d \\ i_q \end{bmatrix} + \begin{bmatrix} \frac{v_d}{L_d} \\ \frac{v_q - \omega_r \lambda_{mpm}}{L_q} \end{bmatrix} \tag{6.2}$$

In the zero voltage injection period, the machine terminal voltage can be assumed to be zero, i.e. v_d , v_q are 0. Then (6.2) may be written as:

$$\begin{bmatrix} \frac{d}{dt} i_d \\ \frac{d}{dt} i_q \end{bmatrix} = \begin{bmatrix} -\frac{R}{L_d} & \frac{L_q}{L_d}\omega_r \\ -\frac{L_d}{L_q}\omega_r & -\frac{R}{L_q} \end{bmatrix} \begin{bmatrix} i_d \\ i_q \end{bmatrix} + \begin{bmatrix} 0 \\ -\frac{\omega_r \lambda_{mpm}}{L_q} \end{bmatrix} \tag{6.3}$$

Equation (6.3) can be used in the real dq-reference frame only, which needs to know the real rotor position. However, the rotor position is unknown in sensorless control system. Therefore, an estimated dq-reference frame (γδ-reference frame) has to be introduced, as shown in Figure 6.3.

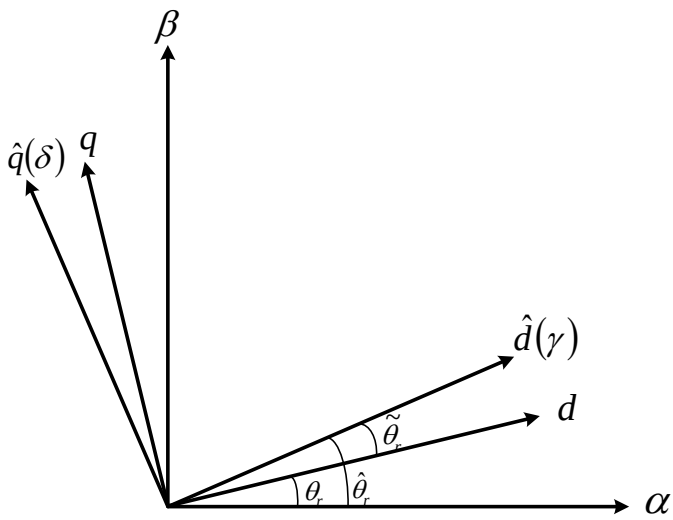

Figure 6.3: Real and estimated dq-reference frames.

The transformation matrix between the real and estimated dq-reference frame may be described as:

$$f(\tilde{\theta}_r) = \begin{bmatrix} \cos\tilde{\theta}_r & \sin\tilde{\theta}_r \\ -\sin\tilde{\theta}_r & \cos\tilde{\theta}_r \end{bmatrix} \tag{6.4}$$

And the transformations for the current variables are:

$$\begin{bmatrix} \hat{i}_d \\ \hat{i}_q \end{bmatrix} = f\left(\tilde{\theta}_r\right)\begin{bmatrix} i_d \\ i_q \end{bmatrix} \tag{6.5}$$

$$\begin{bmatrix} \frac{d}{dt}\hat{i}_d \\ \frac{d}{dt}\hat{i}_q \end{bmatrix} = f\left(\tilde{\theta}_r\right)\begin{bmatrix} \frac{d}{dt}i_d \\ \frac{d}{dt}i_q \end{bmatrix} + \tilde{\omega}_r\begin{bmatrix} 0 & 1 \\ -1 & 0 \end{bmatrix}\begin{bmatrix} \hat{i}_d \\ \hat{i}_q \end{bmatrix} \tag{6.6}$$

where $\tilde{\theta}_r$ is the angle between the real and estimated reference frame; i_d, i_q are the currents in the real dq-reference frame, and $\hat{i}_d$, $\hat{i}_q$ are the currents in the estimated dq-reference frame. By substituting (6.6), equation (6.3) can be represented in the estimated dq-reference frame as:

$$\begin{bmatrix} \frac{d}{dt}\hat{i}_d \\ \frac{d}{dt}\hat{i}_q \end{bmatrix} = f\left(\tilde{\theta}_r\right)\left\{\begin{bmatrix} -\frac{R}{L_d} & \frac{L_q}{L_d}\omega_r \\ -\frac{L_d}{L_q}\omega_r & -\frac{R}{L_q} \end{bmatrix}\begin{bmatrix} i_d \\ i_q \end{bmatrix} + \begin{bmatrix} 0 \\ -\frac{\omega_r\lambda_{mpm}}{L_q} \end{bmatrix}\right\} + \tilde{\omega}_r\begin{bmatrix} 0 & 1 \\ -1 & 0 \end{bmatrix}\begin{bmatrix} \hat{i}_d \\ \hat{i}_q \end{bmatrix} \tag{6.7}$$

then

$$\begin{bmatrix} \frac{d}{dt}\hat{i}_d \\ \frac{d}{dt}\hat{i}_q \end{bmatrix} = f\left(\tilde{\theta}_r\right)\begin{bmatrix} -\frac{R}{L_d} & \frac{L_q}{L_d}\omega_r \\ -\frac{L_d}{L_q}\omega_r & -\frac{R}{L_q} \end{bmatrix}\cdot f^{-1}\left(\tilde{\theta}_r\right)\begin{bmatrix} \hat{i}_d \\ \hat{i}_q \end{bmatrix} + f\left(\tilde{\theta}_r\right)\begin{bmatrix} 0 \\ -\frac{\omega_r\lambda_{mpm}}{L_q} \end{bmatrix} + \tilde{\omega}_r\begin{bmatrix} 0 & 1 \\ -1 & 0 \end{bmatrix}\begin{bmatrix} \hat{i}_d \\ \hat{i}_q \end{bmatrix} \tag{6.8}$$

When the PM machine is working in the FOC drive system, d-axis current reference is usually set to be 0. Therefore, in (6.8), $\hat{i}_d$ may be regarded as 0. The current change on the estimated d-axis may then be described as:

$$\begin{aligned} \frac{d}{dt}\hat{i}_d = {} & \frac{R}{2}\left(\frac{1}{L_d} - \frac{1}{L_q}\right)\hat{i}_q \sin(2\tilde{\theta}_r) - \frac{\lambda_{mpm}}{L_q}\omega_r \sin\tilde{\theta}_r \\ & + \left[\frac{L_q}{L_d} + \left(\frac{L_d}{L_q} - \frac{L_q}{L_d}\right)\sin^2\tilde{\theta}_r\right]\omega_r\hat{i}_q + \tilde{\omega}_r\hat{i}_q \end{aligned} \tag{6.9}$$

In (6.9), the first two terms are predominant. Therefore equation (6.9) may be simplified to:

$$\frac{d}{dt}\hat{i}_d = \frac{R}{2}\left(\frac{1}{L_d} - \frac{1}{L_q}\right)\hat{i}_q \sin(2\tilde{\theta}_r) - \frac{\lambda_{mpm}}{L_q}\omega_r \sin\tilde{\theta}_r \tag{6.10}$$

Considering that when $\tilde{\theta}_r$ is small enough, $\sin\tilde{\theta}_r$ may be approximated by $\tilde{\theta}_r$. Then (6.10) becomes:

$$\frac{d}{dt}\hat{i}_d = \left[R\left(\frac{1}{L_d} - \frac{1}{L_q}\right)\hat{i}_q - \frac{\lambda_{mpm}}{L_q}\omega_r \right] \cdot \tilde{\theta}_r \propto K \cdot \tilde{\theta}_r \tag{6.11}$$

Therefore, the current change on the estimated d-axis during the zero voltage injection period may be observed to be proportional to $\tilde{\theta}_r$. Similar idea has been studied in [4], [5], where the current variation during the zero voltage vector effect time within a normal PWM period was used to estimate the position. However, in this case, the maximum output voltage needs to be carefully limited to guarantee enough time intervals for sampling the current variation. Measuring the current accurately may also become difficult if the noise filters are applied for obtaining a clear current signal. The delay of the noise filters may bring a lot of troubles to the current sampling. By injecting a separate zero voltage PWM period, the voltage determined by the FOC system and the rotor position estimation become independent.

The back-EMF related term $\frac{\lambda_{mpm}}{L_q}\omega_r$ in (6.11) becomes predominant when the machine operates at e.g. above 10% of the rated frequency. Therefore, coefficient *K* becomes minus, and $\frac{d}{dt}\hat{i}_d$ is proportional to $-\tilde{\theta}_r$. The estimated rotor position $\hat{\theta}_r$ and the estimated rotor speed $\hat{\omega}_r$ may then be obtained from a classical PLL controller as shown in Figure 6.4.

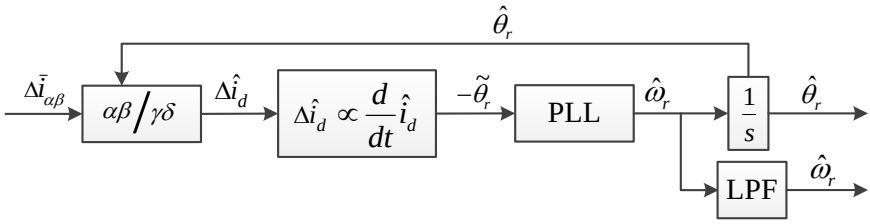

Figure 6.4: Block diagram of PLL controller.

6.3 Simulation and experimental analysis

6.3.1 Simulation results

The zero voltage injection method is first implemented in a simulation model built in Matlab/Simulink. The switching frequency is set as 5k Hz which is the same as the value used in the experiment. The machine parameters are set as the same as the test machine. Due to the algorithm is implemented in the FOC drive system also, the machine and the control system module are the same as the ones used in chapter 5, as shown in Figure 5.2 and 5.3.

Figure 6.5 shows the module used for selecting the voltage outputs between the injection zero voltage and the voltage command from the FOC module. Being different from the INFORM method, the cycle counter for the zero voltage injection method generates a pulse signal between 1 and 2, then the zero voltage can be injection intermittently between two FOC voltage commands.

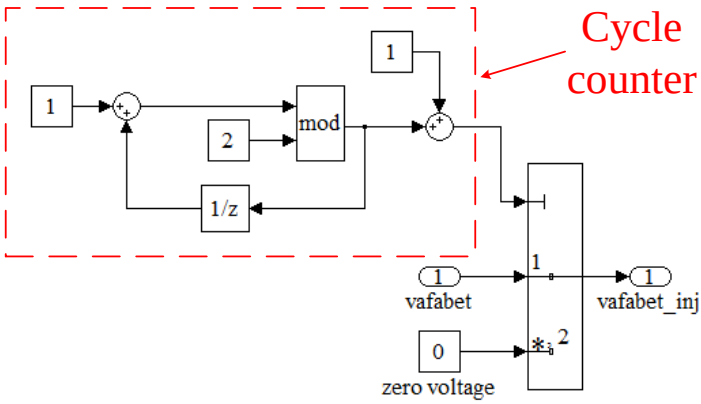

Figure 6.5: Diagram of output voltage selector.

Figure 6.6 shows the voltage outputs and the selector signals. In Figure 6.6, the up row figure shows the selector signal; the bottom row shows the voltage outputs in the αβ-reference frame. When the selector signal is equal to 1, the voltage outputs are selected

as the voltage commands from the PI controller; when the selector signal is equal to 2, the voltage outputs both on the α- and β-axes become zero.

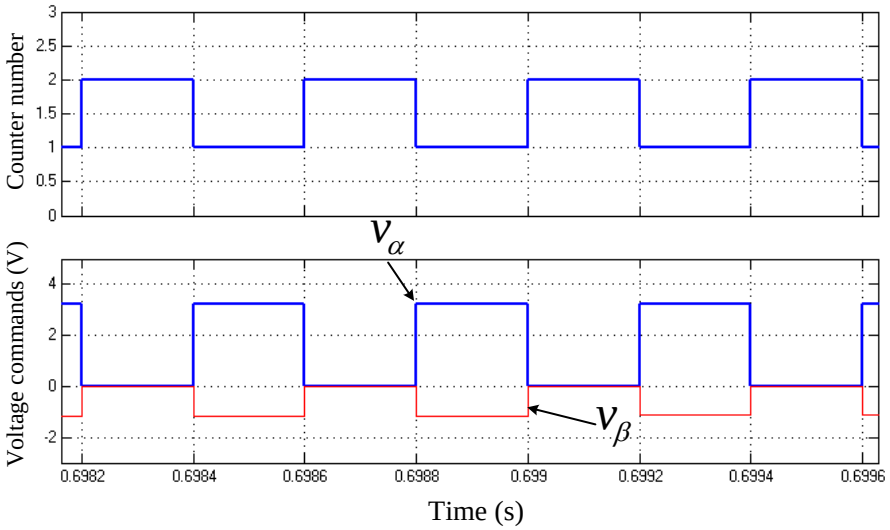

Figure 6.6: Counter signal and voltage commands outputs from the selector.

Figure 6.7 shows the PLL controller used for obtaining the estimated rotor speed and position. Since the calculation of the current samples can give the rotor position error only, therefore a PLL controller is needed for the system.

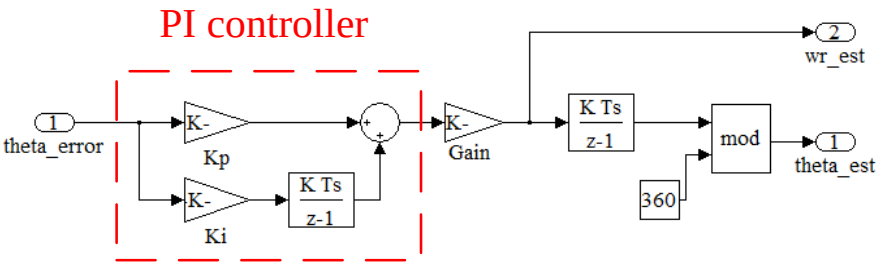

Figure 6.7: Diagram of PLL controller in simulation module.

When the zero voltage injection method is implemented in the simulation model, the real rotor position and speed obtained from the machine module are first used as the feedbacks to validate the algorithm. In this simulation, the PI parameters for the current control loop are set as: $K_p = 30$, $K_i = 8000$; and the parameters for the speed loop are set as the same as before, which are: $K_p = 2$ $K_i = 30$. The PI parameters for the PLL controller are set as: $K_p = 1000$, $K_i = 10000$.

Figure 6.8 shows the drive system performance and the estimated rotor position with the step load. The machine is controlled to operate at 300 rpm, when a 75% rated load is applied to the machine, the current on the q-axis step increases from 0.4 A to 3 A. Since the real rotor position is used for decoupling the currents, the current on the d-axis is maintained at 0 A. There is a -4 degrees DC bias appearing in the rotor position error, which means the real rotor position delays the estimated one by 4 degrees. This may be due to the voltage drop on the stator resistance of the machine. In a further simulation, when the value of the stator resistance is set to be higher than the actual value of the test machine, the DC bias increases with the resistance.

In Figure 6.9, the estimated rotor position is used as the feedback in the simulation, which means the real rotor position will not be involved in the calculation. With the 75% load, the DC bias in the rotor position error increases to -12 degrees. The actual current vector is leading the real q-axis by 12 degrees, and the current on the real d-axis becomes negative. This result illustrates that the current on the d-axis will affect the accuracy of the estimation (i_d term is neglected in (6.9)). The rotor position error between the real and estimated rotor position increases with the decreasing d-axis current.

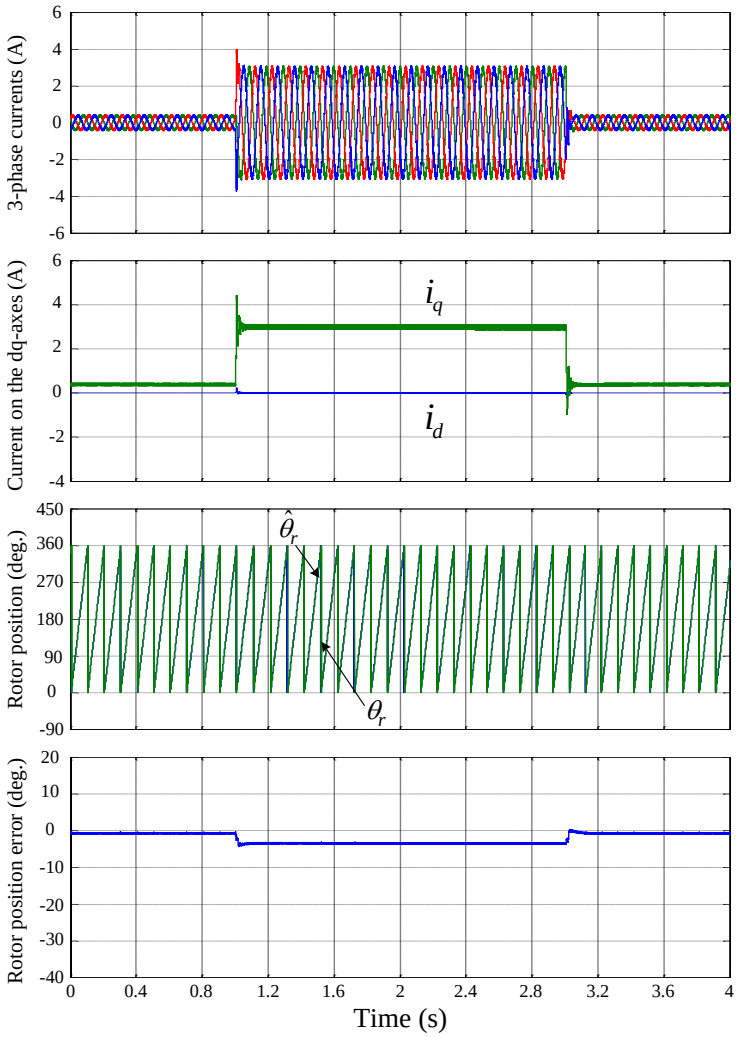

Figure 6.8: Simulation results of zero voltage injection method with 75% rated torque step at 300 rpm (with real rotor position as feedback).

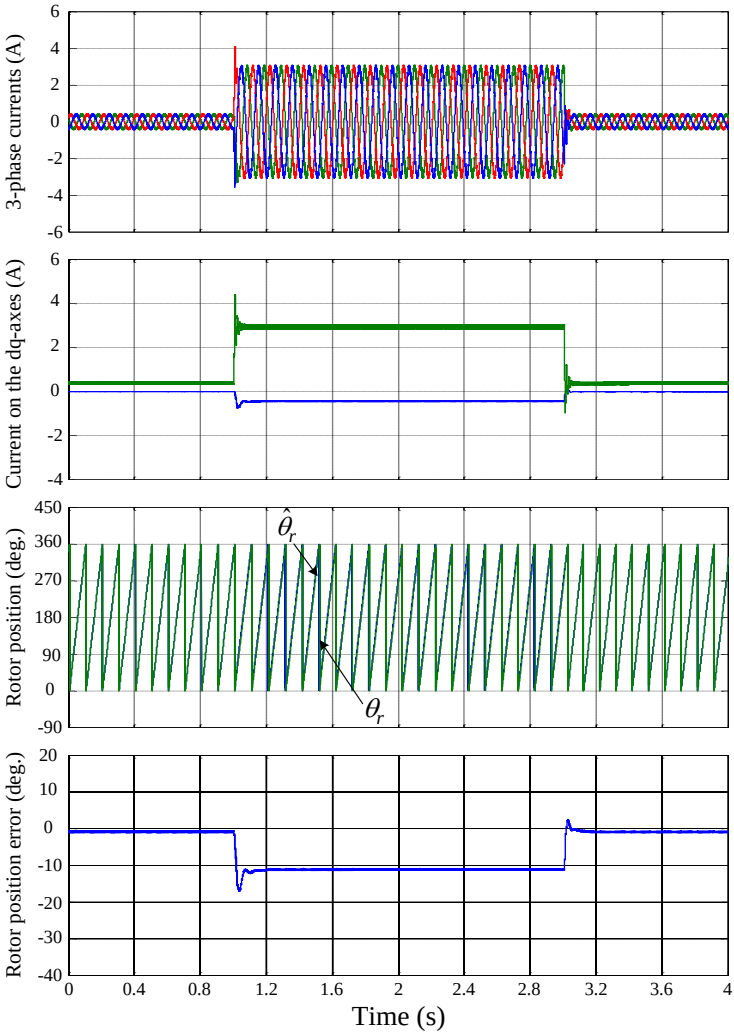

Figure 6.9: Simulation results of zero voltage injection method with 75% rated torque step at 300 rpm (with estimated rotor position as feedback).

6.3.2 Experimental results

The zero voltage injection sensorless control algorithm is then validated in the test system. The switching frequency is set as 5 kHz. The same as the simulation, the parameters for the current loop PI controller are set as $K_p = 30$, $K_i = 8000$; the parameters for the speed loop PI controller are set as $K_p = 2$, $K_i = 30$; and the parameters for the PLL controller are set as $K_p = 1000$, $K_i = 10000$.

Figure 6.10 shows the performance of the practical system and the estimator. The machine speed is controlled at 300 rpm as a constant, and the real rotor position and speed from the encoder are used as the feedbacks. When the machine works without the load, the estimated rotor position has ±2.5 degrees ripple and -3 degree DC bias compares with the real rotor position. When a 75% rated load is applied to the machine, the ripple in the estimated rotor position is narrowed down to ±1 degree, and a -8 degrees DC bias appears in the rotor position error. This enlarged DC bias may be caused by the inverter voltage error as discussed in section 5.4.2.

In Figure 6.11, the estimated rotor position is used in the FOC drive system. When the 75% rated load is applied on the machine, the DC bias in the rotor position error increases to around -24 degrees. The current on the real d-axis is around -1.2 A. This experimental result has a similar characteristic with the simulation result (as shown in Figure 6.9). Because of the sampled background noise and the measurement error, the experimental estimation error is around twice of the simulation one, and the ripples of the current and rotor position are also larger than the simulation.

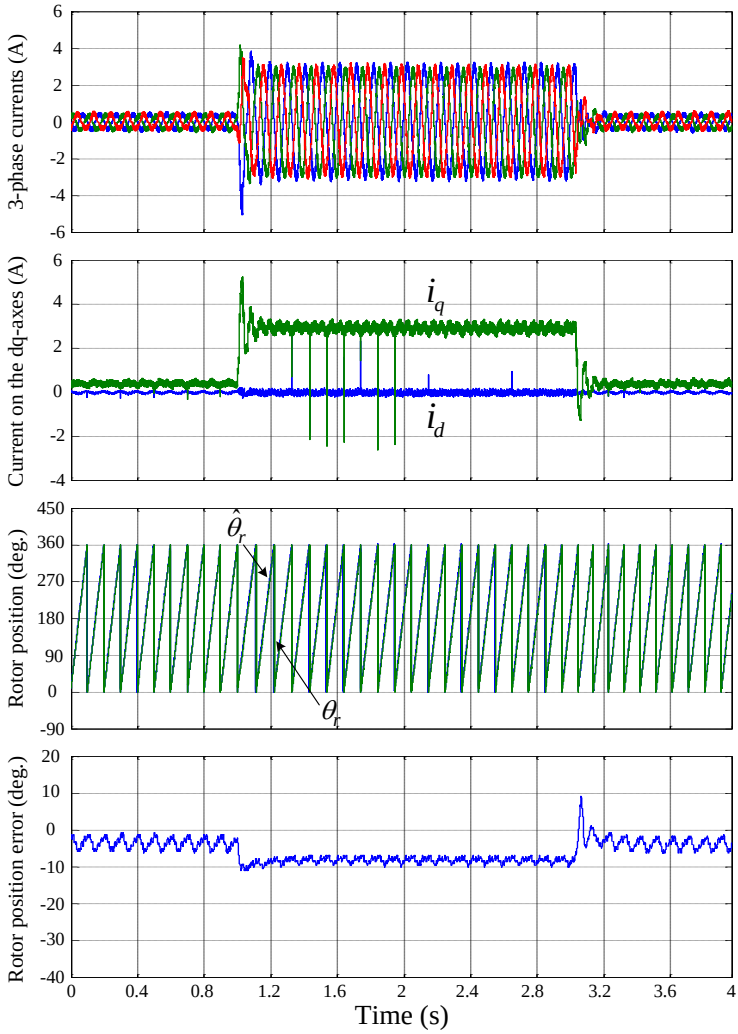

Figure 6.10: Experimental results of zero voltage injection method with 75% rated torque step at 300 rpm (with real rotor position as feedback).

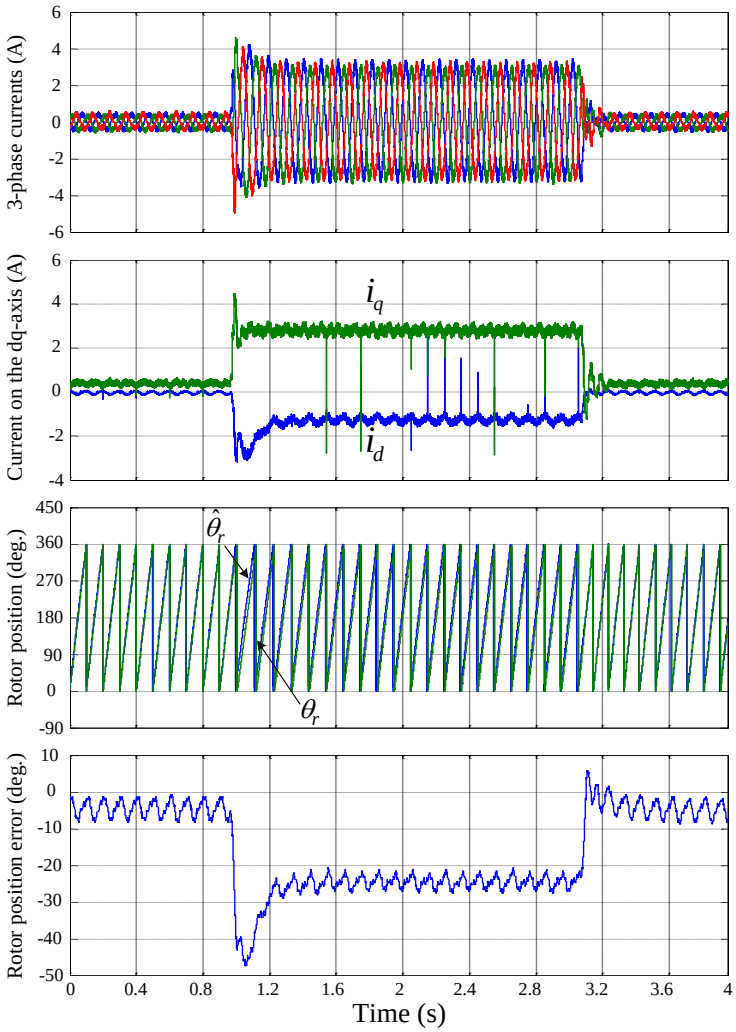

Figure 6.11: Experimental results of zero voltage injection method with 75% rated torque step at 300 rpm (with estimated rotor position as feedback).

6.4 Compensation for the DC bias

6.4.1 Analysis of the DC bias

It should be noticed that for the situation shown in Figure 6.9 and 6.11, since the real position is used to decouple the three-phase currents to the dq-reference frame, the current on the d-axis will be equal to zero. Since there is a position error exists between the real rotor position and estimated rotor position, when the estimated rotor position is used for decoupling the currents, the real d-axis current may not be equal to zero. This may bring a DC error into the estimator.

As shown in Figure 6.4, the PLL controller regulates the estimated rotor position to keep $\frac{d}{dt}\hat{i}_d$ zero in steady state. However, the torque current related term $\frac{L_q}{L_d}\omega_r\hat{i}_q$ in (6.9) brings a DC position error when the $\frac{d}{dt}\hat{i}_d$ term is regulated to be zero. For eliminating this bias position error, a compensation term depending on ω_r and i_q needs to be introduced and added to $\frac{d}{dt}\hat{i}_d$, as illustrated in Figure 6.12.

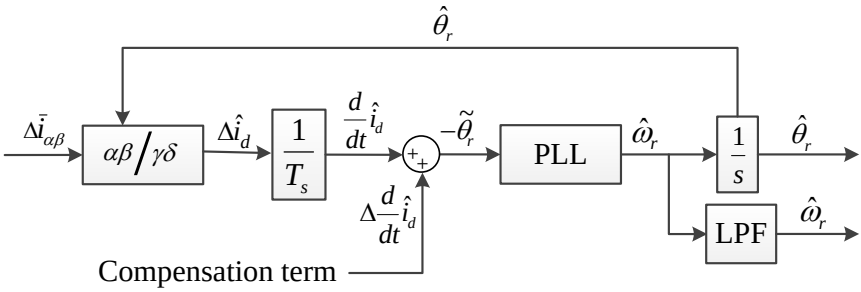

Figure 6.12: Modified diagram of estimator with compensation.

For verifying this compensation term, the compensation values for eliminating the DC bias are recorded with different estimated q-axis current when the machine operates at constant speed. Figure 6.13 shows the experimentally determined compensation values when the machine operates at 300 rpm and 600 rpm respectively. When the speed is

constant, the compensation value has a linear relationship to the current on the estimated q-axis. And the slope of the line decreases when the speed increases. Theoretically, the compensation value should be proportional to the q-axis current and the rotor speed. However, there is an initial value which is used for compensating the rotor position error that may be caused by the inverter voltage error. This compensation term effectively improves the position estimation accuracy, as demonstrated below.

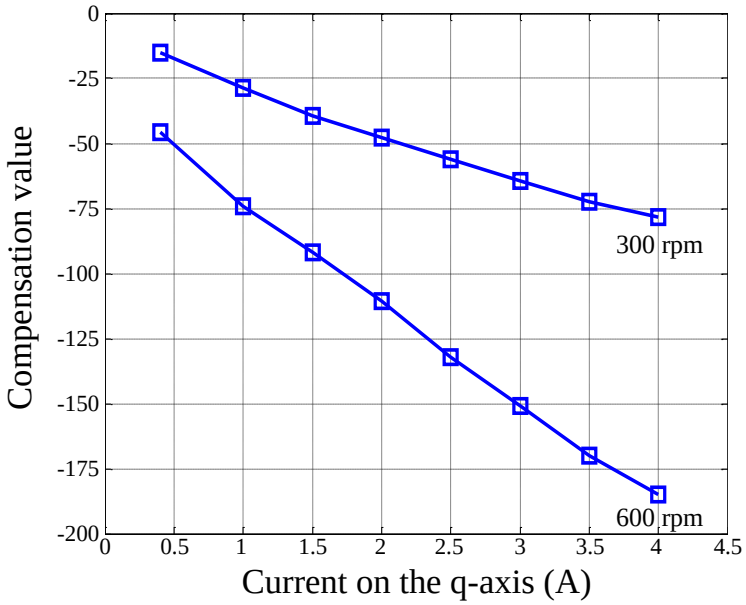

Figure 6.13: Compensation value for $\frac{d}{dt}\hat{i}_d$.

6.4.2 Experimental results with the compensation

Figure 6.14 shows the performance of the drive system with the compensation. The estimated rotor position is used as the feedback. The machine operates at 300 rpm. In the steady state, the rotor position error is nearly 0 both with and without load. In the transient period, the maximum position error is -22.5 degrees when the full rated load is step applied and +8 degrees when the load is suddenly removed. The ripple of the estimated rotor position error is around ±2 degrees for both no-load and loaded operations.

Figure 6.15 shows the experimental results when the machine operates at 600 rpm with the estimated rotor position as the feedback in the FOC system. The compensation term is also applied. The 100% load step results in -15 degrees (load added) and +6 degrees (load removed) position errors, respectively. In the steady state, the ripple in the rotor position error reduces to around ±1 degree.

Figure 6.16 shows the drive performance when the reference speed changes step from 300 rpm to 600 rpm, and then back to 300 rpm. When the speed reference is stepped up, the estimated rotor position error has a +28 degrees fluctuation. When the speed reference is stepped down, the rotor position error has a bigger oscillation, which is around -36 degrees.

Figure 6.17 shows the system performance when the estimated rotor position and speed from the PLL are both used in the drive system. Compared with the speed obtained from the encoder, the estimated speed has a larger ripple. In the steady state, the ripple in the rotor position error increases to around ±2.2 degrees when the machine operates at 600 rpm. When the 100% rated load is applied, the peak value of the rotor position error is around -18 degrees. When the load is removed, the transient error is reduced to -7 degrees.

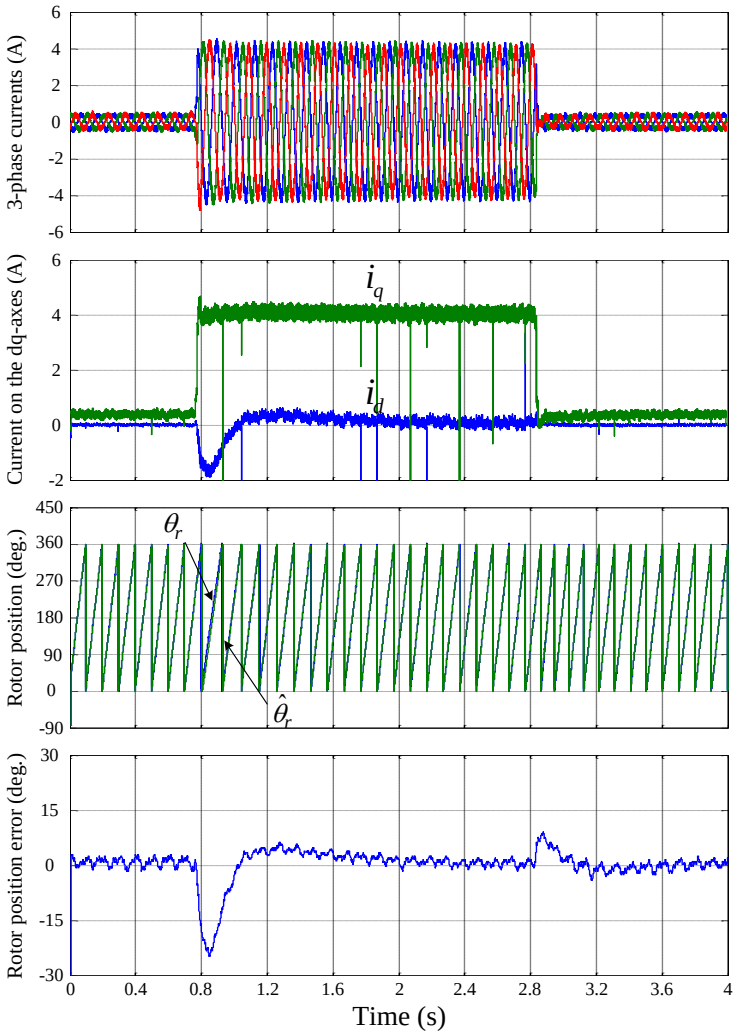

Figure 6.14: Experimental results of zero voltage injection method with 100% rated torque step at 300 rpm (with estimated rotor position as feedback and with compensation).

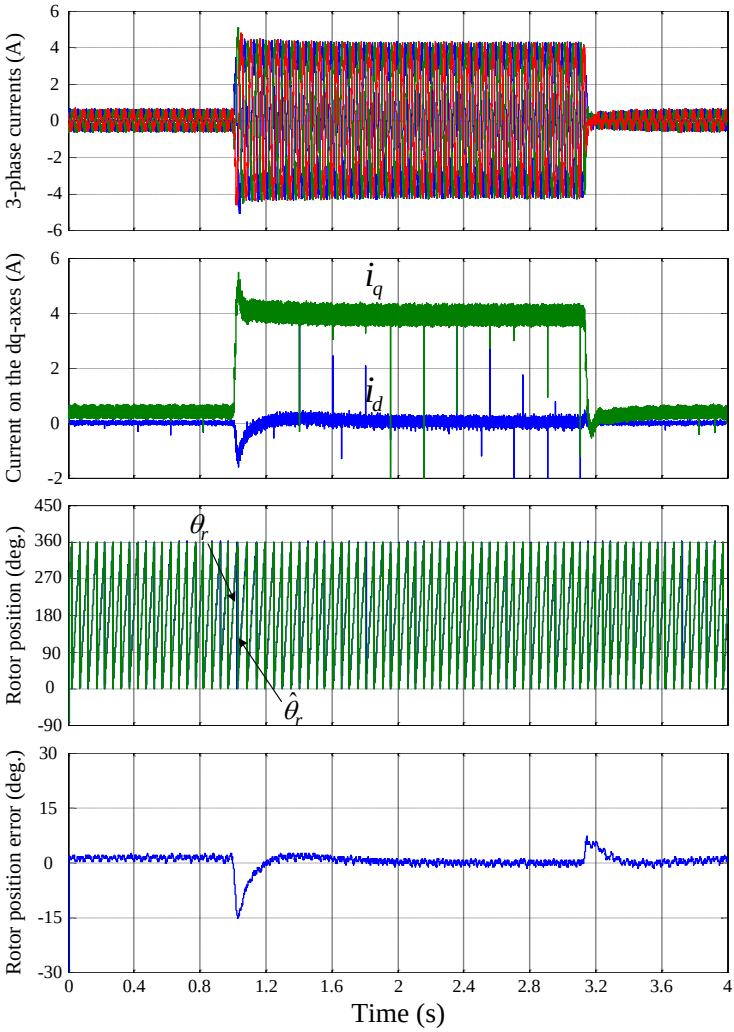

Figure 6.15: Experimental results of zero voltage injection method with 100% rated torque step at 600 rpm (with estimated rotor position as feedback and with compensation).

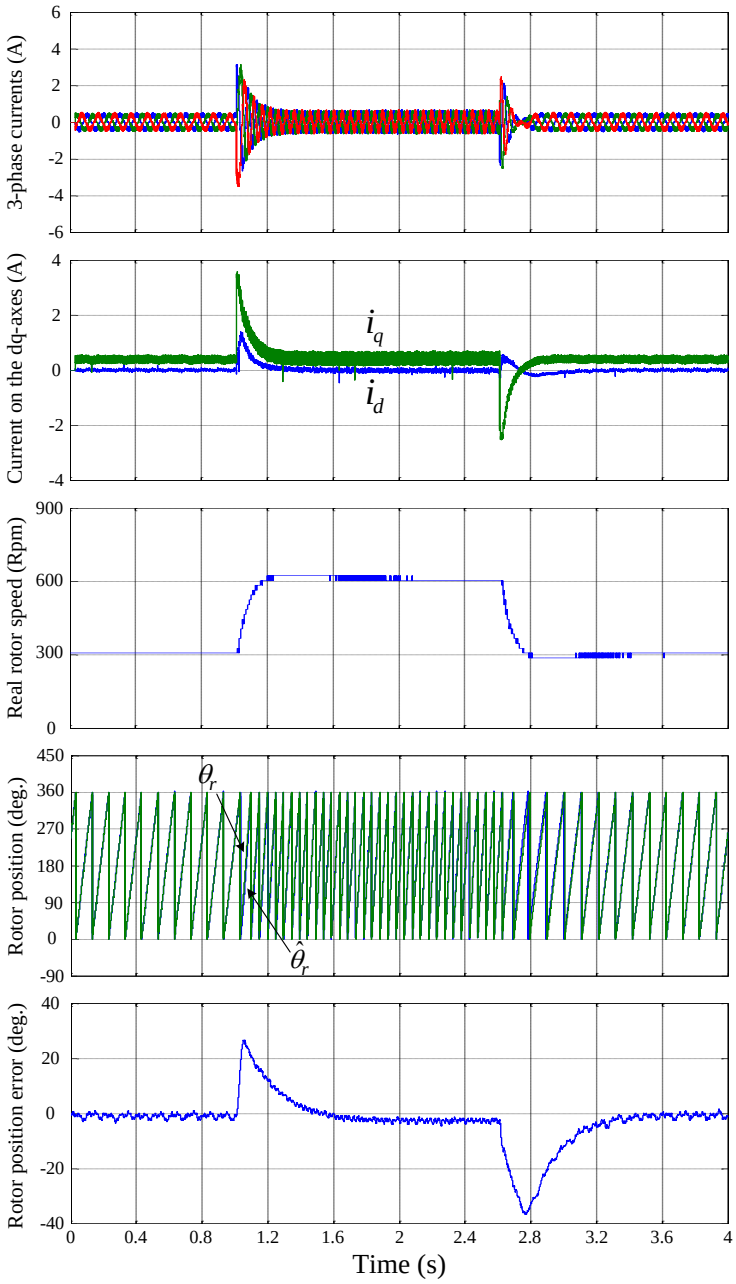

Figure 6.16: Experimental results of zero voltage injection method with speed step from 300 to 600 and to 300 rpm (with estimated rotor position as feedback and with compensation).

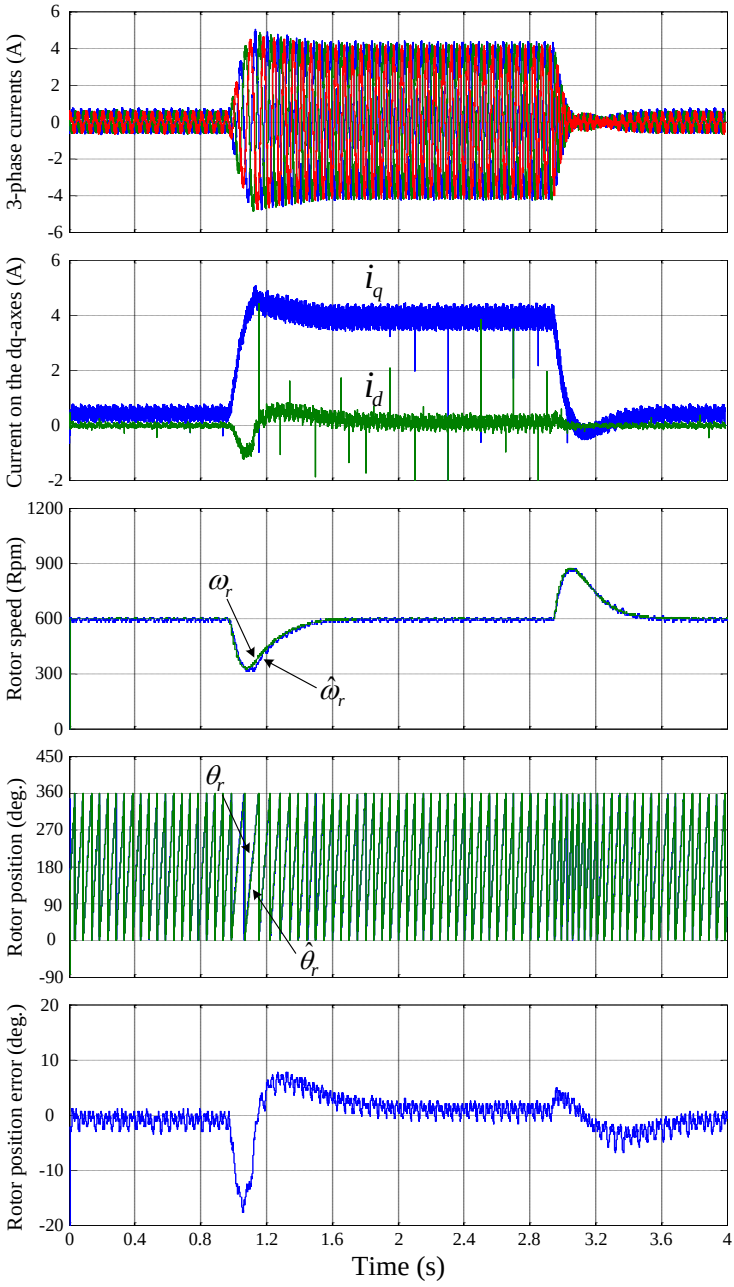

Figure 6.17: Experimental results of zero voltage injection method with 100% rated torque step at 600 rpm (with estimated rotor position and speed as feedback and with compensation).

6.5 Permanent magnet flux linkage online estimation

Besides providing good rotor position estimation, the zero voltage injection method can also be used for the online machine parameters estimation. In most of the PMSM drive systems, machine parameters such as the stator resistance, inductance and the rotor permanent magnet (PM) flux linkage are considered as constants and usually measured offline by using additional instrumentation. However, the values of these machine parameters may change due to e.g. temperature rise [6], [7]. The PM flux linkage may be involved in many control strategies for PMSM, such as rotor position estimation [8], and inductance online measurement [9]. The accuracy of the PM flux linkage value may affect the estimation accuracies and the drive performance consequently [7], [9]. Therefore, a simple and accurate estimation method is proposed for estimating PM flux linkage online. This estimation method is based on the zero voltage vector injection scheme. The q-axis voltage equation in (6.1) indicates that the rotor PM flux linkage may be calculated by using q-axis terminal voltage. In most drive systems, there are no voltage sensors used for measuring the voltage. The inverter voltage error may cause the voltage error between the voltage command and machine real terminal voltage [10]. Therefore it is important to measure and compensate the inverter voltage error when the voltage equation is applied directly for estimating the PM flux linkage. The voltage loss on the inductance has to be taken into account which requires the machine inductance to be known. The inverter voltage error has a nonlinear behavior and the machine inductance may change due to the saturation effect. In addition, when the voltage equation is used for estimating the PM flux linkage directly, current measurement error may also affect the estimation accuracy. Therefore, it will be an advantage that the PM flux linkage estimation may be achieved without knowing the inverter voltage error and the inductance values. The estimation may be also insensitive to current measurement errors. To serve this purpose, the zero voltage injection scheme can be used for estimating the rotor PM flux linkage.

6.5.1 Mathematical analysis of the algorithm

Based on the zero voltage injection scheme which shown in Figure 6.1, in the FOC switching period and in the zero voltage switching period, the corresponding voltage equations for the q-axis may be expressed as:

$$v_q^{(FOC)} = Ri_{q0}^{(FOC)} + L_q \frac{d}{dt} i_q^{(FOC)} + \omega_r L_d i_{d0}^{(FOC)} + \omega_r \lambda_{mpm} \tag{6.12}$$

$$0 = Ri_{q0}^{(Inj)} + L_q \frac{d}{dt} i_q^{(Inj)} + \omega_r L_d i_{d0}^{(Inj)} + \omega_r \lambda_{mpm} \tag{6.13}$$

where di_q / dt term may be approximated by $(i_{q1} - i_{q0})/T_s$ and T_s is the switching period. When the machine operates at steady state, the q-axis current reference may be seen as constant. As shown in Figure 6.18, the current increases during the FOC switching period (period 1.), and decrease in the zero voltage injection period (period 2.) The current loop PI controller will only respond to the current sampled at the beginning of period 1, which is $i_{q0}^{(FOC)}$. Therefore, period 1 and period 2 may be regarded as one control unit period. In steady state, the q-axis current PI controller will force the current sampled at the beginning of the control period ($i_{q0}^{(FOC)}$) to be constant, This means the current variations in period 1 will be opposite to the current variation in period 2, i.e. $\frac{d}{dt} i_q^{(FOC)} = -\frac{d}{dt} i_q^{(Inj)}$.

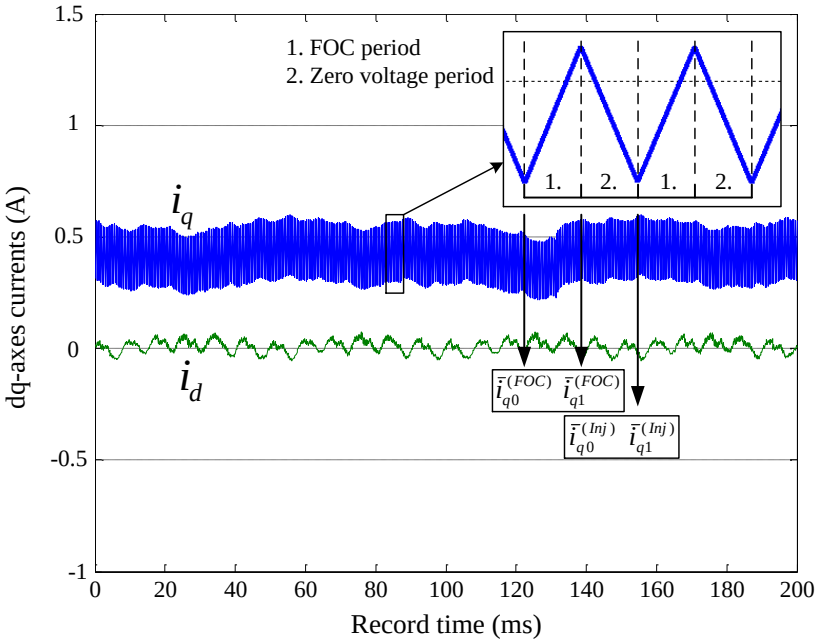

Figure 6.18: Current variation with zero voltage vector injection in steady state.

Therefore, by adding (6.12) and (6.13), the term associated to the inductance will disappear. Considering that d-axis current is controlled to be 0 in the PMSM drive system, (6.12)+(6.13) gives:

$$v_q^{(FOC)} = v_q^* + \Delta v = R\left(i_{q0}^{(FOC)} + i_{q0}^{(Inj)}\right) + 2\omega_r \lambda_{mpm} \tag{6.14}$$

where v_q^* is the voltage command from DSP controller, Δv is the voltage error caused by the inverter.

For minimizing the inverter voltage error effects, (6.14) may be used for two different speeds (denoted with subscripts 1 and 2 respectively), as:

$$v_{q1}^* + \Delta v = R\left(i_{q01}^{(FOC)} + i_{q01}^{(Inj)}\right) + 2\omega_{r1} \lambda_{mpm} \tag{6.15}$$

$$v_{q2}^* + \Delta v = R\left(i_{q02}^{(FOC)} + i_{q02}^{(Inj)}\right) + 2\omega_{r2} \lambda_{mpm} \tag{6.16}$$

When the load on the machine is constant at different speeds, $i_{q01}^{(FOC)} = i_{q02}^{(FOC)}$, $i_{q01}^{(Inj)} = i_{q02}^{(Inj)}$.

Therefore, (6.16)-(6.15) gives:

$$v_{q2}^* - v_{q1}^* = 2\left(\omega_{r2} - \omega_{r1}\right)\lambda_{mpm} \tag{6.17}$$

Then the PM flux linkage may be directly estimated by the voltage commands at different speeds. The machine inductance and the inverter voltage error will not be involved in the estimation.

Since the zero voltage injection method can provide the estimated rotor position with a good accuracy, which is shown in the experimental results in section 6.4. This proposed PM flux linkage online estimation method is also suitable for sensorless operation.

6.5.2 Experimental analysis

This PM flux estimation algorithm is first tested in the sensored FOC system, where the rotor position and speed is obtained from the encoder. Figure 6.19 shows the q-axis voltage commands recorded at different rotor frequencies. Figure 6.20 shows the average value of the voltage command which is constant for a fixed speed. The relationship between the q-axis voltage command and rotor frequency is quite linear (with a constant slope), which validates (6.17).

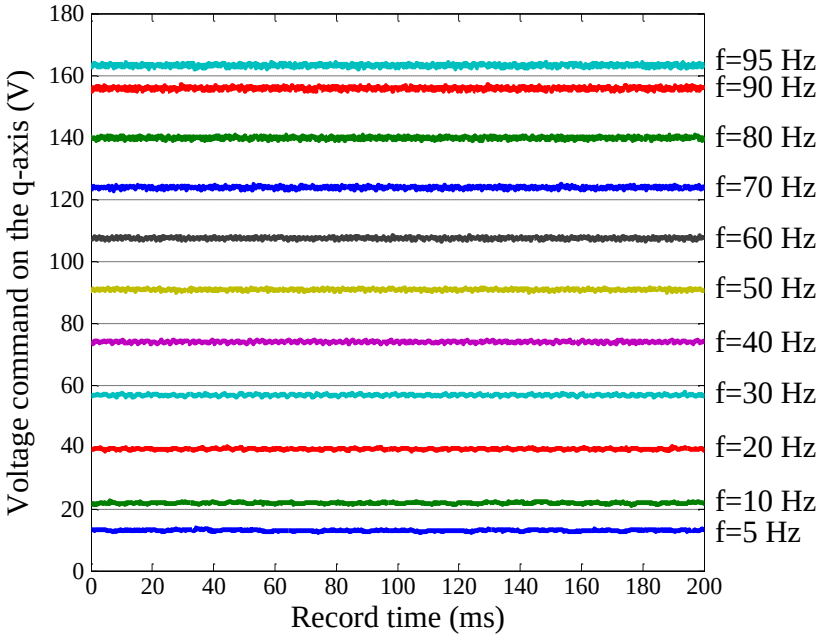

Figure 6.19: Voltage commands at different speeds (with sensored control).

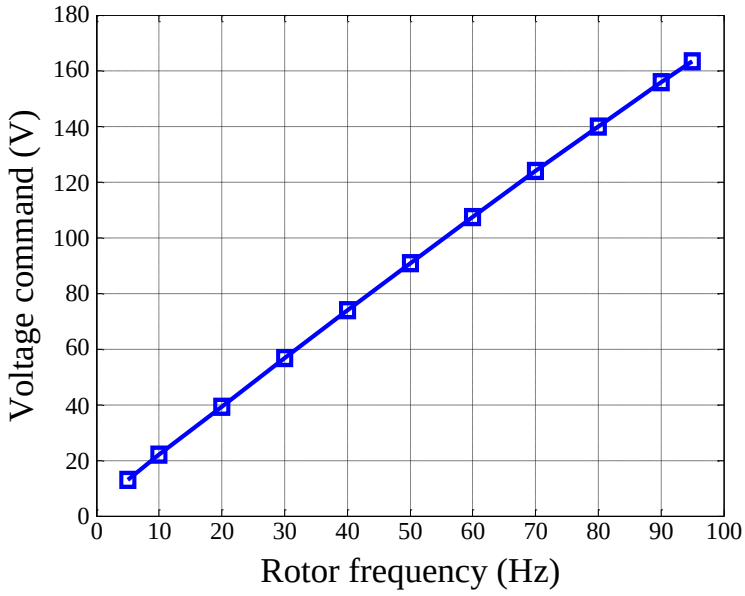

Figure 6.20: Average value of the voltage command vs. speed (with sensored control).

Figure 6.21 compares the estimated PM flux linkage values and the measured values. The blue line is the estimated value and the red line is the value measured from an open-circuit rotating test. The measured PM flux linkage is constant at different speeds, which is around 0.133 Wb. The online estimated PM flux linkage decreases from 0.138 Wb at 5 Hz to 0.130 Wb at 95 Hz. This corresponds to a small estimation error of -2.26% to 3.76%, with respect to the measured value.

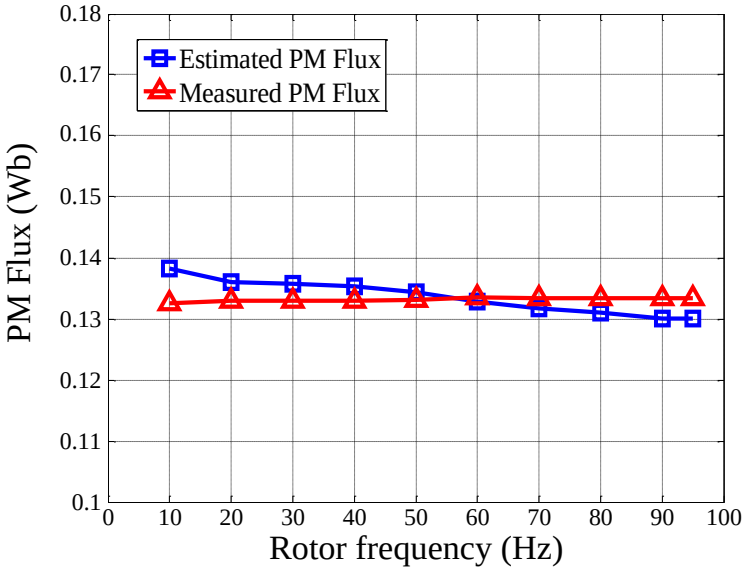

Figure 6.21: Measured and estimated PM flux at different speeds (with sensored control).

Considering that the machine may operate with different load torque when the rotor speed changes, then the stator resistance value needs to be known, and (6.17) will be modified to:

$$v_{q2}^{*} - v_{q1}^{*} = R\left(\left(i_{q02}^{(FOC)} - i_{q01}^{(FOC)}\right) + \left(i_{q02}^{(Inj)} - i_{q01}^{(Inj)}\right)\right) + 2\left(\omega_{r2} - \omega_{r1}\right)\lambda_{mpm} \tag{6.18}$$

Thus, the developed PM flux linkage estimation algorithm can be used with different load. Figure 6.22 shows the results where the stator resistance is considered in the estimation. The linear decrease in the estimated PM flux linkage is eliminated. The error between the estimated value and the measured one may be caused by the inverter voltage error which neglected in (6.17).

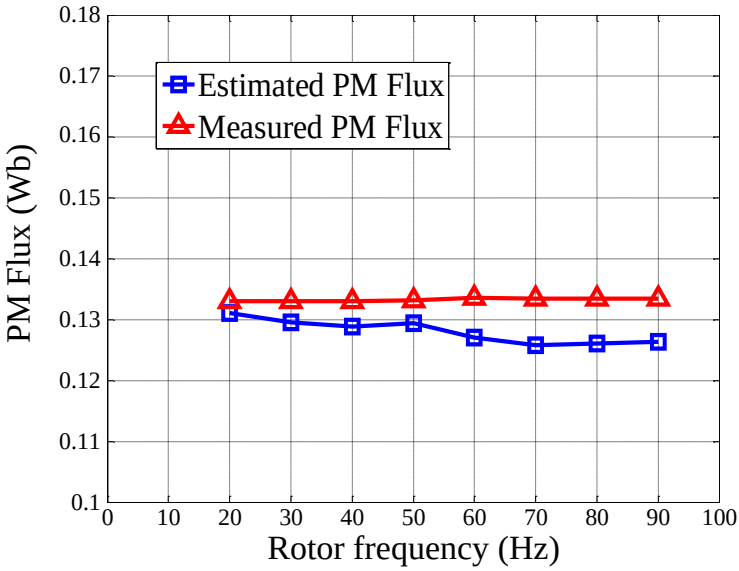

Figure 6.22: Measured and estimated PM flux at different speeds involves resistance (with sensored control)).

The estimation algorithm is then tested in the same system without the encoder. The rotor position and speed estimated from the zero voltage injection method are used as the feedbacks for the control system. The machine operates in sensorless control mode. Figure 6.23 shows the q-axis voltage commands recorded at different speeds. Comparing with Figure 6.19, the voltage commands on the q-axis have more disturbances due to the ripple in the estimated rotor speed. Figure 6.24 shows the average values of the q-axis voltage commands vs. rotor speeds.

Figure 6.25 shows the estimated PM flux linkage value by using (6.17) and the measured value. With respect to the measured value, the estimated ones from exhibit an error between -2.26% to 2.26%. The smallest estimated value is 0.130 Wb, and the largest value is 0.136 Wb. The result shows that this PM flux linkage estimation algorithm works well in a sensorless drive system.

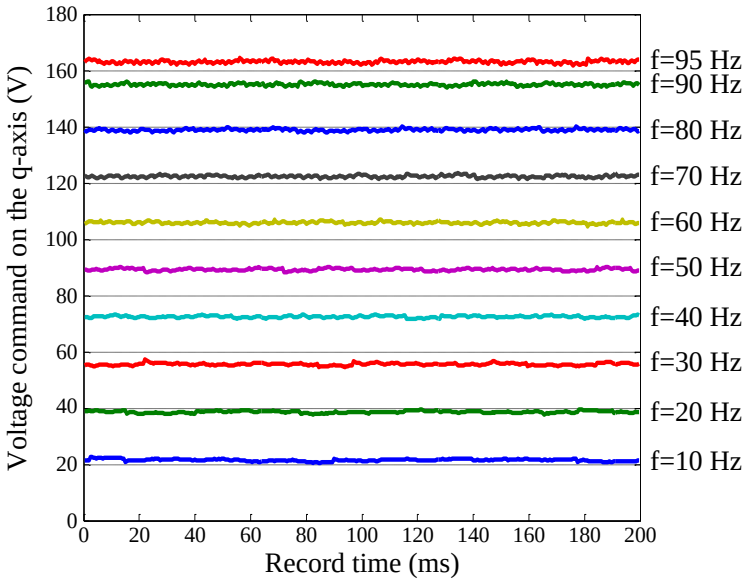

Figure 6.23: Voltage commands at different speeds (with sensorless control).

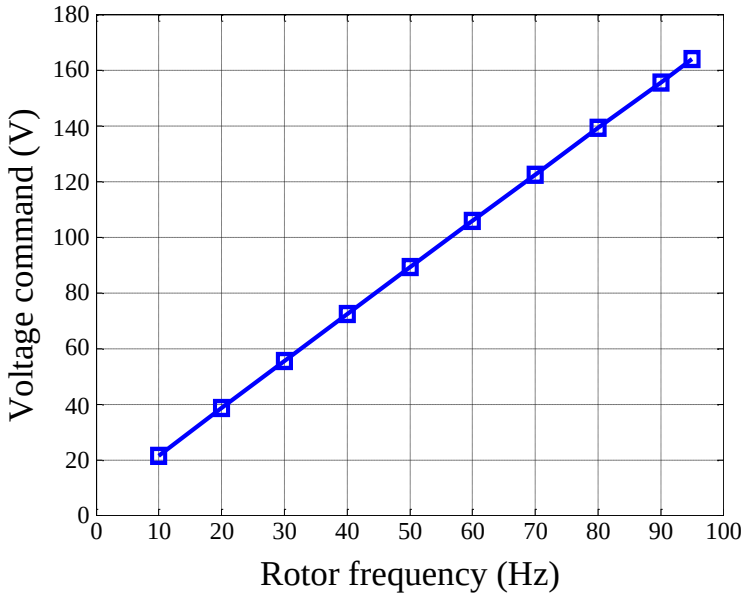

Figure 6.24: Average value of the voltage command vs. speed (with sensorless control).

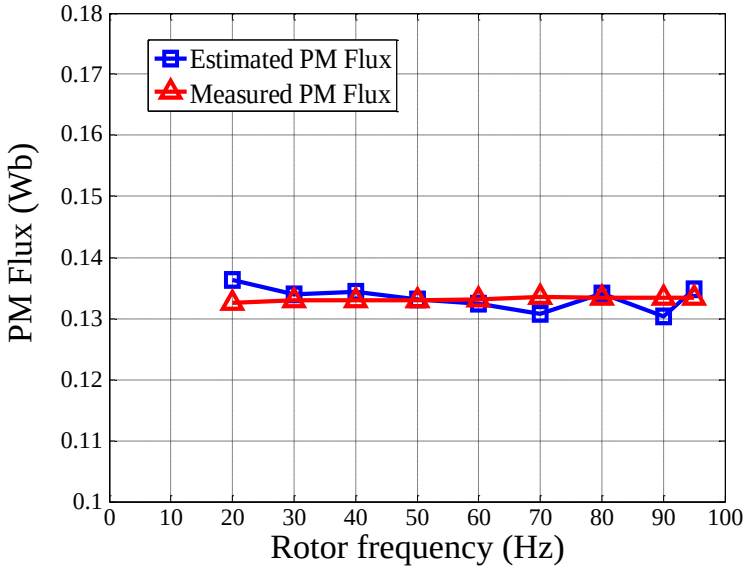

Figure 6.25: Measured and estimated PM flux at different speeds (with sensorless control).

6.6 Summary

The zero voltage injection sensorless control method has been introduced in this chapter. Compared with the INFORM method, the zero voltage injection method inserts one single zero voltage vector between two FOC switching periods. The three-phase currents are then sampled before and after the injection period for calculating the rotor position. For eliminating the nonlinear voltage error, the duty cycles of the injected zero voltage periods are set to be 0. When the zero voltage is injected, the current variation during the injection period is the only variable which is used for estimating the rotor position. Therefore, there is no other machine parameters need to be known in the zero voltage injection method. Compared with the traditional sinusoidal signal injection method, the filter is also unnecessary for the current controller. This may increase the bandwidth for the drive system.

Since there is no voltage output from the inverter during the injection switching period, the current variation caused by the back-EMF voltage is hard to be detected when the

machine operates at low speed. Therefore, the zero voltage injection method is preferred to be used in medium to high speed range.

The zero voltage injection method is implemented both on the simulation model and the experimental platform. The simulation and experimental results show that this sensorless algorithm can provide a good estimated rotor position and speed information when the machine operates at different speeds and with different load conditions. The compensation for the DC bias in the estimated rotor position which related to the torque current and the rotor speed has been also presented in this chapter.

Since the zero voltage injection method provides a good rotor position signal, some potential applications based on this method can be developed. A PM flux linkage online estimation method has been introduced in this chapter. Furthermore, it has the potential to online estimate the inductance by using this sensorless control method.

Bibliography

[1] M. Schroedl, "Sensorless Control of AC Machines at Low Speed and Standstill Based on the "INFORM" Method," *IEEE IAS Annual Meeting,* pp. 270-277, Oct 1996.

[2] J. M. Liu, Z. Q. Zhu, "Novel Sensorless Control Strategy With Injection of High-Frequency Pulsating Carrier Signal Into Stationary Reference Frame," *IEEE Transaction on Industry Applications*, vol. 50, no. 4, pp. 2574-2583, Jul/Aug 2014.

[3] Y. D. Yoon, S. K. Sul, K. Ide, "High-Bandwidth Sensorless Algorithm for AC Machine Based on Square-Wave-Type Voltage Injection," *IEEE Transaction on Industry Applications*, vol. 47, no.3, pp. 1361-1370, May/Jun 2011.

[4] R. Raute, C. Caruana, C. S. Staines, J. Cilia, M. Sumner, G. Asher, "Operation of a sensorless PMSM drive without additional test signal injection," *4th IET Conference on Power Electronics, Machines and Drives*, pp. 616-620, Apr 2008.

[5] R. Raute, "Sensorless Control of AC Machines for Low and Zero Speed Operation without Additional Test Signal Injection," *PhD. Thesis, University of Nottingham, UK,* 2009.

[6] J. Wang, W. Wang, K. Atallah, D. Howe, "Demagnetization Assessment for Three-phase Tubular Brushless Permanent-Magnet Machines," *IEEE Transaction on Magnetics,* vol. 44, no. 9, pp. 2195–2203, Sep 2008.

[7] S. Nandi, H. A. Toliyat, "Condition Monitoring and Fault Diagnosis of Electrical Machines - A Review," *IEEE Industry Applications Conference Thirty-Fourth IAS Annual Meeting,* vol. 1, pp.197-204, Oct 1999.

[8] F. Genduso, R. Miceli, C. Rando, G. R. Galluzzo, "Back EMF Sensorless-Control Algorithm for High-Dynamic Performance PMSM," *IEEE Transaction on Industry Electronics,* vol. 57, no.6, pp. 2092-2100, Jun 2010.

[9] C. Choi, W. Lee, S. O. Kwon, J. P. Hong, "Experimental Estimation of Inductance for Interior Permanent Magnet Synchronous Machine Considering Temperature Distribution," *IEEE Transaction on Magnetics,* vol. 49, no. 6, pp. 2990-2996, Jun 2013.

[10] G. Pellegrino, R. I. Bojoi, P. Guglielmi, F. Cupertino, "Accurate Inverter Error Compensation and Related Self-Commissioning Scheme in Sensorless Induction Motor Drives," *IEEE Transaction on Industry Applications,* vol. 46, no. 5, pp. 1970-1978, Sep/Oct 2010.

Chapter 7

Estimated d-/q-axis Voltage Vector Injection Method

7.1 Introduction

As discussed in chapter 6, the zero voltage injection method uses a single zero voltage pulse for obtaining the rotor position and speed information. However, the terminal voltage of the machine during the injection period used for causing the current ripple is based on the back-EMF. Therefore the zero voltage injection method is preferred to be used in medium to high speed range. When the machine operates at low speed or standstill state, the zero voltage injection method cannot provide the estimated rotor position because the back-EMF voltage is too small to cause the current ripple. In this situation, a new algorithm injects the voltage vector on the estimated d-/q-axis for estimating the rotor position is introduced in this chapter. In this estimated d-/q-axis voltage vector injection method, a single voltage vector is injected between two FOC PWM switching periods. The magnitude of the injection voltage vector is constant, and the voltage vector is always applied on the estimated d- or q-axis. The resultant current variation under this single testing voltage vector is directly linked to the position error. The same as the methods introduced before, this estimated d-/q-axis voltage vector injection method is also affected by the voltage error. Therefore, this method is further developed to reduce the effects of inverter voltage error on the position estimation accuracy by injecting two opposite voltage vectors.

7.2 Estimated d-/q-axis voltage vector injection method

7.2.1 Implementation of the estimated d-/q-axis voltage vector injection method

Similar to the zero voltage injection scheme introduced in section 6.2.1, the needed test voltage vector will be injected between two FOC switching periods, as shown in Figure 7.1. In this estimated d-/q-axis voltage vector injection method, the voltage vector can be applied on the estimated d-axis or q-axis. The current variation due to the injected voltage may be reliably measured and then used for estimating the rotor position. The switching frequency is set to be 10 kHz in this method, and the injection frequency will be half of the switching frequency. The currents are sampled at the beginning of each switching period. The PI controller will respond to the current measured in the beginning of FOC control period (period 1 shown in Figure 7.1) only. Therefore, no filter is needed to extract the high frequency current component for estimating the rotor position or to obtain the fundamental current component for the control.

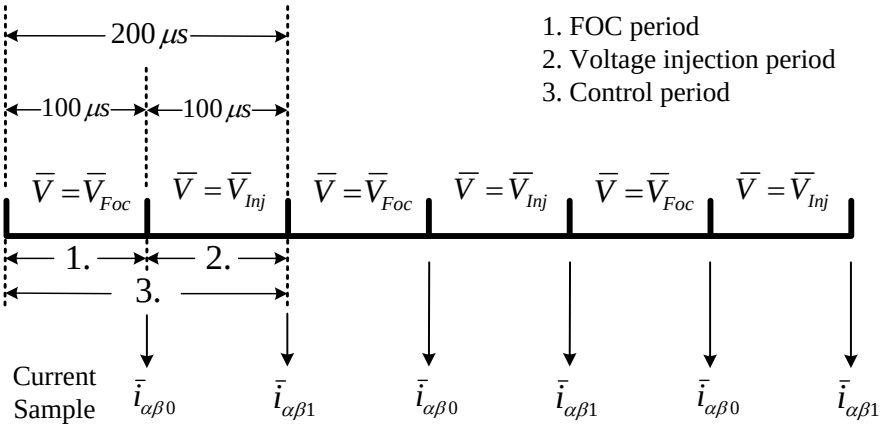

Figure 7.1: Estimated d-/q-axis voltage vector injection scheme in implementation.

7.2.2 Mathematical analysis of the algorithm

The current variation equation in classical INFORM form can be used for the estimated d-/q-axis voltage vector injection method as [1]:

$$\Delta\bar{i}_{\alpha\beta} = \left(c_1 + c_2 e^{j2(\theta_r - \theta_u)}\right)\Delta t\bar{v}_{\alpha\beta} \tag{7.1}$$

where, $c_1 = \dfrac{L_1}{L_1^2 - L_2^2}$, $c_2 = \dfrac{-L_2}{L_1^2 - L_2^2}$, θ_u is the voltage vector angle in the αβ-reference frame, and $\bar{v}_{\alpha\beta} = V_m e^{j\theta_u}$.

Since the injection voltage is needed to be applied on the estimated d- or q-axis, it will be more convenient to transform (7.1) to the estimated rotor reference frame, where it allows to use the injected voltage vector for position estimation. For transforming (7.1) from the stationary αβ-reference frame to the rotating estimated dq-reference frame (also noted as the γδ-reference frame), the estimated rotor position $\hat{\theta}_r$ is introduced, as shown in Figure 7.2. By multiplying $e^{-j\hat{\theta}_r}$ on the both sides, equation (7.1) may be rewritten as:

$$\Delta\bar{i}_{\gamma\delta} = \Delta\bar{i}_{\alpha\beta} e^{-j\hat{\theta}_r} = \left(c_1 + c_2 e^{j2\left(\theta_r - \hat{\theta}_r - \hat{\theta}_u\right)}\right)\Delta t\bar{v}_{\gamma\delta} \tag{7.2}$$

where $\bar{v}_{\gamma\delta}$ is the voltage vector represented with respect to the estimated d-axis (γ-axis), $\hat{\theta}_u = \theta_u - \hat{\theta}_r$ is the voltage vector phase angle in the γδ-reference frame.

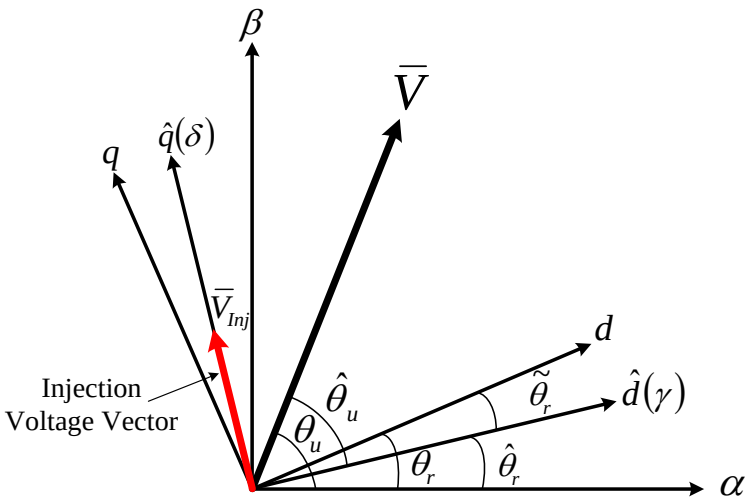

Figure 7.2: Real and estimated rotor reference frames.

As an example, when the injected voltage vector is chose to be aligned with the estimated q-axis (δ-axis), then $\hat{\theta}_u = \frac{\pi}{2}$, $\bar{v}_{\gamma\delta} = V_m e^{j\frac{\pi}{2}}$, as indicated in Figure 7.2. Equation (7.2) may then be represented as:

$$\Delta\bar{i}_{\gamma\delta} = \Delta t c_2 V_m \sin\left(2\tilde{\theta}_r\right) + j\left(\Delta t c_1 V_m - \Delta t c_2 V_m \cos\left(2\tilde{\theta}_r\right)\right) \tag{7.3}$$

where $\tilde{\theta}_r = \theta_r - \hat{\theta}_r$ is the rotor position error. In this situation, the sin component of the position error will be isolated to the real part of (7.3). Therefore, the current variation on the estimated d-axis (γ-axis) will be proportional to the position error, as:

$$\mathrm{Re}\left(\Delta\bar{i}_{\gamma\delta}\right) = \Delta\bar{i}_{\gamma} = k\sin\left(2\tilde{\theta}_r\right) \propto 2k\tilde{\theta}_r \tag{7.4}$$

where $k = \Delta t c_2 V_m$ is a constant. The estimated rotor position and the estimated rotor speed may then be obtained by using the classical PLL controller [2], as shown in Figure 7.3. The same PLL controller is also used in the zero voltage injection method, as discussed in section 6.2.2.

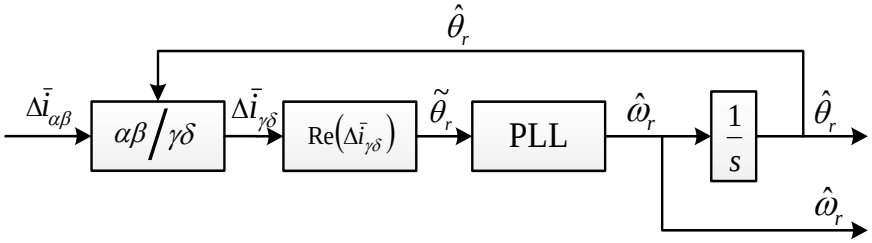

Figure 7.3: Block diagram of PLL controller for recovering the rotor position and speed from the estimated position error.

When the injection voltage vector is applied on the estimated d-axis (γ-axis), then $\hat{\theta}_u = 0$, and $\bar{v}_{\gamma\delta} = V_m e^{j0}$, (7.2) may be developed to:

$$\Delta\bar{i}_{\gamma\delta} = \Delta t c_1 V_m + \Delta t c_2 V_m \cos\left(2\tilde{\theta}_r\right) + j\Delta t c_2 V_m \sin\left(2\tilde{\theta}_r\right) \tag{7.5}$$

The imaginary part of the current variation vector may then be linked to the position error as:

$$\mathrm{Im}\left(\Delta\bar{i}_{\gamma\delta}\right) = \Delta\bar{i}_{\delta} = k\sin\left(2\tilde{\theta}_r\right) \propto 2k\tilde{\theta}_r \tag{7.6}$$

Considering that the rotor position angle may be assumed to be constant during one switching period, the current variation may be transferred from the αβ-reference to the γδ-reference frame by multiplying $e^{-j\hat{\theta}_r}$. Then the current variation in the γδ-reference frame may be obtained by:

$$\Delta\bar{i}_{\gamma\delta} = \left(\Delta i_\alpha + j\Delta i_\beta\right)\left(\cos\hat{\theta}_r - j\sin\hat{\theta}_r\right) \tag{7.7}$$

According to (7.4) and (7.6), the current variation is directly linked to the position error, as:

$$\mathrm{Re}\left(\Delta\bar{i}_{\gamma\delta}\right) = \left(i_{\alpha 1} - i_{\alpha 0}\right)\cos\hat{\theta}_r + \left(i_{\beta 1} - i_{\beta 0}\right)\sin\hat{\theta}_r \tag{7.8}$$

$$\mathrm{Im}\left(\Delta\bar{i}_{\gamma\delta}\right) = -\left(i_{\alpha 1} - i_{\alpha 0}\right)\sin\hat{\theta}_r + \left(i_{\beta 1} - i_{\beta 0}\right)\cos\hat{\theta}_r \tag{7.9}$$

Therefore, the rotor position may then be obtained from the PLL controller by using the measured current variation.

7.3 Simulation and Experimental analysis

7.3.1 Simulation results

The estimated d-/q-axis voltage vector injection method is also first validated in the simulation model. The machine model and the FOC system module are the same as those described in chapter 5 and 6 (as shown in Figure 5.2 and 5.3). Being different from the zero voltage injection method, since the voltage vector is applied on the estimated d- or q-axis, the estimated rotor position needs to be used as the feedback for the injection. Figure 7.4 shows the voltage injection scheme which was implemented in the Matlab/Simulink. $\hat{\theta}_r$ is used for locating the injection voltage vector on the estimated d- or q-axis, and the magnitude of the injection voltage is set as 30 V.

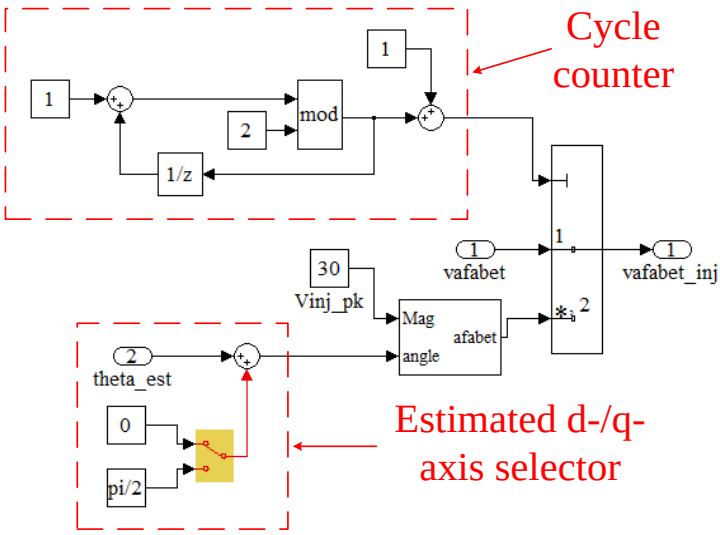

Figure 7.4: Diagram of output voltage selector.

For determining the current ripples caused by the injection voltage, Figure 7.5 shows the current details when the voltage vector is injected on the γ- and δ-axes respectively. The machine is controlled to operate at 9 rpm without the load, and the estimated rotor position is used as the feedback. The position is estimated by using (7.6) and (7.4), correspondingly.

Figure 7.5 shows the current profile when the machine operates at steady state. It may be observed from Figure 7.5(a) that when the voltage is injected on the δ-axis, the real q-axis current will have a larger ripple, as expected. The ripple on the q-axis current is around ±0.2 A, and the ripple on the d-axis current is much smaller. Figure 7.5 (b) shows that when the voltage is injected on the γ-axis, the q-axis current ripple can be greatly reduced to almost 0 A, but the current ripple on the d-axis is around ±0.25 A.

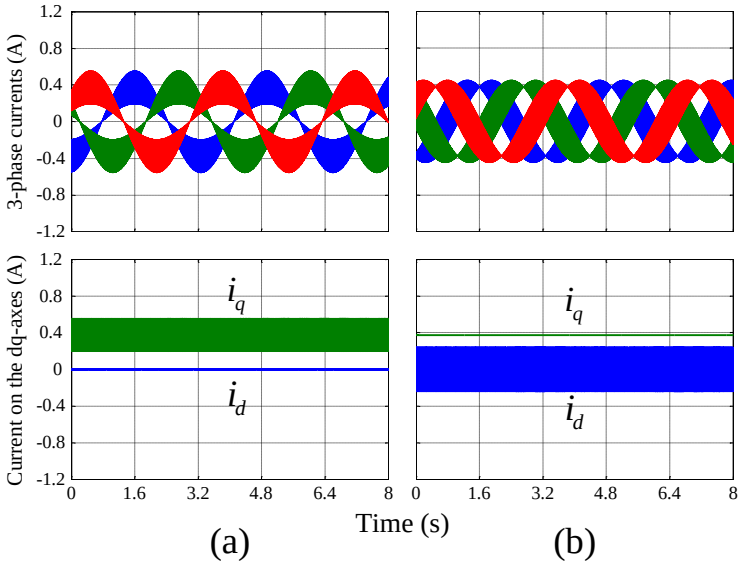

Figure 7.5: Simulation results for the steady state current in the machine real dq-reference frame for the two proposed injection methods. (a) Voltage injected on the δ-axis (b) Voltage injected on the γ-axis.

Figure 7.6 and Figure 7.7 show the system performances when the different injection strategies are applied in the transient FOC system respectively. The estimated rotor position is used as the feedback, and the machine operates at 9 rpm. When the voltage vector is injected on the δ-axis, the PI parameters used in the q-axis current controller is set as: $K_p = 50$, $K_i = 15000$; and the PI parameters used in the d-axis current controller is set as: $K_p = 40$, $K_i = 12000$. On the contrary, when the voltage vector is injected on the γ-axis, the PI parameters used in the q-axis current controller is set as: $K_p = 40$, $K_i = 12000$; and the PI parameters used in the d-axis current controller is set as: $K_p = 50$, $K_i = 15000$. The PI parameters for the rotor speed controller is still set as: $K_p = 2$, $K_i = 30$. The PI parameters for the PLL controller is still set as: $K_p = 30$, $K_i = 200$. As shown in both Figure 7.6 and Figure 7.7, this estimated d-/q-axis voltage vector injection method provides a very good estimated rotor position signal for the system. When the voltage vector is injected on the estimated q-axis, there is a -0.05 degree DC bias in the rotor position error since the 90% rated load applies on the

machine, as shown in Figure 7.6. Figure 7.7 shows the situation when the voltage vector is injected on the estimated d-axis, the DC bias becomes +0.1 degree both with and without the load. These very small DC biases in the estimated rotor position are both caused by the back-EMF term which is neglected since the rotor speed is assumed to be zero ideally. It was observed from simulation that this DC bias will increase when the rotor speed increases, which supports the previous statement.

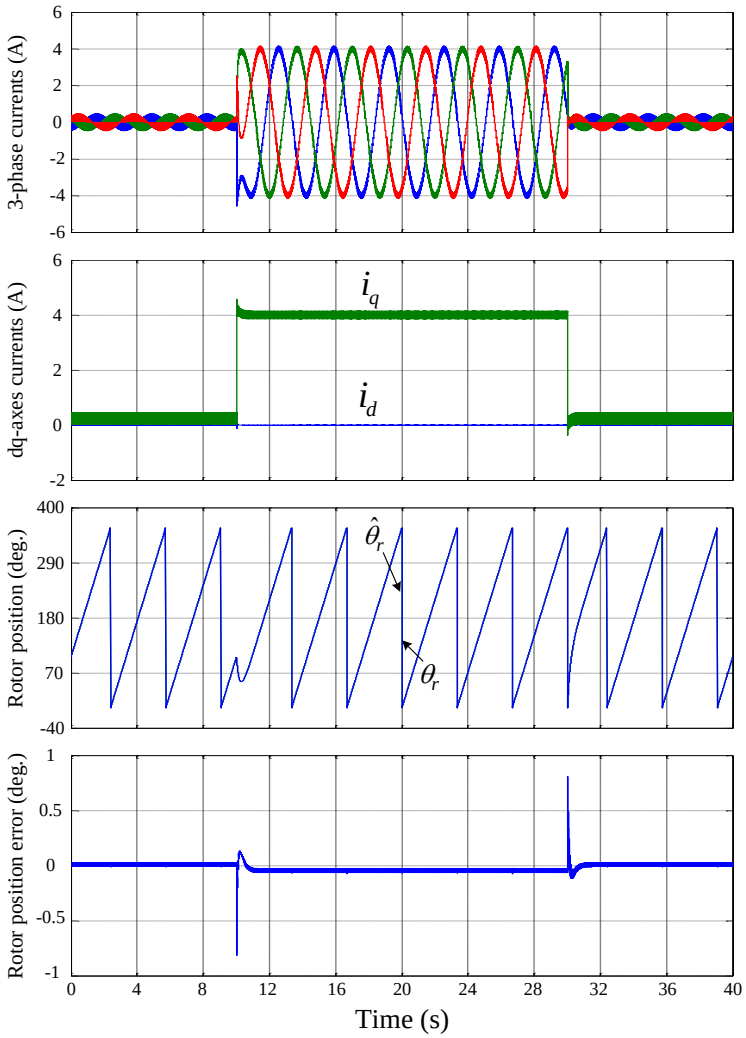

Figure 7.6: Simulation results with 100% rated torque step at 9 rpm (with the δ-axis injection voltage).

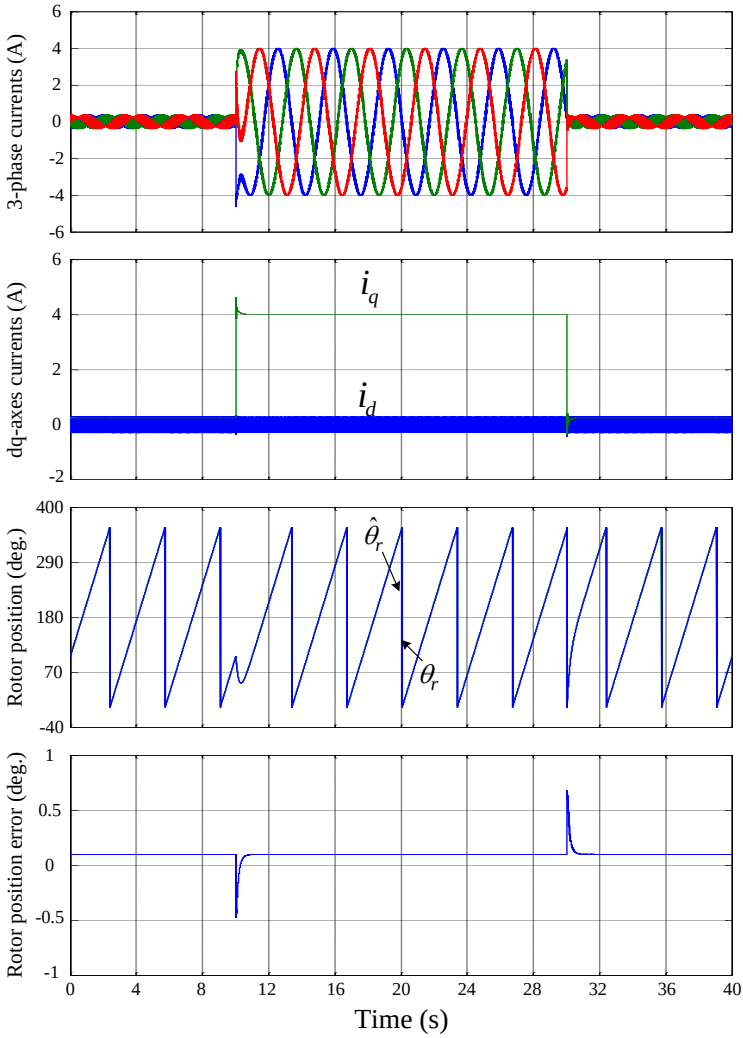

Figure 7.7: Simulation results with 100% rated torque step at 9 rpm (with the γ-axis injection voltage).

7.3.2 Experimental results

The estimated d-/q-axis voltage vector injection method is then implemented on the experimental drive system. The PI parameters used in the experimental system are the same as the values used in the simulation module. Considering the dead-time voltage error, the magnitude of the injection voltage vector is set to be 45 V. The first experiment is to measure the current ripple when the voltage vector is injected into the

control system. The same as Figure 7.5, the voltage is injected on the γ- and δ-axis respectively. Figure 7.8 shows a similar result as Figure 7.5, but the current has a big background noise which comes from the measurement. According to the torque equation of a PMSM, the q-axis current has a predominant influence on the torque. Therefore it is preferred to inject the voltage vector on the estimated d-axis (Figure 7.5(b) and Figure 7.7), which can reduce the ripple in the q-axis current and consequently the torque ripple.

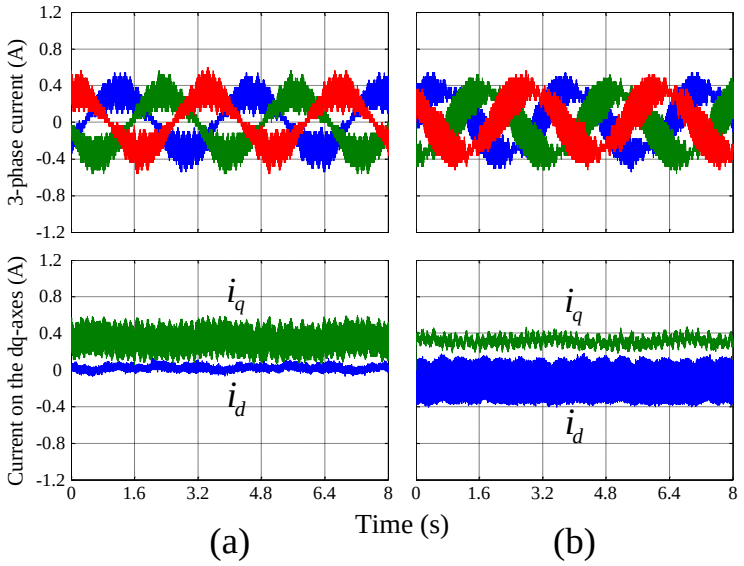

Figure 7.8: Experimental results for the steady state current in the machine real dq-reference frame for the two proposed injection methods. (a) Voltage injected on the δ-axis (b) Voltage injected on the γ-axis.

In this estimated d-/q-axis voltage vector injection method, no filter is used in the current control loop. Therefore, this injection method will have little influence on the current control loop bandwidth.

Figure 7.9 shows the experimental result of the current step responses with and without the injection method. The current step command is given on the d-axis so the machine will not rotate during this transient period. For comparing the performances of the

current-loop controllers, the same PI parameters are used in the current controllers with/without the voltage injection. Figure 7.9(a) shows the d-axis current response without the injection voltage and Figure 7.9(b) shows the d-axis current response with the δ-axis injection voltage. The rise time of the d-axis current is very similar when comparing Figure 7.9(a) with Figure 7.9(b), which is around 0.8 ms.

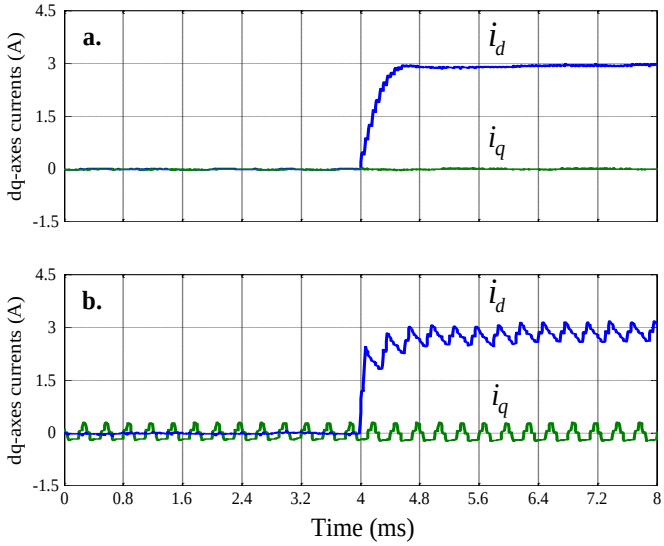

Figure 7.9: Experimental results for the current response with/without voltage injection for position estimation. (a) Without voltage injection. (b) With voltage injection on the δ-axis.

Figure 7.10 and Figure 7.11 show the system performance when the machine operates with load. The injection voltage is still applied on the estimated d- and q-axis respectively. Compared with the simulation results shown in Figure 7.6 and Figure 7.7, the ripple in the estimated rotor position is around ±3.5 degrees. But there is an around -12 degrees DC bias appearing in the rotor position error, which means the estimated rotor position leads the real position by 12 degrees, and the real d-axis current becomes -1.2 A. This DC bias is caused by the inverter voltage error, due to which the injection voltage vector cannot be injected precisely on the target axis due to the voltage error [4], [5]. The estimated rotor position calculated by the current variation will then have a steady state DC bias. Similar DC bias position error may also be observed in many

other methods [6]-[11], where this DC bias error could be up to 18~28 degrees when the machine operates at low speed [11]. For improving the performance of the estimator, this estimated rotor position DC bias needs to be eliminated by minimizing the inverter voltage error effects.

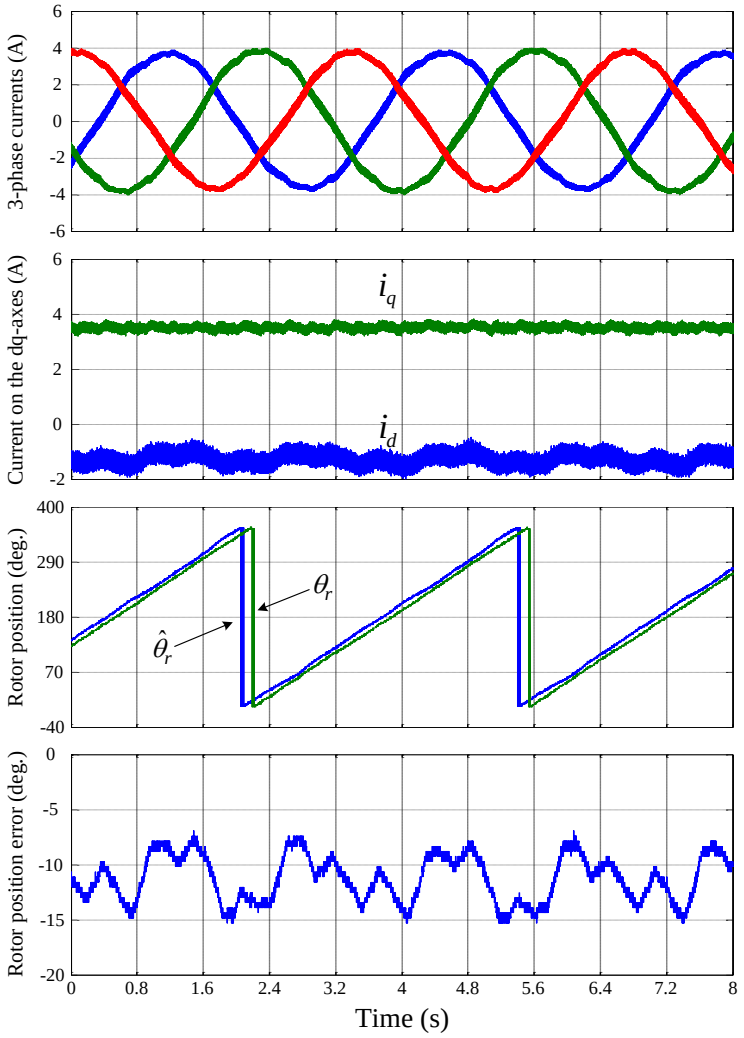

Figure 7.10: Experimental results at steady status of the machine with 90% rated load (with the γ -axis injection voltage).

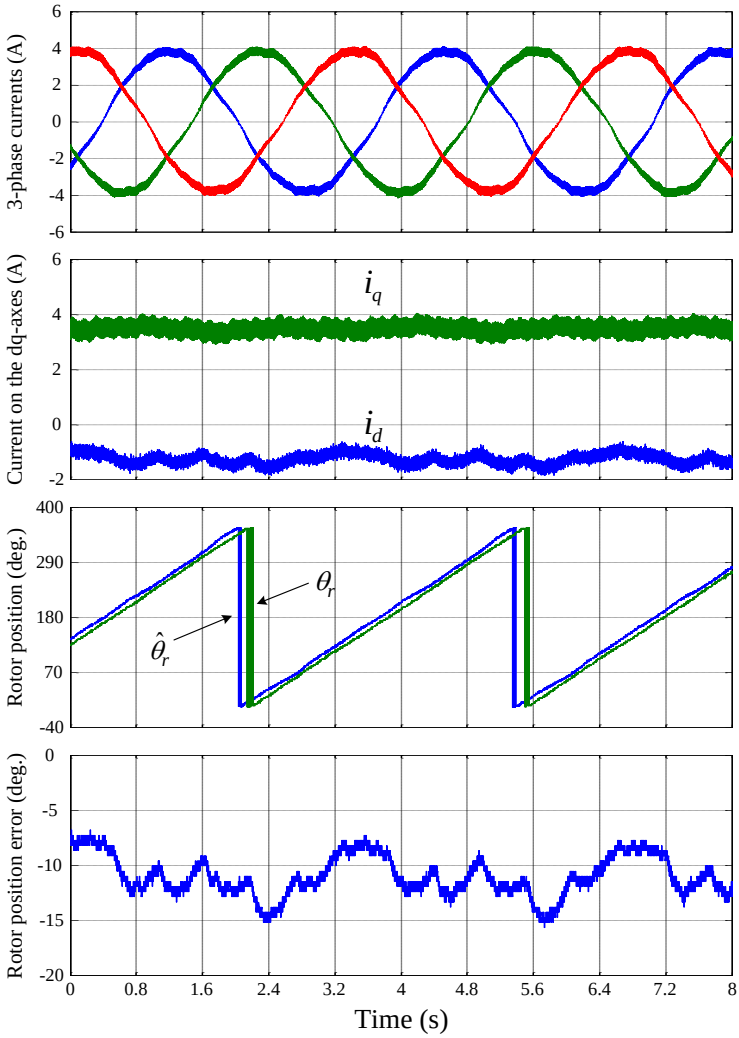

Figure 7.11: Experimental result at steady status of the machine with 90% rated load (with the δ-axis injection voltage).

7.4 Inverter voltage error minimization

7.4.1 Inverter voltage error effects analysis

As it may be observed from (7.1) that, the coefficient C_1 is much larger than C_2. In the estimated d-/q-axis voltage vector injection method, when the voltage is injected on the estimated q-axis, C_1 related term will only appear in the imaginary part of (7.3). The

position error is obtained by utilizing the real part of (7.3). The term associated to C_1 is then eliminated [3]. The INFORM method uses very similar principle [1]. By combining the current variations caused by the three injecting voltage vectors, C_1 related term is finally eliminated. The term associated to C_2 is then used for estimating the position. In the estimated d-/q-axis voltage vector injection method, the voltage vector cannot be injected on the desired axis due to the inverter voltage error. The term associated to C_1 may then not be totally eliminated in the algorithm. Moreover, a small voltage error may be enlarged by C_1. The position estimation accuracy is then significantly affected.

Considering that the inverter voltage error is very difficult to be compensated accurately, especially under the voltage injection method, as discussed in chapter 4. Therefore, the nonlinear inverter voltage error is proposed to be compensated before being applied to the motor terminals.

7.4.2 Implementation of voltage error minimization

Since the injection voltage is not equal to zero or is applied on the stator phase axis, minimizing the voltage error by compensating duty cycle of the gate signal may be too complicated to implement. Therefore, a new strategy of using two opposite injection voltage to offset the inverter voltage error is applied in the drive system. The new injection scheme is illustrated in Figure 7.12. In the new scheme, two voltage vectors with opposite directions are injected consequently following the FOC switching period.

As shown in Figure 7.12, in the first injection period, the voltage vector is injected on the δ-axis ($V_m e^{j\pi/2}$) for example. The second voltage vector on the minus δ-axis ($V_m e^{-j\pi/2}$) is injected consequently in the following switching period. Figure 7.13 shows the diagram of the two opposite injection voltage vectors.

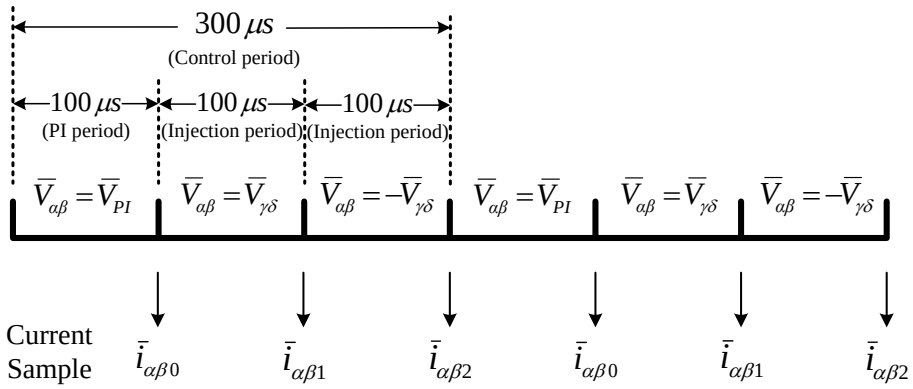

Figure 7.12: Modified voltage injection sequence.

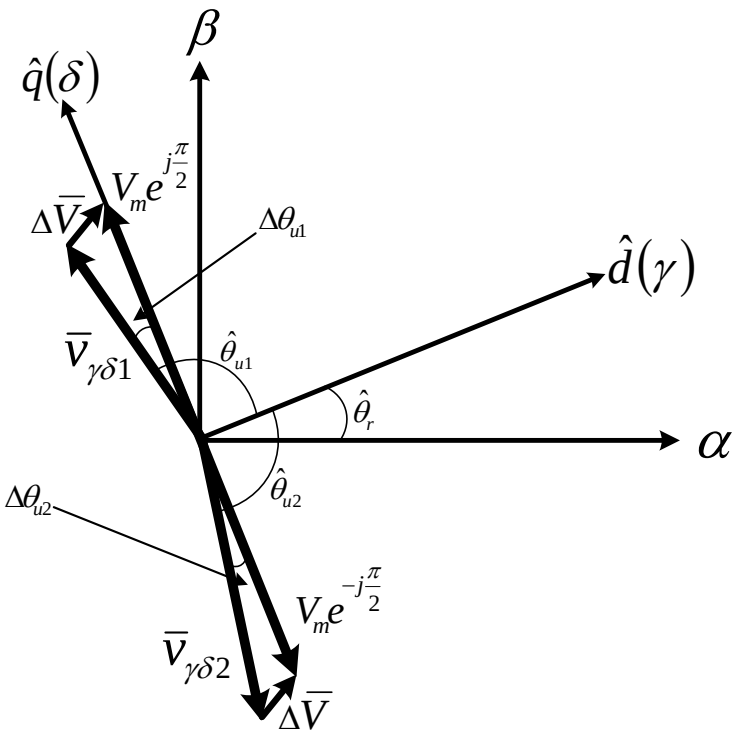

Figure 7.13: Opposite voltage injection scheme for minimizing the voltage error effects.

Assuming that the inverter voltage error will not change during these two injection switching periods, the actual voltage vectors applied to the machine may be expressed as:

$$V_m e^{j\hat{\theta}_{u1}} = V_m e^{j\pi/2} - \Delta\overline{V} \tag{7.10}$$

$$V_m e^{j\hat{\theta}_{u2}} \approx V_m e^{-j\pi/2} - \Delta\overline{V} \tag{7.11}$$

where subscripts 1 and 2 denotes the first injection period and the second injection period, $\Delta\overline{V}$ is the voltage error. Therefore, by following (7.2), the current variations in the estimated dq-reference may be rewritten as:

$$\Delta\bar{i}_{\gamma\delta 1} = \Delta t c_1\left(V_m e^{j\pi/2} - \Delta\overline{V}\right) + \Delta t c_2 e^{j2\tilde{\theta}_r} \cdot e^{-j\hat{\theta}_{u1}} V_m \tag{7.12}$$

$$\Delta\bar{i}_{\gamma\delta 2} = \Delta t c_1\left(V_m e^{-j\pi/2} - \Delta\overline{V}\right) + \Delta t c_2 e^{j2\tilde{\theta}_r} \cdot e^{-j\hat{\theta}_{u2}} V_m \tag{7.13}$$

As shown in Figure 7.13, the two injection voltage vector angles in the estimated dq-reference frame are $\hat{\theta}_{u1} = \frac{\pi}{2} + \Delta\theta_{u1}$, $\hat{\theta}_{u2} = -\frac{\pi}{2} - \Delta\theta_{u2}$. Since $\Delta\theta_{u1} \approx \Delta\theta_{u2}$, it is not difficult to derive that:

$$\mathrm{Re}\left(\Delta\bar{i}_{\gamma\delta 1} - \Delta\bar{i}_{\gamma\delta 2}\right) = 2\Delta t c_2 V_m \cos\left(\Delta\theta_{u1}\right)\sin\left(2\tilde{\theta}_r\right) \tag{7.14}$$

And the angle $\Delta\theta_{u1}$ is very close to zero, (7.14) can be represented as:

$$\mathrm{Re}\left(\Delta\bar{i}_{\gamma\delta 1} - \Delta\bar{i}_{\gamma\delta 2}\right) = 2k\sin\left(2\tilde{\theta}_r\right) \approx 4k\tilde{\theta}_r \tag{7.15}$$

Equation (7.15) shows very similar result to (7.4). However, the inverter voltage error is eliminated in (7.15)

Similar idea can be applied on the estimated d-axis, then the injection voltages become $V_m e^{j0}$ and $V_m e^{j\pi}$. By following the same steps described above, the position error may be obtained from the imaginary part of the current variation term as:

$$\mathrm{Im}\left(\Delta\bar{i}_{\gamma\delta 1} - \Delta\bar{i}_{\gamma\delta 2}\right) = 2k\sin\left(2\tilde{\theta}_r\right) \approx 4k\tilde{\theta}_r \tag{7.16}$$

7.4.3 Experimental results with the voltage error minimization

Figure 7.14 shows the experimental results when the improved method with the voltage error minimization is applied in the sensorless drive system. In this experiment, the estimated rotor position and the speed from the encoder are used as the feedback. Compared to the results shown in Figure 7.10, where only one injection voltage is used, the DC bias in the estimated position during the loaded state has now been largely minimized. The ripple in the estimated position when the machine operates at steady state is around ±3 degrees.

Due to the PLL controller is used for obtaining the estimated rotor position, when the machine operates at a speed lower than 9 rpm, the magnitude of the injection voltage needs to increase from 45 V to 75 V. In this situation, a better estimated rotor position signal can be obtained, and the PI controller for the speed loop has a faster response. As shown in Figure 7.15, when the machine operates at 3 rpm, the higher injection voltage causes a larger ripple in the current, which is ±0.4 A in the q-axis current and ±0.8 A in the d-axis current respectively. The ripple in the estimated rotor position also increases to ±7 degrees with the load, but the transient fluctuation decreases from -20 degrees to -10 degrees when the load is added.

Since the estimated speed from the PLL is used as the feedback for the speed loop, the drive is then under full sensorless control. The drive performance experiencing a step load torque change is shown in Figure 7.16. The magnitude of the injection voltage is set as 45 V. As shown in Figure 7.16, the machine can work with a nearly full rated step load at 30 rpm. The q-axis current ripple is ±0.075 A, and the estimated rotor position ripple is around ±5 degrees.

When the machine is controlled to operate at lower speed, e.g. 6 rpm, 90% rated step load may make the machine unstable during the transient status. This instability is mainly caused by the larger transient fluctuation in the estimated rotor speed. By increasing the injection voltage magnitude to 75 V, a 70% rated load can be step added or removed on the machine successfully. Figure 7.17 shows the system performance in

the transient status. The rotor speed error is around ±90 rpm when the load removes, which is the limit for the speed controller.

Figure 7.18 shows the system performance when the machine operates at 300 rpm (around of the 10% rated frequency) with the step load. Comparing with the situation of operating at 30 rpm (shown in Figure 7.16), the disturbance in the transient states is smaller. However, a fundamental frequency ripple appears in the d- and q-axes currents. This q-axis current ripple may cause the fluctuation in the rotor speed in the steady status. This sinusoidal fundamental frequency ripple may be caused by the back-EMF which is neglected in this sensorless algorithm. Since the rotor speed is up to 300 rpm, the back-EMF voltage cannot be neglected anymore.

Figure 7.19, 7.20 and 7.21 show the full sensorless drive system performances with the varying reference speed commands. There is no load applied on the machine during these experiments. Figure 7.19 shows the experimental results when the reference speed increases step from 30 rpm to 90 rpm. When the speed command reveres from 30 rpm to -30 rpm, the estimated rotor position error is well maintained below 10 degrees during the transient state, as shown in Figure 7.20. Figure 7.21 shows the result when the rotor reference speed increases from 30 rpm to 300 rpm with a slope. Since the reference speed rises as a slope, the real machine speed increases without any fluctuation, and the ripple in the estimated rotor position decreases from ±7 degrees to ±2 degrees when the machine operates stably at 300 rpm.

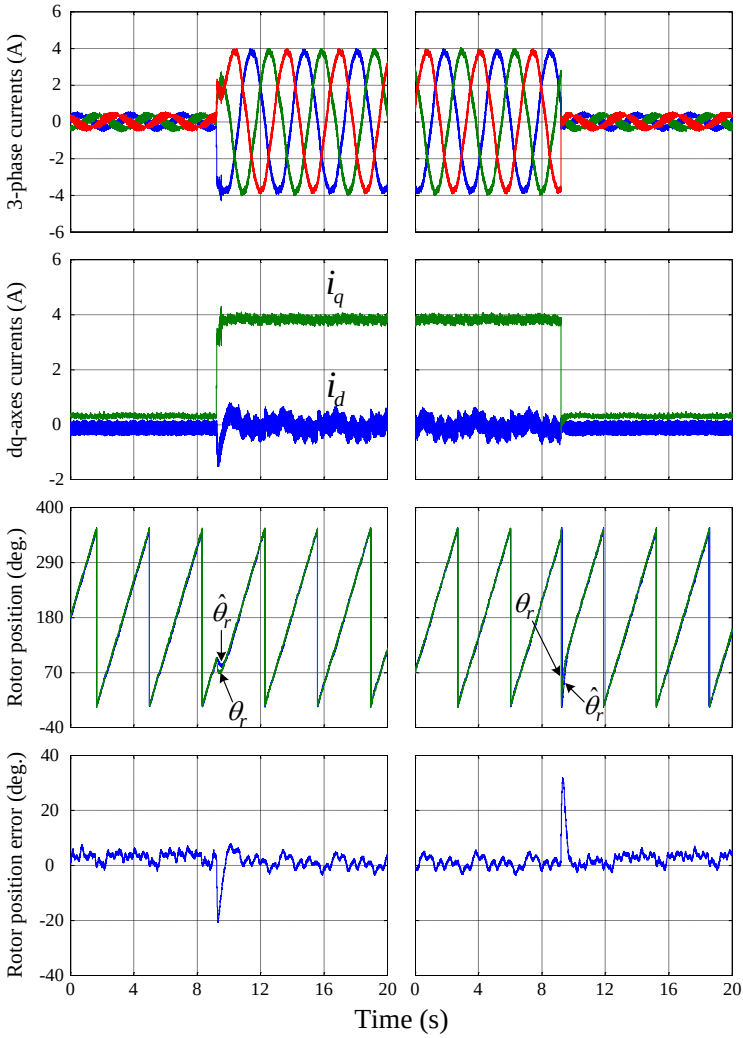

Figure 7.14: Experimental results with 90% rated torque step at 9 rpm (with estimated rotor position as feedback and with opposite voltage injected on the γ-axis injection).

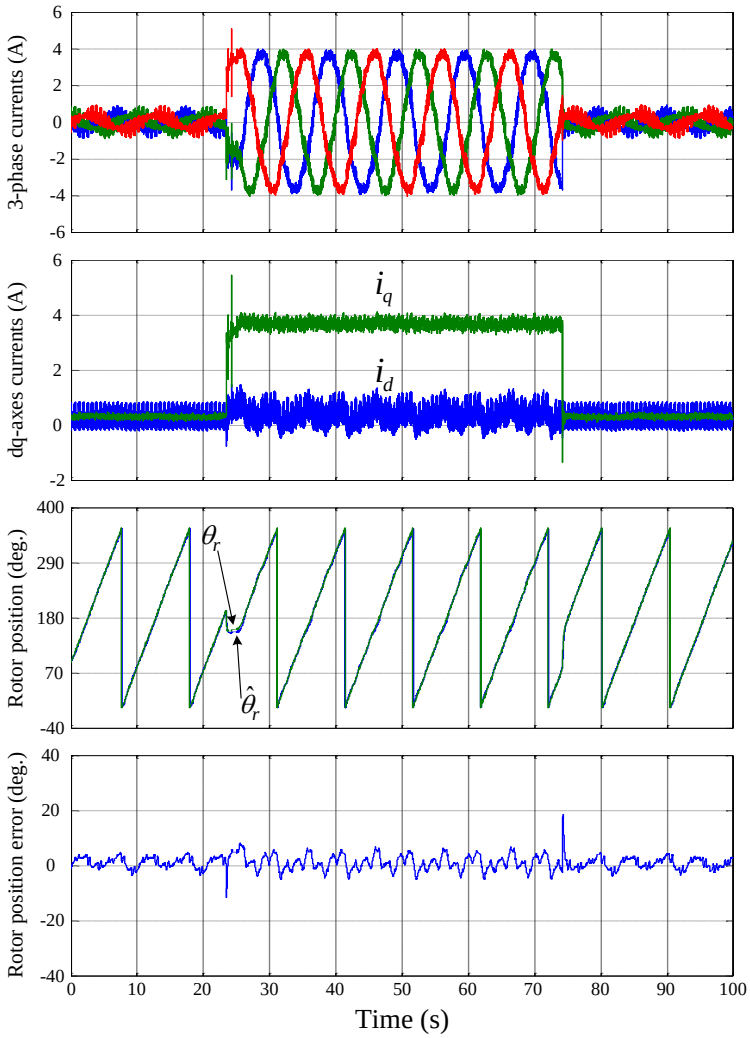

Figure 7.15: Experimental results with 90% rated torque step at 3 rpm (with estimated rotor position as feedback and with opposite voltage injected on the γ-axis injection).

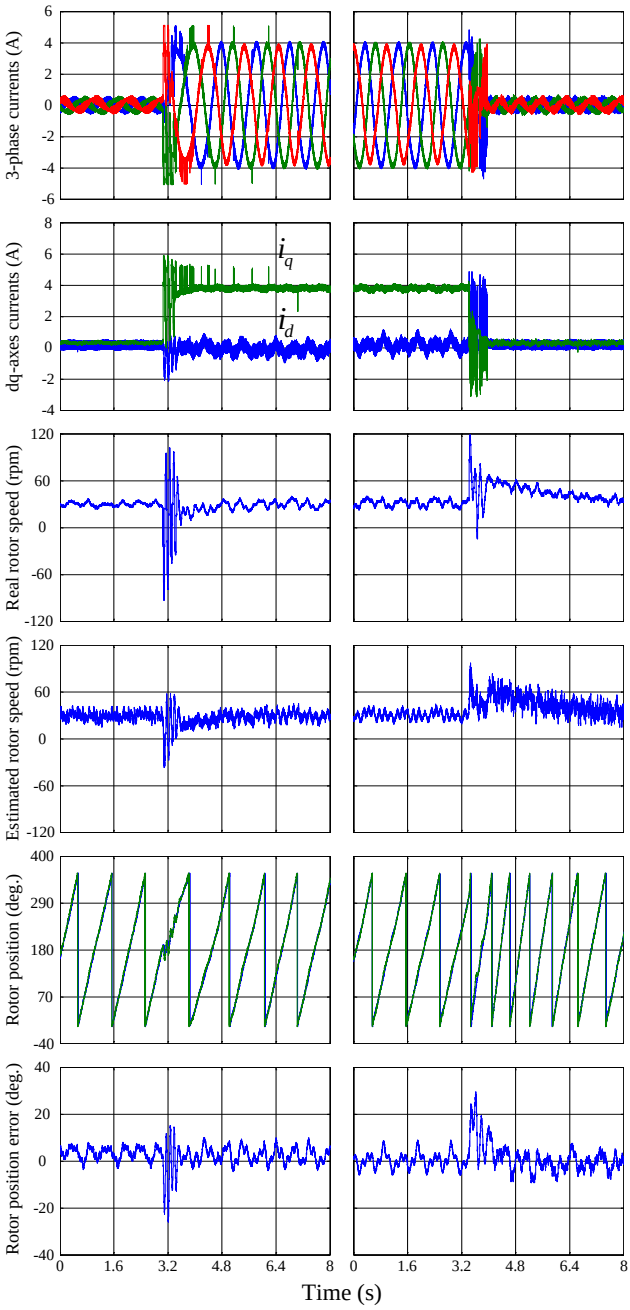

Figure 7.16: Experimental results with 90% rated torque step at 30 rpm (with estimated rotor position and speed as feedback and with opposite voltage injected on the γ-axis injection).

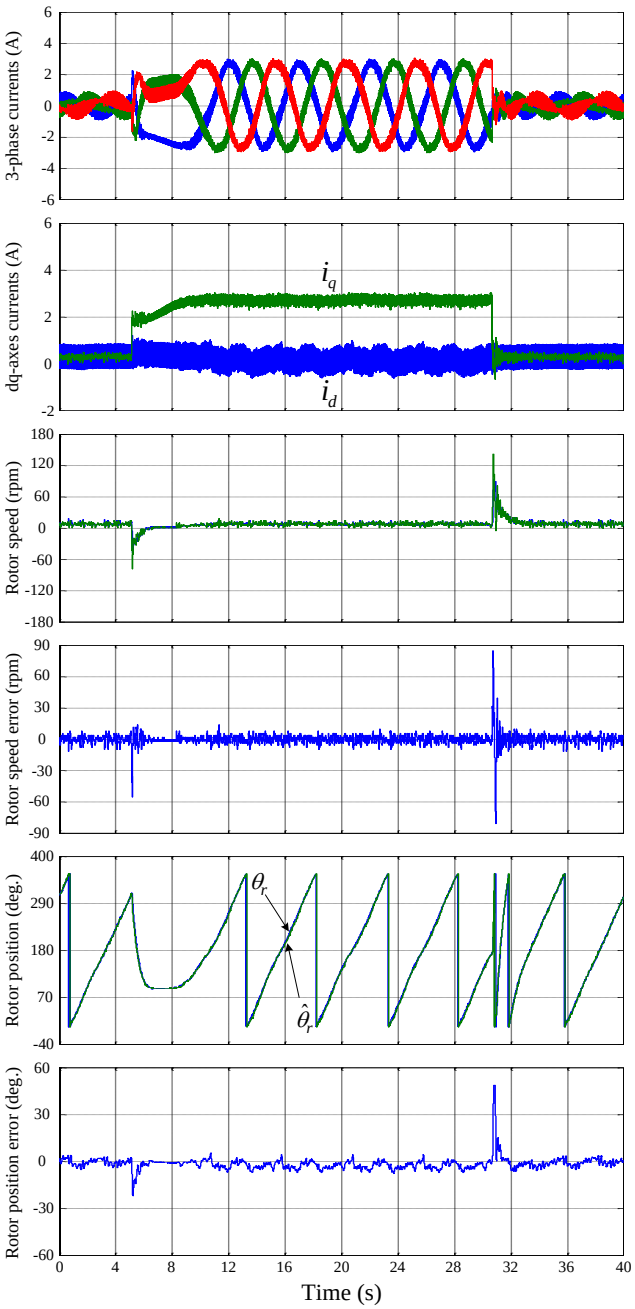

Figure 7.17: Experimental results with 70% rated torque step at 30 rpm (with estimated rotor position and speed as feedback and with opposite voltage injected on the γ-axis injection).

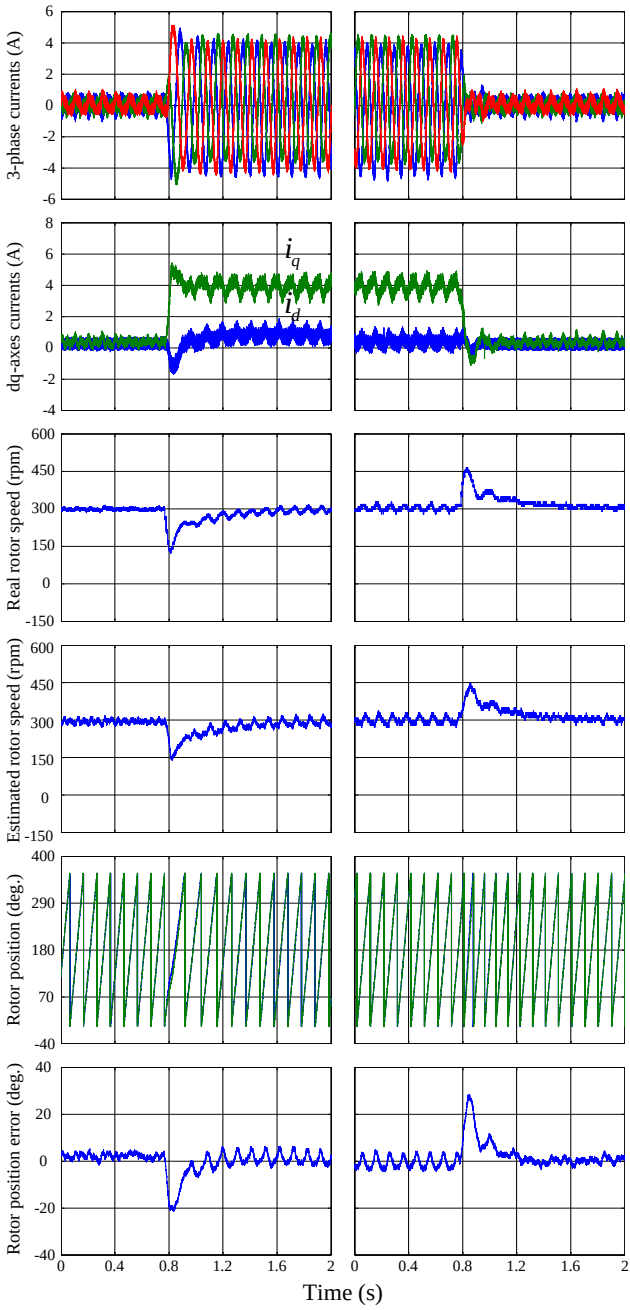

Figure 7.18: Experimental results with 95% rated torque step at 300 rpm (with estimated rotor position and speed as feedback and with opposite voltage injected on the γ-axis injection).

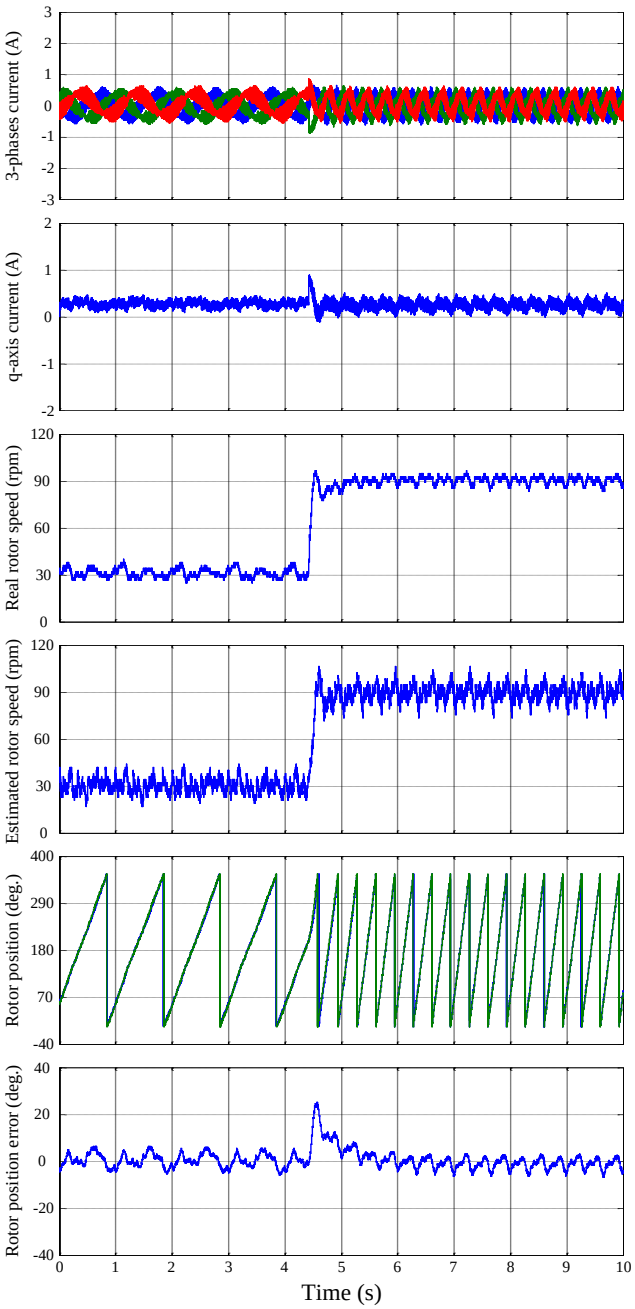

Figure 7.19: Experimental results with speed step from 30 rpm to 90 rpm (with estimated rotor position and speed as feedback and with opposite voltage injected on the γ-axis injection).

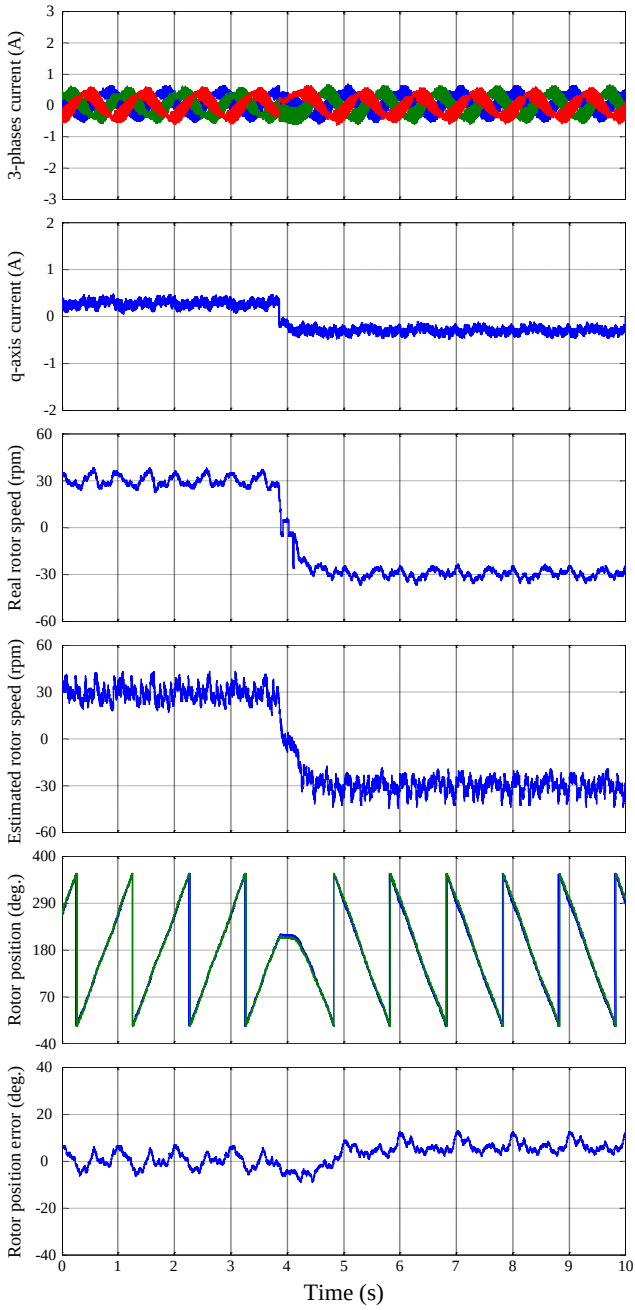

Figure 7.20: Experimental results with speed reverse from 30 rpm to -30 rpm (with estimated rotor position and speed as feedback and with opposite voltage injected on the γ-axis injection).

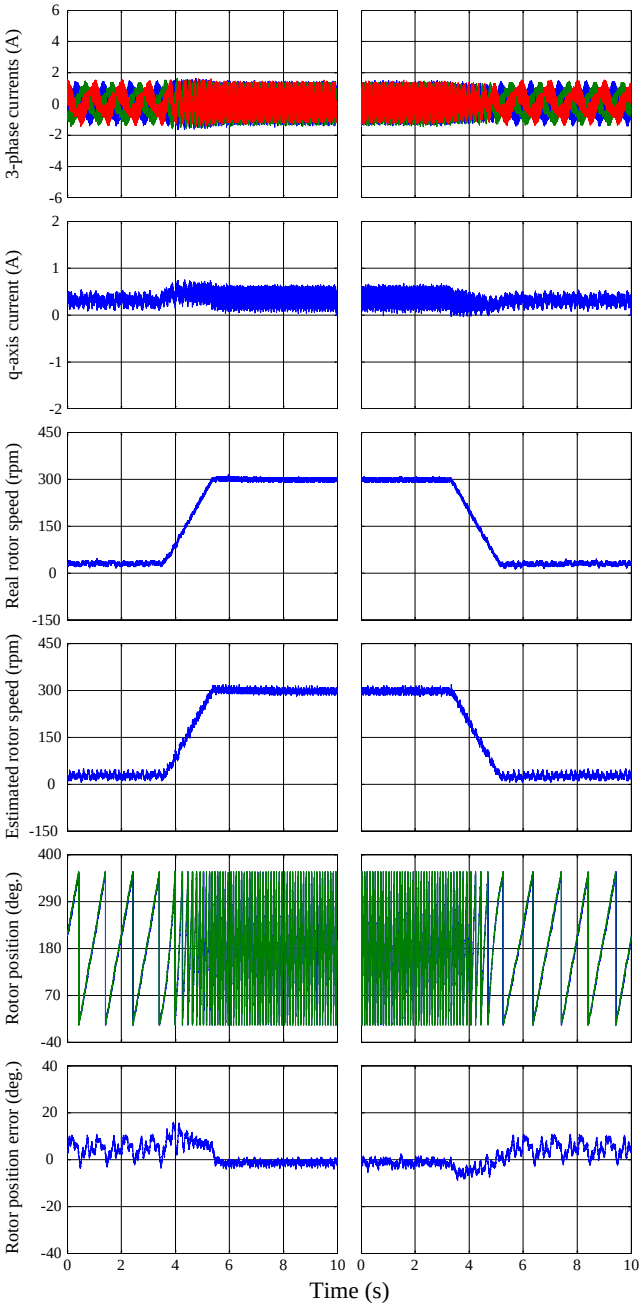

Figure 7.21: Experimental results with slope rising speed from 30 rpm to 90 rpm (with estimated rotor position and speed as feedback and with opposite voltage injected on the γ-axis injection).

7.5 Summary

The estimated d-/q-axis voltage vector injection sensorless control method has been presented in this chapter. In this method, the single voltage vector with a constant magnitude is injected on the estimated d-, or q-axis between two FOC switching periods. The current variations during the injection period are directly used for estimating the rotor position.

Compared with the classical INFORM method, there is only one voltage pulse needs to be injected in each control period. Therefore, the control frequency of this method is twice as the INFORM method, and the current distortion is also smaller than the INFORM method. There is no machine parameters involved in the calculation for the rotor position, and the filters are also unnecessary in the current control loop although this sensorless method is based on voltage injection.

However, the inverter voltage error will affect the estimation accuracy like in other voltage injection based sensorless control methods. This disturbance caused by the voltage error can be well eliminated by using an additional injection voltage pulse, as discussed in this chapter. The compensation voltage vector is injected on the opposite axis with the same magnitude, thus the number of the injection periods becomes two. In this way, the inverter voltage error can be greatly compensated in the rotor position estimation.

The experimental results show that the estimated d-/q-axis voltage vector injection algorithm provides an accurate estimated rotor position and speed. The sensorless drive exhibits a good performance in different operation conditions.

Bibliography

[1] M. Schroedl, “Sensorless Control of AC Machines at Low Speed and Standstill Based on the “INFORM” Method,” *IEEE IAS Annual Meeting,* pp. 270-277, Oct 1996.

[2] J. L. Chen, T. H. Liu, C. L. Chen, "Design and implementation of a novel high-performance sensorless control system for interior permanent magnet synchronous motors," *IET Electric Power Application,* vol. 4, no. 4, pp. 226-240, Apr 2010.

[3] O. Benjak, D. Gerling, "Review of position estimation methods for PMSM drives without a position sensor, part III: Methods based on saliency and signal injection," *International Conference on Electrical Machines and Systems,* pp. 873-878, Oct 2010.

[4] G. T. Shen, W. X. Yao, B. Chen, K. Wang, K. Lee, Z. Y. Lu, "Automeasurement of the Inverter Output Voltage Delay Curve to Compensate for Inverter Nonlinearity in Sensorless Motor Drives," *IEEE Transaction on Power Electronics,* vol. 29, no. 10, pp. 5542-5553, Oct 2014.

[5] Z. D. Zhang, L. Y. Xu, "Dead-Time Compensation of Inverters Considering Snubber and Parasitic Capacitance," *IEEE Transaction on Power Electronics,* vol. 29, no. 6, pp. 3179-3187, Jun 2014.

[6] M. J. Corley, R. D. Lorenz, "Rotor position and velocity estimation for a salient-pole permanent magnet synchronous machine at standstill and high speeds," *IEEE Transaction on Industry Applications,* vol. 34, no. 4, pp. 784-789, Jul/Aug 1998.

[7] J. H. Jang, S. K. Sul, J. I. Ha, K. Ide, and M. Sawamura, "Sensorless drive of surface-mounted permanent-magnet motor by high-frequency signal injection based on magnetic saliency," *IEEE Transaction on Industry Applications,* vol. 39, no. 4, pp. 1031-1039, Jul/Aug 2003.

[8] J. Holtz, "Acquisition of Position Error and Magnet Polarity for Sensorless Control of PM Synchronous Machines," *IEEE Transaction on Industry Applications,* vol. 44, no. 4, pp. 1172-1180, Jul/Aug 2008.

[9] J. M. Liu, Z. Q. Zhu, "Novel Sensorless Control Strategy With Injection of High-Frequency Pulsating Carrier Signal Into Stationary Reference Frame," *IEEE Transaction on Industry Applications,* vol. 50, no. 4, pp. 2574-2583, Jul/Aug 2014.

[10] D. Paulus, P. Landsmann, and R. Kennel, "Sensorless field-oriented control for permanent magnet synchronous machines with an arbitrary injection scheme and direct angle calculation," *Symposium on Sensorless Control for Electrical Drives*, pp. 41-46, Sep 2011.

[11] I. Boldea, M. C. Paicu, G. D. Andreescu, F. Blaabjerg, " 'Active Flux' DTFC-SVM Sensorless Control of IPMSM," *IEEE Transaction on Energy Conversion*, vol. 24, no. 2, pp. 314-322, Jun 2009.

Chapter 8
Conclusion

This chapter presents the conclusions of the dissertation and the future works.

8.1 Conclusions

Sensorless control for PMSM has been increasingly studied and researched for over 20 years. Different kinds of sensorless algorithms have been successfully used in the industrial applications. However, since the sensorless methods are more and more applied on the different types of PM machines, the parameters of the machine such as stator resistance, inductances on the dq-axes or PM flux linkage may be needed in the rotor position estimation. Therefore, the parameter independent sensorless control methods can bring a lot of advantages into the PMSM drive system. Comparing with the sensorless methods which rely on the machine parameters, the parameter independent sensorless control methods are more stable and universal. There is no need to use the additional equipment to measure the machine parameters for the drive system, and the sensorless control algorithm will not be affected by the changes of the machine parameters. Conversely, the parameter independent sensorless control methods can provide an online estimation for the machine parameters.

The main work of this dissertation was to introduce some voltage pulse injection based parameter independent sensorless control methods which can estimate the rotor position and speed directly by the current variations cause by the injection voltage. These sensorless algorithms are all very easy to implement in the drive system. The currents sampled on the three phases are the only variables used in the estimation, thus the machine parameters will not be involved in the algorithms. No low pass filters or

band pass filters are needed for the current controller in these sensorless methods, so the drive system may have a higher bandwidth and better performance.

In different voltage pulse injection based methods, the INFORM method is a classical voltage injection method which was proposed by Manfred Schroedl. The INFORM method is easy to implement and yields good results ideally. However, the inverter voltage error may seriously affect the performance of this method. A simple nonlinear voltage error compensation strategy was introduced to improve the INFORM method. The nonlinear voltage error of the inverter is first limited to one phase only and then compensated through a measured inverter voltage error curve. This compensation method can largely minimize the effects of the inverter voltage error. A sector estimation method based on the INFORM injection scheme was proposed consequently. In this method, the rotor position error between the real rotor position and estimated one was controlled within ±15 degrees even experiencing step load change dynamics.

Being different from the INFORM method, two different voltage pulses injection methods which use only one injection switching period for estimating the rotor position were introduced in this dissertation. In the INFORM method, three voltage vectors are injected on the a-, b- and c-axes sequentially. Thus three switching periods are needed for the rotor position estimation. In these two proposed voltage injection method, a single voltage vector is injected between two FOC commanded PWM switching periods. Therefore, the injection frequency is half of the inverter switching frequency, and the control frequency of the zero voltage vector injection method is twice as the INFORM method.

In the zero voltage injection method, there is no voltage output from the inverter during the injection period. The back-EMF voltage is used as the injection voltage. The current variations may be detected when the back-EMF voltage is high enough. Therefore, the zero voltage injection method is preferred to be used in the medium to high speed range. Both simulation and experimental results have shown that the zero voltage injection method can provide a good performance for the rotor position estimator and the drive system. A PM flux linkage online estimation method based on

the zero voltage injection schemes was also proposed. The experimental results have shown a good accuracy for the estimation at different operation speed conditions.

In the new estimated d-/q-axis voltage vector injection method, the single voltage vector with a constant magnitude is applied on the estimated d- or q-axis as the injection voltage. Similar to the zero voltage injection method, the current ripples during the injection period are used for calculating the rotor position. This sensorless method can be used at very low speed and standstill condition. However, the inverter nonlinear voltage error may bring a DC bias into the estimated rotor position. For compensating the inverter voltage error, an additional switching period is sacrificed in this proposed method. The experimental results have shown that the estimated d-/q-axis voltage vector injection method based sensorless drive system exhibits a great performance in both steady state and different transient operation conditions when the machine operates at a very low speed.

8.2 Future work

Three parameters independent sensorless control methods have been discussed in detail in the dissertation. There still have some interesting topics about the sensorless control of PMSM that are worth to be investigated. The topics can be developed in the future research work and are listed as below:

- **Nonlinear voltage error compensation.**

  In the voltage injection based sensorless control methods, the accuracy of the injection voltage may affect the estimation accuracy of the rotor position. The voltage error from the inverter cannot be avoided in any drive systems. As discussed in chapter 4, the inverter nonlinear voltage error may be very difficult to be compensated accurately in all three phases. Since the voltage error on one single phase will be affected by the currents on the other two phases, a compensation method considering the currents on all three phases needs to be carefully investigated. The reasons for the effects come from different phases currents need to be deeply studied. Then maybe a 3-D table

for the inverter voltage error depending on three-phase currents may then be established and used for the compensation.

- **Machine parameters online estimation.**

  In the parameter independent sensorless control algorithm, the machine parameters will not be involved in the estimation. Since the estimator can provide good estimated rotor position information, the machine parameters may be calculated by the voltage equations of the machine with the estimated rotor position. As an example, the PM flux linkage online estimation has been illustrated in the dissertation. Therefore, other machine parameters such as the resistance and inductance may be also estimated accurately online. Some new parameter estimation algorithms based on the parameters independent sensorless control method could be developed in the future.

- **Parameter independent sensorless control without voltage injection.**

  The parameter independent sensorless control methods presented in the dissertation are all based on the voltage injection. However, the voltage injection based methods bring a large distortion into the current, and the injection period may also decrease the control frequency of the drive system. Therefore, using the current variation inside the PWM switching period to estimate the rotor position is a good topic to be researched. A non-zero voltage vector will change the current in the single switching period. How to detect the current variation inside the switching period and then use this variation to calculate the rotor position will be an interesting and valuable idea for the sensorless control.

- **Validating the parameter independent sensorless control method in different drive system.**

  Due to the limited experimental equipment, all the proposed parameter independent sensorless algorithms are tested in the same drive platform. These sensorless methods should be applied in the drive systems with different power sizes. The performance of the estimator can then be well tested and

compared. The smooth changeover from one type of parameter independent algorithm to another one has a significant importance for the industrial applications. Also adaption on the different power size motor and inverter is very important for further investigations.

Appendix A
Reference Frame Transformations

A.1 Clarke transformation

Clarke transformation is used for converting the variables from the three-phase stationary reference frame into the two-phase stationary reference frame (abc-reference frame to αβ-reference frame). Figure B.1 shows the diagrams of the Clarke transformation.

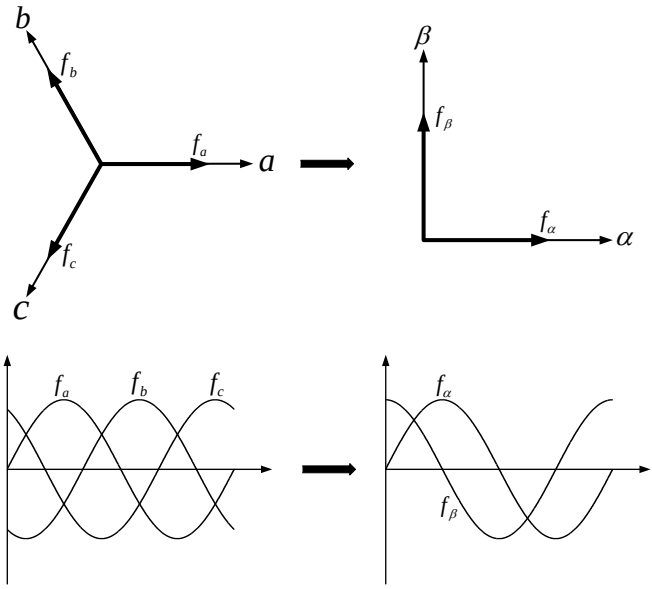

Figure A.1: Clarke transformation.

The Clarke transformation is expressed as:

$$f_\alpha = \frac{2}{3} f_a - \frac{1}{3} f_b + \frac{1}{3} f_c \tag{B.1}$$

$$f_\beta = \frac{2\sqrt{3}}{3} f_b - \frac{2\sqrt{3}}{3} f_c \tag{B.2}$$

where $f_a + f_b + f_c = 0$, (B.1) and (B.2) can be simplified as:

$$f_\alpha = f_a \tag{B.3}$$

$$f_\beta = \frac{2\sqrt{3}}{3}(f_b - f_c) \tag{B.4}$$

A.2 Inverse Clarke transformation

Inverse Clarke transformation is used for converting the variables from the two-phase stationary reference frame into the three-phase stationary reference frame (αβ-reference frame to abc-reference frame). Figure B.2 shows the diagrams of the inverse Clarke transformation.

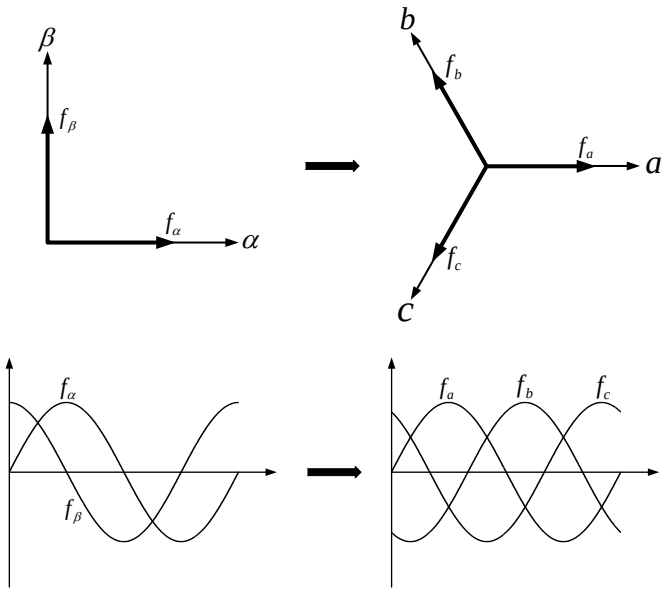

Figure A.2: Inverse Clarke transformation.

The inverse Clarke transformation is expressed as:

$$f_a = f_\alpha \tag{B.5}$$

$$f_b = -\frac{1}{2} f_\alpha + \frac{\sqrt{3}}{2} f_\beta \tag{B.6}$$

$$f_b = -\frac{1}{2} f_\alpha - \frac{\sqrt{3}}{2} f_\beta \tag{B.7}$$

A.3 Park transformation

Park transformation is used for converting the variables from the two-phase stationary reference frame into the two-phase rotating reference frame (αβ-reference frame to dq-reference frame). Figure B.3 shows the diagrams of the Park transformation.

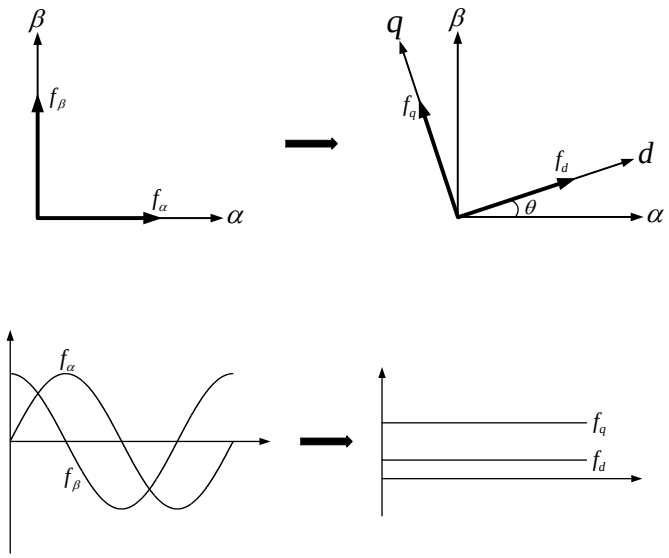

Figure A.3: Park transformation.

The Park transformation is expressed as:

$$f_d = f_\alpha \cos(\theta) + f_\beta \sin(\theta) \tag{B.8}$$

$$f_q = -f_\alpha \sin(\theta) + f_\beta \cos(\theta) \tag{B.9}$$

A.4 Inverse Park transformation

Inverse Park transformation is used for converting the variables from the two-phase rotating reference frame into the two-phase stationary reference frame (dq-reference frame to αβ-reference frame). Figure B.4 shows the diagrams of the inverse Park transformation.

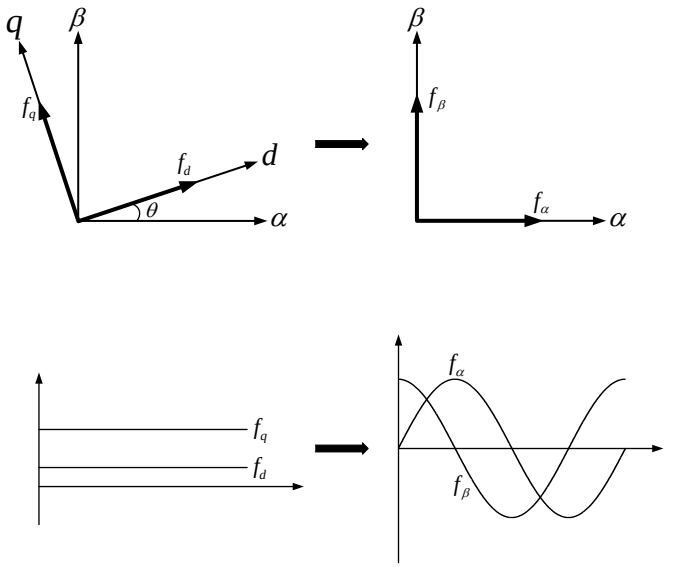

Figure A.4: Inverse Park transformation.

The Park transformation is expressed as:

$$f_\alpha = f_d \cos(\theta) - f_q \sin(\theta) \quad \text{(B.10)}$$

$$f_\beta = f_d \sin(\theta) + f_q \cos(\theta) \quad \text{(B.11)}$$

Appendix B

System Parameters

B.1 PM machine parameters

Type	-	Danfoss HR92C4-44S
Number of poles	-	4
Rated power	-	470 W
Rated speed	-	2850 rpm
Rated frequency	-	95 Hz
Rated torque	-	1.5 Nm
Rated phase voltage	-	380 V
Rated phase current	-	2.9 A
Maximum speed	-	6000 rpm
Maximum phase voltage	-	450 V
Maximum phase current	-	16 A
Stator resistance	-	2.35 Ω
d-axis inductance	-	10.0 mH
q-axis inductance	-	13.4 mH
Rotor permanent magnet flux linkage	-	0.133 Wb

B.2 Load machine parameters

Type	-	GETA GmbH GP115.30
Rated power	-	500 W
Rated speed	-	6000 rpm
Rated voltage	-	170 V

Rated current	-	4 A

B.3 Inverter specifications

Type	-	Danfoss FC-302P3K0T5E20H1
Rated power	-	3.0 kW
Rated Input voltage	-	380V
Rated Input current	-	5.7A
Maximum Input voltage	-	500 V
Maximum Input current	-	6.5 A
Input frequency	-	50~60 Hz
Rated Output voltage	-	380 V
Rated Output current	-	6.3 A
Maximum Output voltage	-	500 V
Maximum Output current	-	7.2 A
Output frequency	-	0~1000 Hz
Dead-time setup	-	2μs

B.4 PI parameters for the controllers

1. INFORM method

- Speed loop:

Ki	-	30
Kp	-	2

- d-axis current loop:

Ki	-	20000
Kp	-	70

- q-axis current loop:

Ki	-	20000
Kp	-	70

2. Zero voltage injection method

- Speed loop:

  Ki - 30

  Kp - 2

- d-axis current loop:

  Ki - 8000

  Kp - 30

- q-axis current loop:

  Ki - 8000

  Kp - 30

- Phase lock loop:

  Ki - 10000

  Kp - 1000

3. Estimated d-axis injection method

- Speed loop:

  Ki - 30

  Kp - 2

- d-axis current loop:

  Ki - 15000

  Kp - 50

- q-axis current loop:

  Ki - 12000

  Kp - 40

- Phase lock loop:

  Ki - 200

  Kp - 30

4. Estimated q-axis injection method

- Speed loop:

  Ki - 30

  Kp - 2

- d-axis current loop:

  Ki - 12000

  Kp - 40

- q-axis current loop:

  Ki - 15000

  Kp - 50

- Phase lock loop:

  Ki - 200

  Kp - 30

Appendix C
DSP Programme Flow

Code Composer Studio (CCS) v4 is used as the human-computer interface for controlling the drive system in this dissertation. The programme code is written and debugged in this software. In the programme, there is only one EPWM interrupt is used, the main programme flow is shown as Figure C.1. A dead loop is used for detecting the parameters input and the enable command. When the enable flag is equal to 1, the programme goes into the interrupt function. In the interrupt programme, the current and the rotor position are sampled by the ADC and QEP modules at first. And then the estimated rotor position and control algorithm are calculated. The duty cycle for the inverter gate signals is then given and loaded into the EPWM register. After the DAC output, the functions in the interrupt programme is finished. When the enable flag is detected to be 0, the interrupt programme will stop and go back to the dead loop.

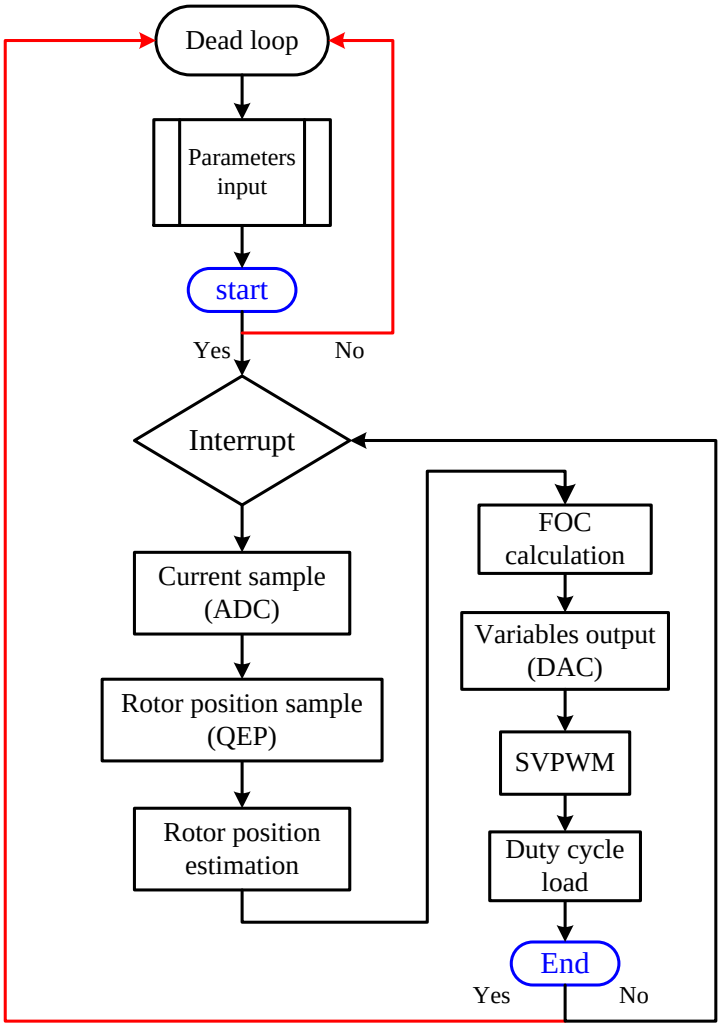

Figure C.1: Programme flow.

SELECTED PUBLICATIONS

Paper 1

(*Journal Paper*)

Minimum Voltage Vector Injection Method for Sensorless Control of PMSM for Low-Speed Operations

Ge Xie, Kaiyuan Lu, Sanjeet Kumar Dwivedi, Jesper Riber Rosholm and Frede Blaabjerg

The paper has been accepted in the
IEEE Transaction on Power Electronics.

Paper 2

(*Journal Paper*)

Permanent Magnet Flux Online Estimation Based on Zero Voltage Vector Injection

Ge Xie, Kaiyuan Lu, Sanjeet Kumar Dwivedi, Jesper Riber Rosholm and Weiming Wu

The paper has been accepted in the
IEEE Transaction on Power Electronics Letters.

Paper 3

(*Conference Paper*)

High bandwidth zero voltage injection method for sensorless control of PMSM

Ge Xie, Kaiyuan Lu, Sanjeet Kumar Dwivedi and Jesper Riber Rosholm

The paper has been published in the
2014 17th International Conference on Electrical Machines and Systems (ICEMS),
pp.3546-3552, Oct 2014.

Paper 4

(*Conference Paper*)

Improved INFORM Method by Minimizing the Inverter Nonlinear Voltage Error Effects

Ge Xie, Kaiyuan Lu, Sanjeet Kumar Dwivedi and Jesper Riber Rosholm

The paper has been accepted in the
2015 2nd Workshop on Electrical Machines Design Control and Diagnosis
(WEMDCD).